Karlsruhe Institute of Technology

Biomimetics for Efficient Oil Water Separation: From Natural Oil Sorbents to Bioinspired Micro- and Nanostructured Polymeric Sorbents and Membranes

Zur Erlangung des akademischen Grades einer
Doktorin der Ingenieurwissenschaften (Dr.-Ing.)
von der KIT-Fakultät für Maschinenbau
des Karlsruher Instituts für Technologie (KIT)
angenommene

Dissertation

von

M.Sc. Claudia Zeiger

Referenten: PD Dr. Hendrik Hölscher
Prof. Dr. Jan Gerrit Korvink
Prof. Dr. Wilhelm Barthlott

Tag der mündlichen Prüfung: 04.06.2018

Kurzfassung

Bionik hat es sich zur Aufgabe gemacht, von der Natur zu lernen und natürliche Mechanismen und Effekte technisch nutzbar zu machen. Nach dem Prinzip „survival of the fittest" hat die Evolution über die vergangenen Jahrmillionen hochgradig spezialisierte Lebewesen hervorgebracht, die perfekt an ihre natürliche Umgebung angepasst sind. Blätter der Wasserpflanzen *Salvinia* (Schwimmfarn) und *Pistia stratiotes* (Wassersalat) weisen beispielsweise auf ihrer Oberfläche hierarchische Mikro- und Nanostrukturierungen auf, die das Überleben der Pflanzen sicherstellen, auch wenn diese unter Wasser gezogen werden. Die Pflanzenblätter sind bedeckt von Trichomen, einer mikroskaligen, haarigen Struktur, die die Pflanzenblätter superhydrophob (wasserabweisend) macht. Gleichzeitig sind die Blätter superoleophil (ölaufnehmend), wodurch sie selektiv Öl aus Öl/Wasser-Gemischen absorbieren. Die Absorptionsfähigkeit von Pflanzenblättern mit "haariger" Oberfläche wird mit der von superhydrophoben Lotusblättern ohne Haare verglichen, sowie mit künstlichen Absorbern. Anhand der verschiedenen Typen von Trichomen, die innerhalb der Gattung der Schwimmfarne (*Salvinia*) existieren, wird der Einfluss der Trichomform auf die Ölabsorptionsfähigkeit der Pflanzenblätter untersucht. Inspiriert durch solche natürlichen Oberflächen, ist Nanopelz eine Polymerfolie, die von Mikro- und Nanometer großen Haaren bedeckt ist. Wie sein natürliches Vorbild ist auch Nanopelz superhydrophob und superoleophil, und absorbiert somit selektiv Öl aus Öl/Wasser-Gemischen. Es werden verschiedene Weiterentwicklungen des bekannten Nanopelzes vorgestellt, darunter unter anderem wiederverwendbarer Nanopelz aus Formgedächtnispolymer. Außerdem wird ein neues Herstellungsverfahren vorgestellt, welches es ermöglicht, Nanopelz großflächig herzustellen und den Weg hin zu einer industriellen Herstellung von Nanopelz ebnet. Die Separationseffizienz von Nanopelz wird außerdem erhöht, indem Nanopelzfolien mikroperforiert werden. Die so hergestellten Membranen eigenen sich zur Filtration von Öl/Wasser-Gemischen. Sie lassen selektiv Öl durch die Poren hindurchfließen und halten Wasser zurück. Durch Plasmabehandlung der Nanopelzmembranen wird ein unterwassersuperoleophober Filter hergestellt. Im Vergleich zum ursprünglichen Nanopelzfilter hat dieser invertierte Eigenschaften und lässt Wasser durch die Poren hindurchfließen, Öl hingegen nicht. Typische Parameter der Membranen werden analysiert und mit theoretischen Werten verglichen, und die Filterleistung von Nanopelz wird anhand der Trennung von Öl/Wasser-Gemischen demonstriert. So wurde unter anderem ein Gemisch aus Rohöl und Wasser mithilfe von plasmabehandeltem Nanopelz getrennt. Das Wasser war nach der Trennung augenscheinlich frei von Ölrückständen.

Abstract

According to the idea of biomimetics, applying principles of living nature to technical applications means making use of highly specialized and optimized mechanisms that have proved themselves over billions of years. Due to natural selection and according to the biological principle "survival of the fittest", living organisms perfectly adapted to their natural environment. Leaves of aquatic plants such as *Salvinia* (water fern) and *Pistia strationtes* (water lettuce), for example, are covered by a hierarchical micro- and nano structure, which helps them to survive when dragged under water. Due to their "hairy" trichome structure, the leaves are superhydrophobic and superoleophilic and therefore selectively absorb oil from oil/water mixtures. Oil absorption capacity of four *Salvinia* species with different trichome types and of water lettuce (*Pistia stratiotes)* is quantified. By comparing oil absorption of *Salvinia* and *Pistia* leaves with trichomes (hairs) to Lotus *(Nelumbo nucifera)* leaves with no trichomes, the influence of presence and morphology of trichomes on oil absorption is examined. Specifically, the influence of trichome shape on oil absorption is analyzed by comparing oil absorption of different hair types of *Salvinia molesta*. Subsequently, artificial nanofur inspired by *Salvinia* leaf surface structure is investigated. Polymeric nanofur consists of dense layer of micro- and nanosized hairs and is superhydrophobic and superoleophilic just as its natural role model. Various improvements are presented, including reusable nanofur from shape memory polymer. Also, new nanofur fabrication process is introduced which allows upscaling and paves the way towards industrial fabrication of nanofur. Nanofur oil/water separation efficiency is increased by punching holes into nanofur to fabricate a nanofur membrane. Membranes with special wetting properties enable selective removal of either oil or water from oil/water mixtures by filtration. Superhydrophobic/superoleophilic nanofur membrane lets oil permeate through and retains water. The as-prepared oil-removing membrane is converted into underwater superoleophobic water-removing membrane by argon plasma treatment. Plasma treated nanofur selectively lets water permeate through and therefore separates water from oil/water mixtures. Characteristic values such as membrane permeability and breakthrough pressures are analyzed and experimental results are compared to theoretical values, and the efficiency of both types of membranes for oil/water separation is demonstrated. For example, a mixture of crude oil and water was separated by filtration, and no oil was observed in the collected water.

Acknowledgments

This work would not have been possible without the support of numerous persons and institutions. I would like to express special thanks to Prof. Dr. Jan Konvink for giving me the opportunity to carry out my research project at the Institute of Microstructure Technology (IMT), Karlsruhe Institute of Technology (KIT) between 2014 and 2018. It is an honor to thank Prof. Dr. Wilhelm Barthlott for making it possible for me to collaborate with the Nees Institute for Biodiversity of Plants at the University of Bonn and for sharing his immense knowledge on plant surfaces and biomimetics with me.

I would like to express my sincere gratitude to my supervisor Dr. Hendrik Hölscher for his continuous support throughout my research activities, for his patience, motivation and inspiring discussions, and to Dr. Maryna Kavalenka for her guidance and support. I thank my colleagues for their collaboration, the lively debates, their critical feedback and their support in the laboratory, in particular Matthias Worgull, Norbert Schneider, Marc Schneider, Andreas Striegel, Paul Abaffy, Markus Guttmann, Richard Thelen, Felix Vüllers, Tobias Förtsch, Christian Lutz and Julia Syurik.

Furthermore, I am indebted to the students I supervised: Jana Kumberg, Hanna Wund, Isabelle C. Rodrigues da Silva, Matthias Heger and Alexander Storz. They executed countless experiments and achieved remarkable results, and it was a pleasure to pass on my knowledge to them and to learn from them in return.

Prof. Dr. Wilhelm Barthlott and the Botanical Gardens of the University of Bonn kindly provided *Salvinia, Pistia stratiotes* and *Nelumbo nucifera* plants. It is my pleasure to thank Matthias Mail for his support and for interesting discussions. Experiments were partly executed using the facilities of the Karlsruhe Nano Micro Facility (KNMF). I thank MiRO Mineralölraffinerie Oberrhein GmbH & Co. KG for the crude oil samples and the viscosity measurements.

I am very much indebted to the Carl Zeiss Foundation for the financial support through a personal scholarship.

Last but not the least, I would like to thank my family and friends for their sincere encouragement and inspiration, and for continuously supporting me throughout writing this thesis.

Karlsruhe, June 2018

Claudia Zeiger

Contents

1. Introduction

1.1 Biomimetics - Learning from Nature

"I think the biggest innovations of the twenty-first century will be the intersection of biology and technology." (Steve Jobs) [1]

In the interdisciplinary field of biomimetics, principles from biology are applied to the synthesis of materials, systems or machines. [2] According to the idea of evolution by natural selection as proposed by Charles Darvin [3], the principle of "surviving of the fittest" leads to a constant improvement of living nature for more than 420 million years. [4] Organisms adapt to their environment, develop mechanisms, structures, and materials for improved camouflage or successful courtship, for effectively escaping from predators or to defy natural influences and extreme conditions such as heat and cold, floods and droughts, sun and darkness, storms or fire. While less adapted animals and plants become extinct, survival of the fittest can ensure the survival of the best adapted species. For example, the antireflective properties of moth eyes ensure invisibility of the moths in the darkness. [5,6] Beetles of the species *Merimna atrata*, whose larvae develop in freshly burnt wood, have infrared organs to detect fires from long distances. [7,8] Various aquatic and semiaquatic animals use specific mechanisms to reduce drag and move faster in water. The riblet structures on the skin of sharks is aligned in the direction of the water flow and reduces drag by reducing the turbulent vortices, [9] and penguins create a coat of small air bubbles to move faster in water. [10,11]

Applying principles of the living nature to technical applications means making use of highly specialized and optimized mechanisms that have proved themselves over millions of years. Therefore, biomimetics reduces the development effort and/or leads to improved solutions by making use of the groundwork evolution carried out. Living nature encompasses an estimated number of 10 million plants and animals, which can potentially serve as prototypes for engineers. [12] Well known historic examples for biomimetic technologies are airplanes, which are inspired by birds, and hook-and-loop tape, which is inspired by the fruits of burdock plants. Also, swim suits inspired by shark skin increase the speed of swimmers in the water. [9,13] Another wide field of biomimetic research are surfaces of

plants. They are often multifunctional, and do for example reflect or absorb light, create color by spectral radiation, reduce water loss, stay dry and keep an air layer underwater, reduce the adhesion for insects or avoid contamination. [12] Self cleaning surfaces, for example, mimic the surface structure and properties of Lotus leaves, and the artificial nanofur surface inspired by the leaves of the aquatic plants *Salvinia* and *Pistia* possesses similar multifunctional properties as its role models. The surface of the polymeric nanofur foil is covered by hierarchical micro- and nanosized hairs. It retains an air layer underwater [14] and is highly transmissive for light [15]. Also, it is superhydrophobic (water repelling) and superoleophilic (oil affine) (see Ch. 2.1) and therefore selectively absorbs oil from oil/water mixtures. [16]

In this thesis, the oil absorption mechanism of such surfaces is investigated. Oil absorption by a bioinspired, artificial nanofur surface is compared to its natural role models. Also, the oil absorption mechanism of different superhydrophobic leaf surfaces is studied. The observations and the achieved results on the one hand lead to identification of efficient and environmentally friendly oil absorption materials, and on the other hand can help to improve the bioinspired nanofur surface. Subsequently, various improvements and new developments concerning the variety and the fabrication efficiency of nanofur and its usage for oil/water separation are presented. This includes the oil/water filtration by microporous nanofur and the implementation of reusable nanofur, as well as an adapted nanofur fabrication process. Prior to that, an introduction to oil spills and oil/water separation methods is given in the following section.

1.2 Oil Spills and Oil Spill Cleanup

Oil and petroleum products are among the most important energy resources and raw materials in the world. The products which are based on crude oil include gasoline, oils, asphalt, domestic fuel oil, vaseline, and polymers. [17] The enormous worldwide consumption of oil and petroleum products leads to increased oil exploration, production, transportation, refinement, storage, and processing activities, which are accompanied by a high risk of oil spillage and aquatic pollution. [18–20] Although crude oil is a naturally occurring product, it causes a massive negative impact on the environment (see Fig. 1.1) and public health when spilled in unfavorable places and conditions. [17] Crude oil, commonly known as petroleum or "black gold", is composed of hydrocarbon deposits and other organic materials. It is formed through heating and compression of organic materials leading to biological, chemical, and geochemical processes. The oldest known crude oil deposits were formed over 500 million years ago. [21]

Crude oil is typically obtained by drilling, where onshore drilling relates to drilling holes under the earth's surface, and offshore drilling refers to drilling underneath the seabed. In particular offshore drilling is accompanied by a high risk of oil being spilled into the surrounding sea water. One example is the Deepwater Horizon Blowout in 2010 where an estimated amount of 780 000 m^3 of oil discharged into the Gulf of Mexico. [22, 23] Also, the transportation of oil on oil tankers frequently leads to enormous oil spills, such as the spill caused by the oil tanker Exxon Valdez which struck a reef in 1989 and spilled over 40 000 m^3 of crude oil. [24] Common oil spill response techniques include in-situ burning, which is the process of burning oil floating on the sea at or close to the origin of an oil

spill. However, the resulting fire and the potentially toxic smoke can have a negative impact on the environment and on human health. [25] Another common response technique is the chemical dispersion of spilled oil. An oil slick is broken up into small droplets which spread in the water and therefore can be degraded by naturally occuring microorganisms. Depending on the used dispersant, however, this goes along with the aquatic toxicy of the chemicals which are dispensed to the sea water. [25] Aside from such gigantic accidents, smaller amounts of oil are released into the environment every day by incidents such as leaking pipelines or by the inappropriate disposal of oily wastewater. [26] As even small accidental oil spills have a potentially negative impact on the environment and public health, removing the spilled oil from water is highly desirable. Also, industrial processes, such as removing oil from machine cooling water, require methods for an efficient oil/water separation. Although oil and water are two immiscible liquids, separating oil/water mixtures keeps challenging scientists and engineers around the world. Therefore, developing efficient and sustainable methods for separating oil/water mixtures and cleaning oil spills is of great significance for various applications. [27–30]

Figure 1.1: Oil spills and their impact. **A,B)** During the Deepwater Horizon Blowout, an estimated amount of 780 000 m^3 of oil discharged into the Gulf of Mexico. [22,23] **C)** Bird suffering from spilled oil. (A) NOAA's National Ocean Service, reprinted from [31], B) Daniel Beltrá, courtesy Catherine Edelman Gallery, reprinted from [32], C) Getty Images, reprinted from [33]

Removing oil by absorption is the method of choice for many applications, where a sorption material is immersed into the oil and transforms the oil into a semisolid state by absorbing it. [34] Subsequently, the absorbed oil is removed from the water together with the sorbing material. Common absorbing materials include natural sorbents such as saw dust, as well as artificial granulate sorbing materials. However, many sorbents commonly used to collect spilled oil absorb large amounts of water in addition to the oil and have a limited oil absorption capacity. This leads to an increased material consumption as well as an increased weight of soaked sorbent materials, and therefore to increased handling and disposal costs. To overcome these challenges, materials with special wetting properties, which repel water while absorbing oil (superhydrophobic/superoleophilic, see Ch. 2.1) are required. [35–40] Novel approaches for fabricating such materials focus on polymeric sponges, metal meshes, and fabrics, modified or coated with metal or metal oxide, nanoparticles or silicon compounds. [41–47] However, many of these technical materials are potentially harmful to the environment during production, usage or disposal, or are economically inefficient. [48] In contrast, the use of environmental friendly methods inspired by nature or based on biological materials is a promising approach in the search for a solution for effective and efficient oil/water separation methods. [16, 35, 49–51]

1.3 Overview and Approach of this Thesis

In this thesis, a biomimetic solution for oil/water separation and oil spill cleanup is presented in its entirety. The structure of the thesis is illustrated in Fig. 1.2. First, the fundamentals of surface wetting, special wetting properties, and microstructure fabrication technologies are summarized in Ch. 2. This includes hot embossing, hot pulling and nanothermoforming as well as an introduction to shape memory polymers and to contact angle measurement. Next, natural materials for efficient and selective oil absorption are identified and the absorption mechanism of these materials is investigated (Ch. 3). The oil absorption capacities of four *Salvinia* species, water lettuce *Pistia stratiotes* and Lotus leaves are compared to artificial oil sorbents, and the influence of the surface structures on the oil absorption is investigated. Leaves of the water fern *Salvinia* both serve as oil sorbents and as a role model for nanofur as an artificial, bioinspired oil/water separation material. In Ch. 4 several enhancements of nanofur are presented. This includes methods for reusing the nanofur by washing and by fabricating nanofur from a shape memory polymer, as well as new fabrication methods for an increased fabrication efficiency which allows the upscaling of nanofur fabrication.

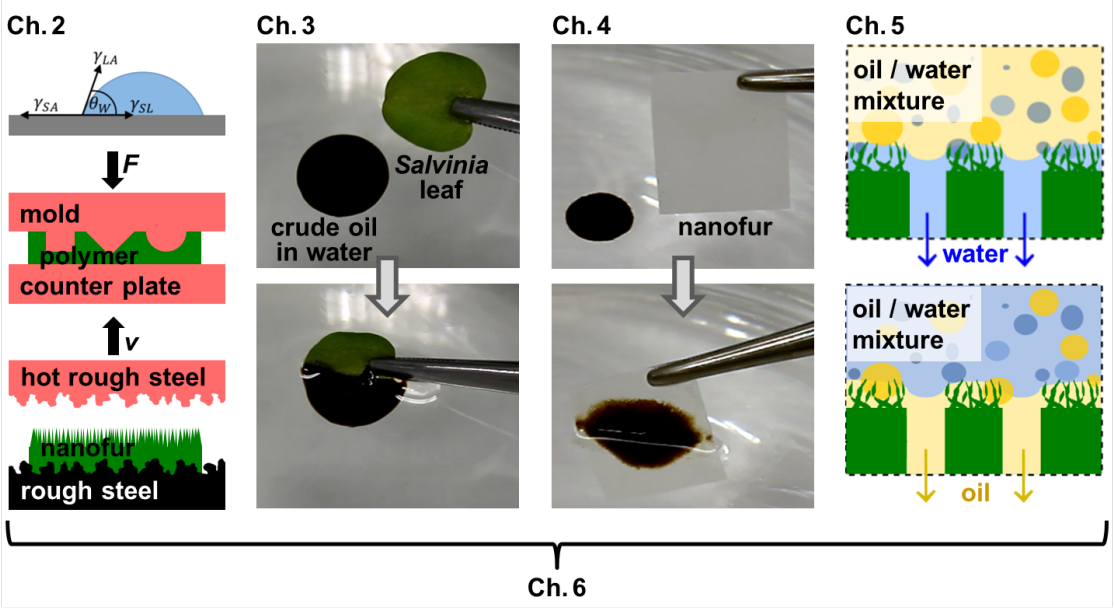

Figure 1.2: Overview of the structure of this thesis. In Ch. 2, the fundamentals of surface wetting and of the replication technologies hot embossing and hot pulling are summarized. The oil absorption by natural oil sorbents such as *Salvinia* leaves is investigated in Ch. 3. Next, several enhancements of nanofur for oil absorption are presented in Ch. 4. By microperforation, nanofur is converted into a membrane for selective oil/water separation. Both oil-removing and water-removing membranes separate oil/water mixtures as presented in Ch. 5. A summary of the thesis is finally given in Ch. 6.

By microperforation, nanofur foils are converted into membranes for selective oil/water separation. Both oil-removing and water-removing membranes separate oil/water mixtures in a gravity-driven filtration process as presented in Ch. 5. Various filtration setups for oil/water filtration are installed and the results demonstrate the separation capability of

the fabricated membranes. Also, the performance of nanofur membranes is measured and the experimental results are compared to the theoretical values. A summary of the thesis and an outlook on possible applications derived from the achieved results are finally given in Ch. 6.

2. Fundamentals, Materials, and Methods

This thesis focuses on oil absorption and oil/water separation by surfaces with special wetting properties. Both natural and bioinspired artificial surfaces are investigated. Artificial surfaces are produced using fabrication techniques such as hot embossing, hot pulling, and nanothermoforming. The fundamentals of these fabrication techniques, of surface wetting properties, and of contact angle measurement are presented in this chapter. Also, the shape memory polymers Tecoflex® and Tecoplast®, which play a central role in this thesis, are introduced.

2.1 Surface Wetting Properties

Wetting is the process that happens when a liquid comes in contact with a solid surface. [12] When a water droplet touches a solid surface, it can spread out to a thin film. Alternatively, the droplet can remain in a more or less spherical shape, maintaining little contact with the surface. Wettability of a surface results from a force balance between cohesive forces (intermolecular forces between identical molecules) and adhesive forces (intermolecular forces between molecules of different substances). The adhesive forces between the liquid and the solid phase cause the liquid to spread on the surface. In contrast, the cohesive forces between water molecules inside the water droplet, such as forces from hydrogen bondings and van der Waals forces, force the liquid towards a spherical shape, which minimizes the contact with the solid surface. This is because the molecules on the surface of the droplet have more energy than the molecules inside the droplet. The energy difference between the molecules at the surface and the molecules in the bulk is called interfacial energy. In other words, interfacial energy is the work which is needed to increase the size of the interface between two adjacent, immiscible phases. [52]

2.1.1 Contact Angle

Surface wettability is quantified by the contact angle (CA) θ, which is measured where the liquid-vapor interface meets the solid surface (see Fig. 2.1a), and is theoretically described by the Young equation

$$\gamma_{SG} - \gamma_{SL} - \gamma_{LG} cos(\theta) = 0\,, \tag{2.1}$$

where γ_{SG}, γ_{SL} and γ_{LG} denote the solid-gas, solid-liquid, and liquid-gas interfacial energy (see Fig. 2.1a). The Young equation is based on the assumption of a thermodynamic equilibrium of the liquid, solid and gas phases. When the liquid is water and the surrounding gas phase is air, the water contact angle (WCA) θ_W, or, more precisely, the water in air contact angle is measured. Analogously, the oil-in-air contact angle (OCA) is the CA of an oil droplet on a surface, surrounded by air. The air as surrounding gas phase can be replaced by another vapor or immiscible liquid phase. In this thesis, the CA of a water droplet on a solid surface with oil as surrounding medium, for example, is referred to as water-in-oil CA, and vice versa.

Surfaces are classified into groups, describing their wetting behavior. For water (or oil) droplets, these are: [53]

- $\theta_W < 10°$: superhydrophilic (or superoleophilic)
- $10° \leq \theta_W < 90°$: hydrophilic (or oleophilic)
- $90° < \theta_W \leq 150°$: hydrophobic (or oleophobic)
- $150° < \theta_W$: superhydrophobic (or superoleophobic)

While high energy materials tend to be hydrophilic, low energy materials are more hydrophobic. Due to a lower surface energy of oil compared to water, the OCA of most materials is smaller than their WCA, i.e. most materials are oleophilic. Hydrophobicity, in contrast, can be achieved by a surface coating with low energy materials. [54, 55] One prominent example for hydrophobic coating materials is polytetrafluorethylene (PTFE). However, the water contact angle of flat surfaces will not exceed 120°. [56, 57] Higher contact angles and superhydrophobic wetting properties always result from a combination of the material properties and the surface structure or roughness, which enhances the intrinsic CA of the flat surface. According to the Wenzel [58] and Cassie-Baxter [59, 60] models, hydrophilic surfaces become more hydrophilic when roughness is added to the surface, and hydrophobic materials become more hydrophobic. More recent experimental results have shown that surfaces with low wettability (hydrophobic, superhydrophobic) can also be created from materials with an intrinsic CA $< 90°$. More precisely, the intrinsic CA$= 65°$ was suggested as the critical CA above which superhydrophobic surface properties can be achieved by adding roughness. [61, 62] The Wenzel and Cassie-Baxter models imply that water droplets on rough or micro-/nanostructured superhydrophobic surfaces can, as illustrated in Fig. 2.1b,c, either sit on top of the surface structure only touching their tips, with air trapped under the droplet (Cassie-Baxter state), or infiltrate the structure (Wenzel-state).

In addition to the WCA, the roll-off angle and the contact angle hysteresis are other important parameters that describe the wetting properties of surfaces. The roll-off angle is defined as the minimum tilting angle required to make a droplet roll off the surface. Due to infiltration of the liquid into the surface structure and resulting pinning effects, droplets in Wenzel state typically have a high roll-off angle. While rolling down a tilted surface, the advancing CA (downstream CA) and the receding CA (upstream CA) are not equal,

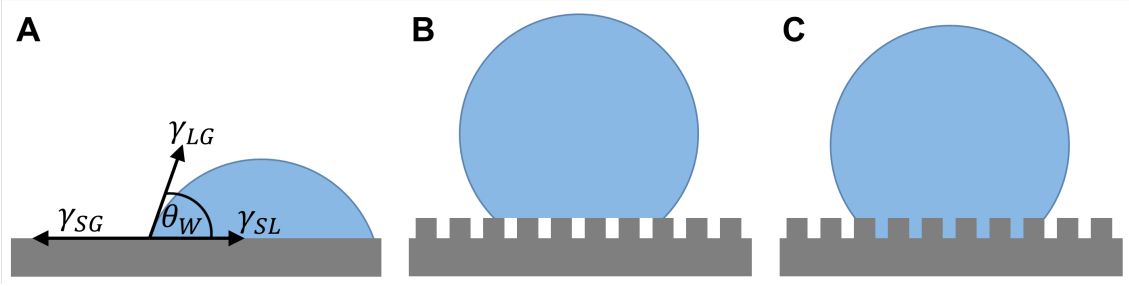

Figure 2.1: Water contact angle and superhydrophobic wetting states. **A)** Water contact angle θ_W is measured where the liquid-vapor interface meets the solid surface. The contact angle is theoretically described by the Young equation (Eq. 2.1), where γ_{SG}, γ_{SL} and γ_{LG} denote the solid-gas, solid-liquid and liquid-gas interfacial energy. [63] On rough or micro/nanostructured superhydrophobic surfaces, droplets can either **B)** sit on top of the structure only touching their tips, with air trapped under the droplet (Cassie-Baxter state) or **C)** infiltrate the structure (Wenzel-state).

with the advancing CA being higher than the receding. The difference between advancing and receding CA is defined as contact angle hysteresis. The typically high roll-off angles of droplets in the Wenzel state come along with a high CA hysteresis. Droplets in the Cassie-Baxter state, in contrast, typically have a low contact angle hysteresis and a low roll-off angle, which is due to the air trapped in the structure.

2.1.2 Contact Angle Measurement

Contact angles as a quantification method for surface wetting properties can be measured with a CA measuring system. In this thesis, the contact angle measurement and contour analysis system OCA 40 (DataPhysics Instruments GmbH, Filderstadt, Germany) [64], which is shown in Fig. 2.2a, was used. The contact angle measurement system consists of an adjustable sample table, an electronic syringe unit, and a high-resolution video camera. The contact angles are calculated from images of droplets sitting on the surface, which are recorded by a camera (see Fig. 2.2b,c) with DataPhysics software SCA 20 [64], using the sessile drop measurement and the ellipse fitting method. The baseline was determined manually whenever the software failed to identify a correct baseline. The droplet volume used for the measurements varies between 1 µL and 5 µL, as smaller droplets lead to more accurate results of the measurements, but on the other hand cannot be placed on superhydrophobic surfaces, as gravity and adhesion to the surface are not strong enough to overcome the adhesion of the droplet to the needle.

2.2 Methods and Materials for Microstructure Fabrication

In this section, materials and methods for the microstructure fabrication are presented that are essential for the subsequent chapters. This includes the explanation of the replication methods hot embossing, hot pulling, and nanothermoforming, as well as an introduction to thermoplastic polymers and shape memory polymers in particular.

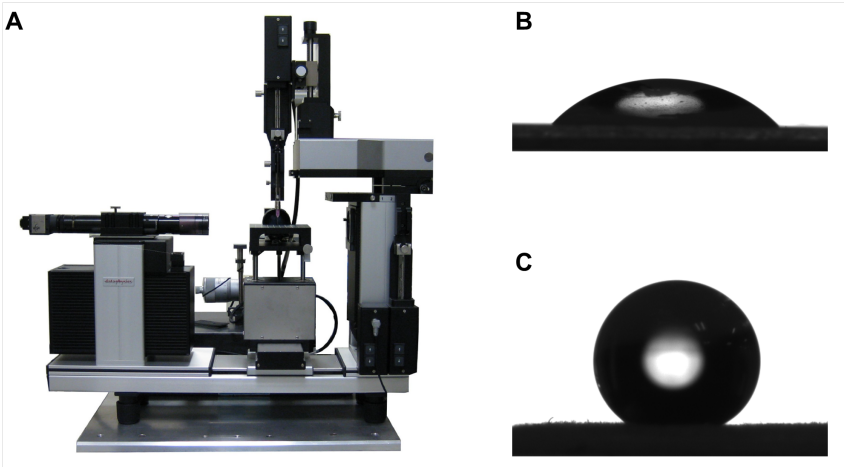

Figure 2.2: Contact angle measurement. **A)** Contact angle measurement system OCA 40 by Dataphysics [64]. The contact angle measurement system consists of an adjustable sample table, an electronic syringe unit and a high-resolution video camera. Reprinted from [65], **B)** Camera picture taken with OCA 40, showing a water droplet on a hydrophilic surface and **C)** on a hydrophobic surface.

2.2.1 Thermoplastic Polymers

Polymers are macromolecules, composed of repeated units which are strung together to long chains or more complicated structures. Thermal replication methods, such as hot embossing and hot pulling, require the meltability of the used polymers. Thermoplastic polymers become soft and moldable when they are heated above a certain temperature, the glass transition temperature T_g, and they become solid when they are cooled below this temperature. The softening happens due to the weakening of intermolecular forces when the temperature increases. Thermoplastic crystalline polymers additionally possess the melting temperature T_m, above which the polymer chains in the crystalline portions of the polymer sample lose their crystal structures and become a disordered liquid. In this thesis, T_s refers to the softening temperature of the polymer, which is the relevant temperature for thermal replication processes. The group of thermoplastic polymers includes classical polymers such as polyethylene (PE), polypropylene (PP), polycarbonate (PC) and poly(methyl methacrylate) (PMMA). In addition, thermoplastic shape memory polymers and thermoplastic biopolymers qualify for thermal replication methods.

2.2.2 Shape Memory Polymers

Shape memory polymers (SMP), first mentioned in a patent specification in 1941, [66] are mechanically active polymers that can remember their former shape (permanent shape) after having been deformed to a temporary shape. They remain in the temporary shape until the recovery is triggered. Triggers causing the recovery of the original shape depend on the specific shape memory polymer and include external stimuli such as heat, pH-change, magnetic induction, and light. The shape memory effect of polymers results from their molecular architecture. Netpoints or hard segments determine the permanent shape, and reversible crosslinks of soft segments fix the temporary shape. [67–70] One example of a shape memory polymer is heat shrinkable tubing made from polytetrafluoroethylene.

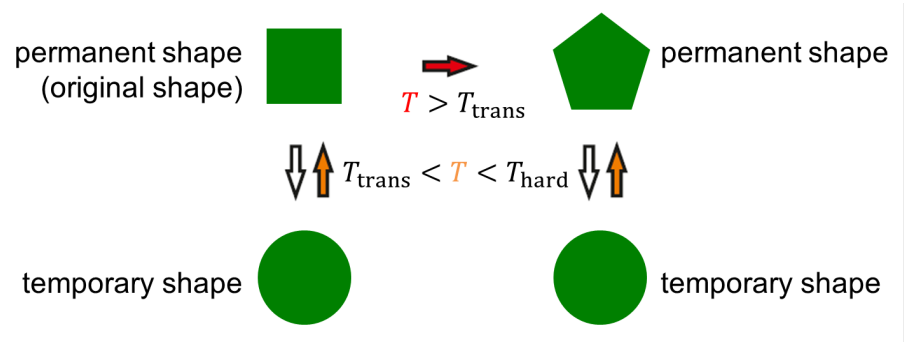

Figure 2.3: Thermoplastic thermoresponsive shape memory polymers can remember their permanent shape after having been deformed to a temporary shape. They remain in the temporary shape until the recovery is triggered by heating the polymer up to a temperature $T > T_{trans}$. The process of temporary deformation and recovery is repeatable several times. The permanent shape can be changed by deforming the SMP at $T > T_{hard}$.

In this thesis, thermoplastic, thermoresponsive SMPs (see Fig. 2.3) are used to obtain smart surfaces. A permanent shape can be created by molding the polymer at temperatures around or above the glass transition temperature of the hard segment T_{hard}. Applicable replication methods are hot forming processes such as hot embossing, injection molding or transfer molding. The temporary shape is created by deforming the polymer sample at a temperature around glass transition temperature of the soft segment T_{trans}, and well below T_{hard} in order to avoid any influence on the permanent shape or its redefinition. The soft segments of the polymer chains melt and allow a deformation of the sample, while the netpoints formed by the hard segments remain unchanged. Cooling down the sample well below T_{trans} fixes the temporary shape until the polymer is heated up to T_{trans} again, which softens the crosslinks and triggers the recovery of the permanent shape. The driving force for the recovery of the permanent shape is the entropy elasticity of the soft segments. The soft segments are in an orientated confirmation when in temporary shape, and they gain entropy when the permanent shape is recovered and the soft segments move to a random confirmation. [67–70]

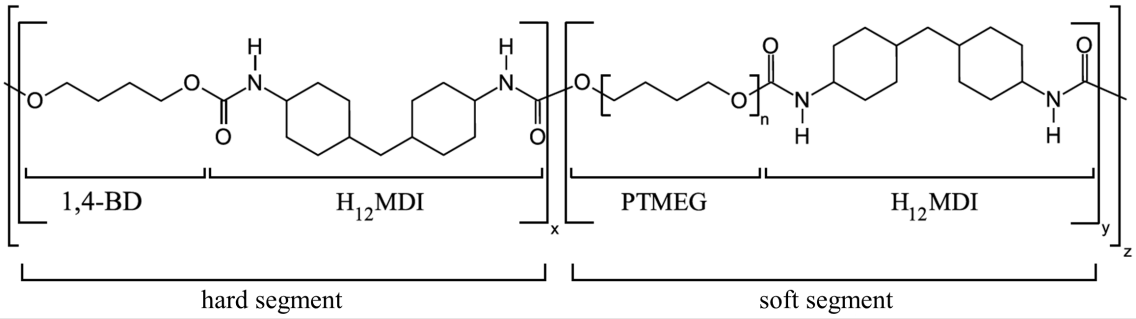

Figure 2.4: Structural formula of the shape memory polymer Tecoflex EG-72D® (TFX). The hard phase of TFX contains of 1,4-BD and H_{12}MDI molecules. The soft phase contains of PTMEG and H_{12}MDI.

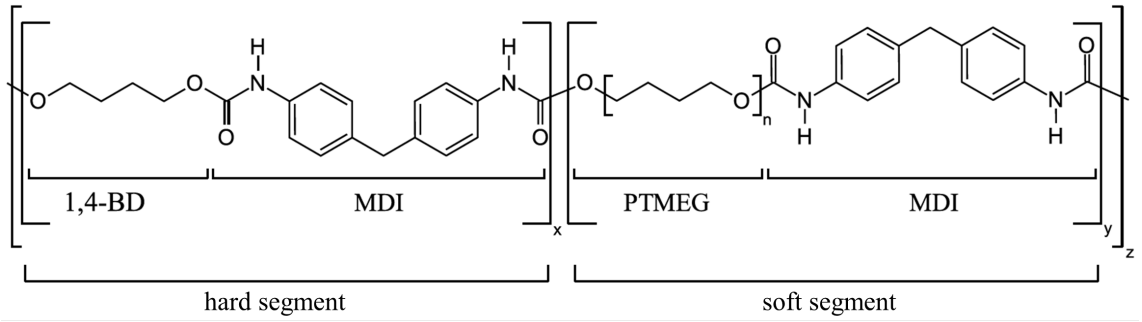

Figure 2.5: Structural formula of the shape memory polymer Tecoplast TP-470® (TP). The hard phase of TP contains of 1,4-BD and MDI molecules. The soft phase contains of PTMEG and MDI.

The two SMPs used in this thesis are Tecoflex EG-72D® (TFX) and Tecoplast TP-470® (TP). TFX can be synthesized by a polyaddition reaction of methylene bis(cyclohexyl isocyanate) (H_{12}MDI), poly(tetramethylene glycol) (PTMEG), and 1,4-butanediol (1,4-BD) which leads to a two-phase microstructure. The hard phase contains of (1,4-BD) and (H_{12}MDI) molecules and the soft segments contain of (PTMEG) and (H_{12}MDI) as illustrated in Fig. 2.4. [67–72] The synthetization and the molecular structure of TP are similar to TFX, with (H_{12}MDI) being replaced by methylene diphenyl diisocyanate (MDI), as can be seen in Fig. 2.5. [71, 72]

2.2.3 Hot Embossing

Hot embossing is an established micro replication technology, where a microstructured master (mold) is replicated in a thermoplastic polymer (see Sec. 2.2.1). Hot embossing is executed using a hot embossing machine (see Fig. 2.6) which consists of a stiff frame with normally four guiding pillars and two crossbars. One crossbar is fixed, while the other is movable in z-axis direction through a precise motion system. Between the two crossbars, heating/cooling units are fixed. Tools such as mold inserts and substrate plates are fixed on the heating/cooling units. A vacuum chamber surrounds the tools and the temperature units when closed. [73]

During the hot embossing process (see Fig. 2.7), a polymer foil is placed between the mold and the counter plate, and all three of them are heated up to the molding temperature. By applying a force, the polymer is pressed into the cavities of the mold. While the mold insert and the polymer are cooled, the applied force is maintained. When the demolding temperature is reached, the polymer sample is demolded. More detailed, the hot embossing process consists of five main steps, which are illustrated in Fig. 2.7. [73]

A) Closing and evacuating: After placing the polymer foil between the substrate plate and the mold, the vacuum chamber is closed and evacuated. A touch force between the mold insert, the polymer foil and the substrate plate is applied. Evacuation of the vacuum chamber is necessary to avoid air bubbles inside the cavities, and leads to the measured negative force peak (a) in Fig. 2.7. Typical pressures are in the range of 1 mbar. The applied touch force is typically between 100 N and 500 N, and is indicated by a small positive force peak (b) in Fig. 2.7.

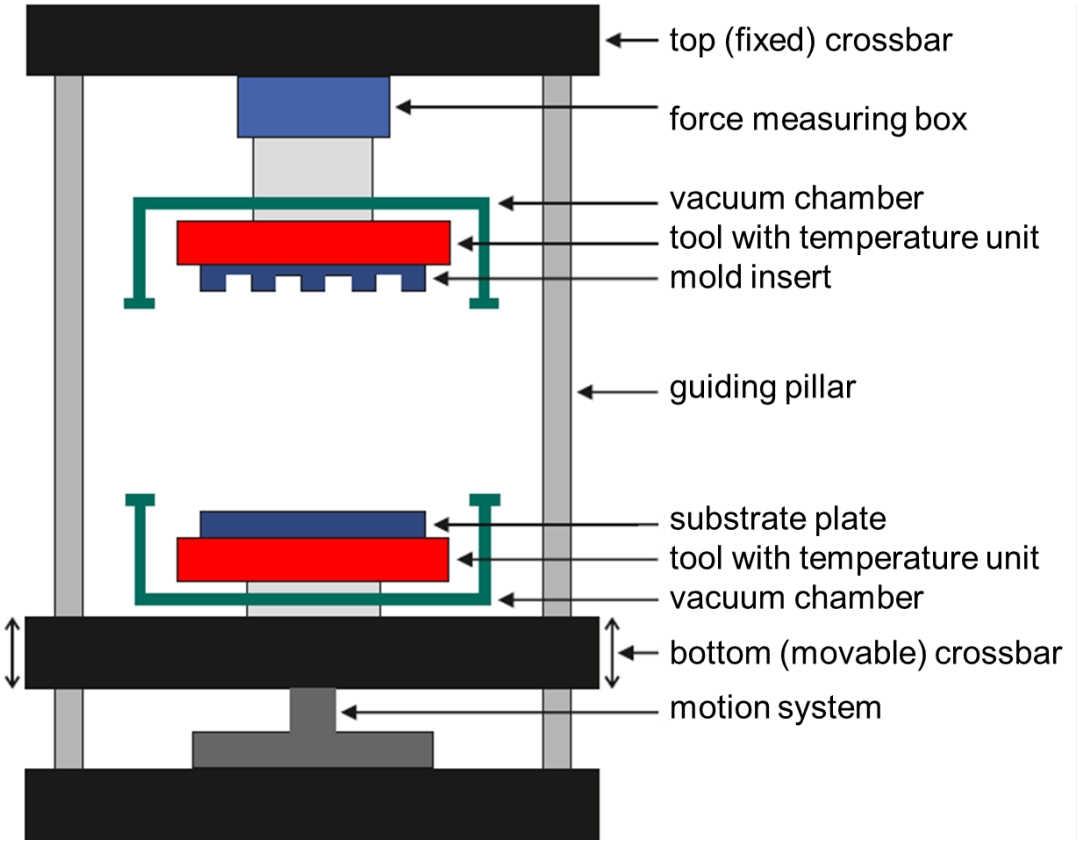

Figure 2.6: Hot embossing machines consists of a stiff frame with four guiding pillars and two crossbars. The top crossbar is fixed and the bottom crossbar is movable through a precise motion system. Between the two crossbars, heating/cooling units and tools are fixed. [73]

B) Heating: Mold and substrate plate are heated, while the touch force is maintained until the molding temperature is reached. The polymer foil is heated through the substrate plate and the mold by heat conduction, and gets soft. This leads, on the one hand, to a thermal expansion of the polymer foil and, therefore, to an increase of the distance between the mold and the substrate plate. On the other hand, once the softening temperature of the polymer is reached, the creeping of the polymer leads to a decrease of the distance between the mold and the substrate plate.

C) Molding: When the embossing temperature is reached, the molding step is executed, starting with a continuous movement of the crossbar (C1 in Fig. 2.7), which leads to an exponential increase of the force. Typical embossing velocities are in the range of 1 mm/min. After reaching the defined force (e), the process switches to force-controlled embossing, where the force is kept at a constant level (C2 in Fig. 2.7) for a defined holding time. As the polymer creeps under constant force, the residual layer thickness decreases, which causes the counter plate to move towards the mold.

D) Cooling: After maintaining a constant temperature and force for a defined holding time, the cooling process starts. As the force is kept constant, the distance between the mold and the substrate plate decreases due to thermal contraction of the polymer.

E) Demolding: When the demolding temperature, which is below the softening temperature of the polymer, is reached, the demolding step starts. Typically, a rough substrate plate is used to ensure the adhesion of the polymer residual layer to the substrate plate. When the adhesion to the substrate plate is higher than the adhesion of the microstructures in the mold cavities, the microstructures can be demolded by moving the crossbar. Demolding is initiated by a constant motion of the crossbar at a low velocity, typically around 1 mm/min. The negative peak (h) in Fig. 2.7 indicates the resulting tensile forces. After demolding, the embossing chamber is vented, which results in a peak of the measured force (i in Fig. 2.7), and opened.

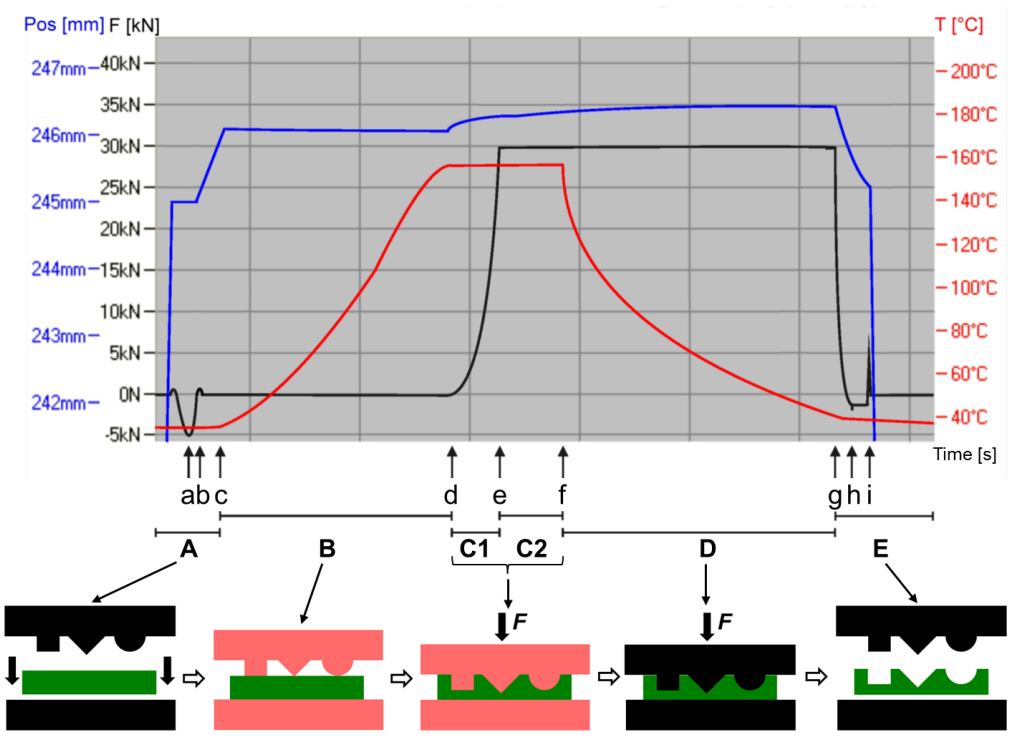

Figure 2.7: Hot embossing process and typical force-path-temperature diagram. **A)** A Polymer foil is placed between mold and counter plate. Closing and evacuating the vacuum chamber (a) and applying touch force between mold insert, polymer foil, and substrate plate (b). Subsequently, heating of the mold and the substrate plate **(B)** begins (c). When the molding temperature is reached (d), the molding step starts with a continuous movement of the crossbar **(C1)** and exponential increase of the force. The polymer is pressed into the cavities of mold. After reaching the defined force (e), the process switches to force-controlled embossing, where the force is kept at a constant level **(C2)** for a defined holding time. **D)** After the holding time, cooling starts (f) maintaining a constant force. **E)** When the demolding temperature is reached (g), demolding is initiated (h) by a constant motion of the crossbar, and the embossing chamber is vented (i) and finally opened. [73]

Th demold high aspect ratio structures with parallel sidewalls, the precise guiding of the moving crossbar is crucial to ensure that the movement happens exclusively in z-direction and that the structures are not destroyed during the demolding step. A characteristic of

hot embossing is that structures with undercuts cannot be demolded. An alternative fabrication technique that compensates this disadvantage is presented in Ch. 2.2.4. Another characteristic of hot embossing is the comparably long cycle time which varies between several minutes and some hours. Therefore this replication technique is commonly used for research and development, small batch series, and high precision replication with high aspect ratio micro- and nanostructures. [73] It is a fundamental technology, and is the basis for the hot pulling process which is explained in the following sections. For the replication of larger areas and for industrial fabrication of structured polymer foils, however, hot embossing is executed on a roll-to-roll machine (roller embossing or roll-to-roll embossing). This allows the structuring of polymer foils in a continuous process as illustrated in Fig. 2.8. A structured top roller serves as a mold and a smooth, potentially soft bottom roller serves as a supporting roller, analogously to the substrate plate in hot embossing, but with no adhesion of the polymer to the roller. Heat is supplied through the rollers, typically mainly through the structured top roller, with a roller temperature set above the softening temperature of the polymer. Force is applied on the top roller, which is pressed against the bottom roller. Typical roller speeds between 0.5 mm/s and 1.5 mm/s, and a typical roller width of at least 1 m lead to the efficient large-scale fabrication of structured polymer foils. [73] However, roller embossing faces characteristics and challenges arising from the rotation of the mold. The height and aspect ratio of the molded structures is limited and the producibility of vertical structure walls correlates with the roller radius. The fabrication of roller molds is significantly more complex compared to the fabrication of flat molds. [74] Also, the roller mold temperature is constant over the fabrication process and needs to be set accurately. Despite these challenges, roll-to-roll machines are used for various industrial replication processes. [73] The implementation of nanofur fabrication in a roll-to-roll process is presented in Ch. 4.5.

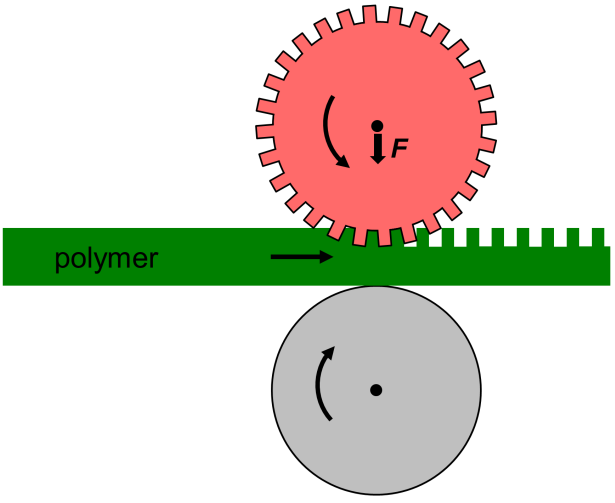

Figure 2.8: Roll-to-roll embossing allows the structuring of polymer foils in a continuous process. The structured top roller serves as a mold, and the bottom roller serves as a supporting roller, analogously to the substrate plate of a hot embossing machine. Heat is supplied through the rollers, typically mainly through the structured top roller. Force is applied on the top roller, which is pressed against the bottom roller.

2.2.4 Nanothermoforming

Hot embossing allows the fabrication of micro- and nanostructures on polymer surfaces, but can only be applied to surface structures with no undercuts. If undercuts are present, the surface structures are destroyed during demolding. In nature, however, structures with undercuts appear on surfaces of many living organisms. One famous example is the surface structure of the *Morpho rhetenor* butterfly. *Morpho* butterflies are famous for their bright and iridescent blue color that is visible from hundreds of meters. [75] This special color does not originate from pigments but from sophisticated Christmas-tree like surface structures that are illustrated in Fig. 2.9. Ridges with approximately 0.5 µm to 1 µm periodicity possess a Christmas-tree like cross sectional structure. The resulting multilayer structure formed by layers of chitin and air causes constructive interference of light in the range of blue wavelengths and destructive interference of red light. [76, 77] In contrast to colors caused by pigments, structural colors do not fade under environmental influences such as UV light. When air is one of the materials forming the multilayer structure, a change of the surrounding medium causes a color change, which is due to the change in the refractive index. If for example ethanol is poured onto a *Morpho* butterfly wing, the main peak of reflectance shifts and color changes from blue to green. [78]

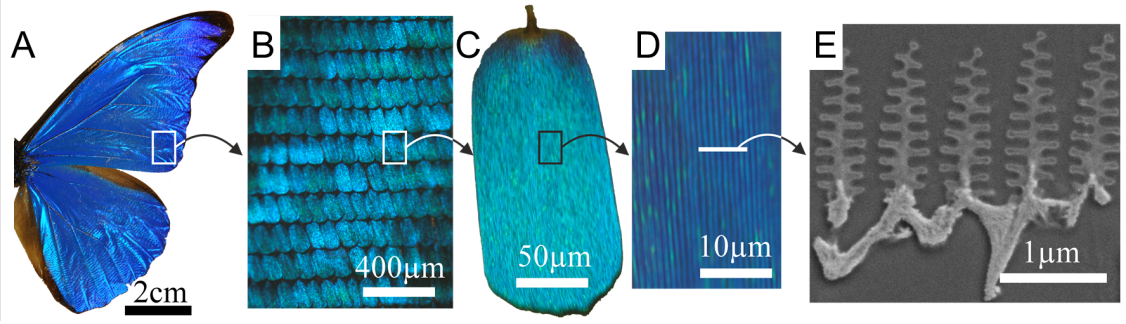

Figure 2.9: Surface structure of blue *Morpho* butterfly wing. **A)** Photo of a wing of a *Morpho rhetenor* butterfly. The bright and iridescent blue color is not caused by pigments but by a sophisticated surface structure. **B)** Microscope image of scales covering the wing and **C)** a single scale. **D)** Groove-like structure of the scale surface is visible on the microscope image. **E)** Cross section (transmission electron microscopy (TEM) image) showing the Christmas-tree like structure of the grooves. This structure serves as a multilayer and causes interference, which results in the blue color of *Morpho* butterflies. (TEM image (E) was kindly provided by Dr. Radwanul H. Siddique.)

A wide range of replication methods has been applied to *Morpho* structures. But most approaches require natural butterfly wings or scales as a master copy and the artificial structures are fabricated by reproducing the natural structures, which precludes upscaling and a large-area fabrication. Cook *et al.* [79], for example, coated a *Morpho* scale with silicon dioxide using chemical vapor deposition. The *Morpho* scale material was then removed by heat treatment. Similar techniques include the replication by coating organic templates with Al_2O_3 [80], TiO_2 [80,81], ZnO [82,83], SnO_2 [81,84], and polydimethylsiloxane [85]. Watanabe *et al.* [86], in contrast, did not use an organic template but fabricated

a *Morpho*-like surface structure by focused ion beam technology. Siddique *et al.* [87] fabricated Christmas-tree like structures by e-beam lithography. Such fabrication techniques, however, are limited to small areas due to high fabrication time and costs.

An established large-scale fabrication technique for such microstructures with undercuts is microthermoforming. A polymer foil is structured with a secondary structure by hot embossing, and the structured foil is subsequently deformed at a lower temperature to add a primary structure. For the deformation step, air is used to press the structured polymer foil into a macro- or microstructured mold. Due to the comparably low temperature, the secondary surface structure is preserved. [73] Truly three-dimensional structures can be fabricated by microthermoforming, but the minimum structure size of the primary structure is limited by the minimum foil thickness. The thickness of the polymer foil must not exceed half the size of the smallest cavity to be filled, and a polymer foil with a thickness of several hundred nanometers is too fragile for the microthermoforming process. *Morpho*-like structures therefore cannot be fabricated by microthermoforming. [88]

For the large-area fabrication of *Morpho*-like structures and for the replication of sophisticated micro- and nanostructures with undercuts on large areas, nanothermoforming was developed. Nanothermoforming allows the fabrication of complex, hierarchical micro- and nanostructured surfaces by utilizing a shape memory polymer as active mold. [88] As explained in Ch. 2.2.2, shape memory polymers recover from a temporary shape to a previously defined permanent shape when a specific external stimulus is applied. Here, Tecoplast TP-470® (TP) serves as active mold for nanothermoforming. Nanothermoforming is highly scalable and allows the fabrication of nanostructures with undercuts on areas as large as those that can be fabricated by hot embossing. The hierarchical structures fabricated by nanothermoforming combine a primary (often micrometer size) structure with a secondary (often nanometer size) structure that superimposes the primary structure. Nanothermoforming is a five step process that contains three hot embossing steps as well as one spincoating step and one heating step, as illustrated in Fig. 2.10. [88]

A shape memory polymer is used as an active mold, which adds the primary structure to the secondary structured polymer foil. In the first hot embossing step, the primary structure is embossed into the shape memory polymer at a temperature $T > T_{\mathrm{hard}}$ which defines the primary structure as the permanent shape of the SMP. After that, the permanent structure is temporarily flattened in a second hot embossing step at $T < T_{\mathrm{hard}}$. Third, a thin polymer foil is spincoated on the surface of the temporarily flattened SMP. After complete drying, a secondary structure is embossed into the spincoated foil (fourth step). Here, the applied embossing temperature needs to be below T_{trans} of the SMP to preserve its permanent shape, and high enough to allow the structuring of the spincoated polymer. In the last step, the SMP with the spinoated, structured foil on top is heated up to a temperature that triggers the recovery of the permanent structure of the SMP. This leads to the deformation of the nanostructured polymer foil and results in a hierarchically micro- and nanostructured surface. As no demolding step is required after the last step, structures with undercuts can be fabricated using this technology. [88]

As shown in Fig 2.11, a hierarchical surface structure that is comparable to the Christmas-tree like structure of the *Morpho* butterfly was fabricated by nanothermoforming. The atomic force microscope (AFM) images of a 3 µm grid (primary structure) and a 400 nm

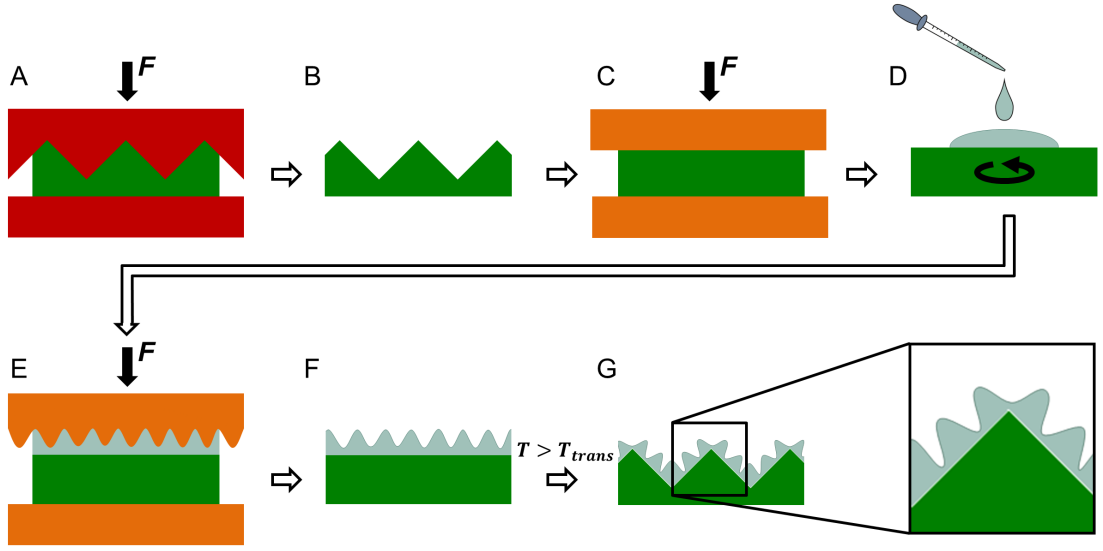

Figure 2.10: Schematic of the nanothermoforming process. **A)** Primary structure is replicated into a SMP as permanent shape (**B**) and **C)** temporarily flattened by hot embossing. **D)** An ultrathin polymer foil is spincoated on the flat SMP surface and **E)** structured by hot embossing (secondary structure **F**). **G)** Heat triggers the shape memory effect and the SMP recovers its permanent shape. Acting as an active mold, the SMP deforms the thin spincoated structured foil.

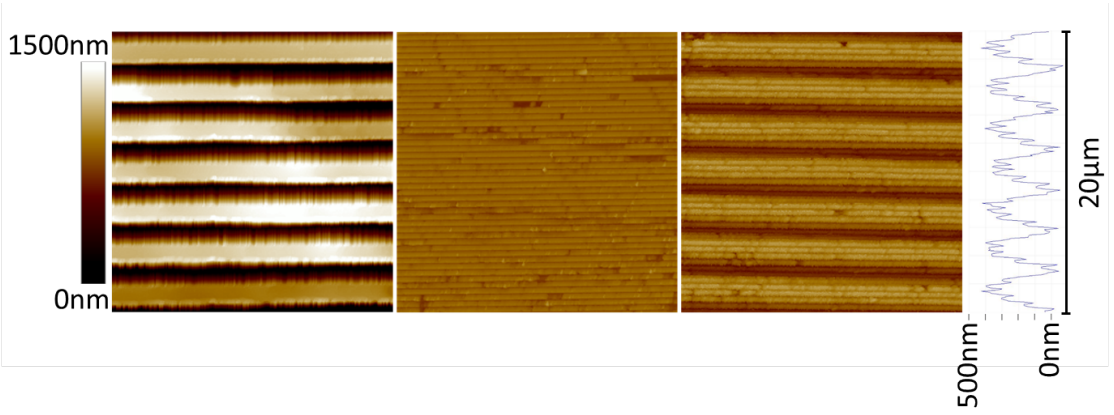

Figure 2.11: Topography (atomic force microscopy images) of the primary and the secondary structure, as well as the nanothermoformed combined structure mimicking the *Morpho* surface. The 3 µm grid (primary structure, left) is superimposed by a 400 nm grid (secondary structure, middle), which results in the hierarchical structure (right), that is similar to the Christmas-tree like structure of the butterfly *Morpho rhetenor*.

grid are shown. In the third AFM image, the combined structure is presented, which is the result of the nanothermoforming process and reveals that nanothermoforming was executed successfully.

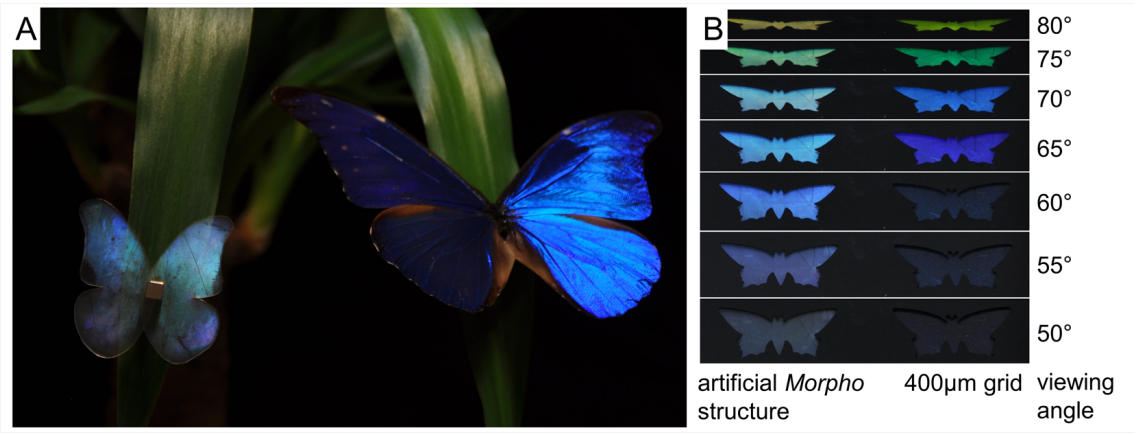

Figure 2.12: Blue *Morpho*-like polymer structure. **A)** Comparison a of blue *Morpho* butterfly (right) and the artificial nanothermoformed structure (left). The natural role model possesses a bright and iridescent blue color that does not originate from pigments but from Christmas-tree like surface structures. The biomimetic polymeric butterfly fabricated by nanothermoforming has a similar blue color and does not contain any pigments, the color is caused by the sophisticated nanothermoformed surface structure. **B)** Demonstration of the large viewing angle over which the blue color of the artificial *Morpho* structure (left) can be observed. The artificial *Morpho* structure appears blue at viewing angles between 55° and 70°, whereas the simple 400 µm grid is blue only at viewing angles of 65° to 70°.

Not only the surface structure of the polymeric surface is similar to the natural structure. Also, the properties of the fabricated surface are comparable to its natural role model. As can be seen in Fig. 2.12a, the polymeric butterfly (left) has a bright and iridescent blue color similar to the *Morpho rhetenor* butterfly (right). Also, the artificial *Morpho* like structure appears blue over a significantly larger viewing angle compared to a simple 400 nm grid, as can be seen in Fig. 2.12b. [88]

In this thesis, nanothermoforming is combined with the hot pulling of nanofur. The combination of nanothermoforming and hot pulling techniques results in a nanothermoformed nanofur surface. The aim is to fabricate a primary microstructure superimposed by nanofur as a secondary structure. An adapted nanothermoforming process as well as the resulting nanothermoformed nanofur are presented in Ch. 4.2.1 and Ch. 4.2.2.

2.2.5 Hot Pulling and Nanofur State of the Art

Hot pulling as a technology for the fabrication of micro- and nanostructured polymeric surfaces was first mentioned by Kolew [89], who fabricated fiber-like surfaces and high aspect ratio pillars from polycarbonate. Hot pulling is executed using a hot embossing machine (see Ch. 2.2.3), but in contrast to the hot embossing process, the mold insert

and the polymer foil are not cooled below T_s before demolding. The polymer sticks to the cavities of the mold insert, and the demolding process executed above the softening temperature of the polymer causes the elongation of the polymer by hot pulling. As Kolew [89] uses a mold insert with a regular hole structure, the hot pulling process leads to long pillars being pulled from the polymer surface while opening the tool. Compared to classical hot embossing, this enables the fabrication of structures with a higher aspect ratio. However, a sophisticated mold with high fabrication costs is needed, and the density of the surface coverage with pillars is strictly limited by the number of holes in the mold.

Röhrig *et al.* [16] enhanced this technology and invented nanofur, which is a polymeric surface covered by a dense layer of randomly distributed high aspect ratio hairs with diameters in the micro- and nanometer range and micro- to millimeter length. Nanofur is fabricated from polycarbonate (PC) foils by a hot pulling process, which is illustrated in Fig. 2.13a. In contrast to hot embossing and the original hot pulling process described by Kolew [89], Röhrig *et al.* [16] heat up the mold to the process temperature before the mold touches the surface of the polymer. A rough steel plate with random structure serves as a mold and is fabricated by sandblasting in a two-step sandblasting process. For the first sandblasting step, coarse aluminum silicate clinker (0.2 mm - 1.4 mm) is used, for the second step fine-grained aluminium oxide F230, F320 or F400. [14–16, 49, 90, 91]

To fabricate nanofur from PC, a PC foil with a thickness of approximately 1 mm is fixed on a rough bottom plate by hot embossing. During the hot pulling process, the sandblasted mold is heated to a temperature above the softening temperature of the polymer (for PC nanofur $T \approx 215°C$) and pressed into the polymer film. The polymer surface melts and flows into the cavities of the rough mold. The retraction of the heated mold results in an elongation of the softened polymer and in the formation of a cratered polymer surface covered with high aspect ratio micro- and nanohairs. [14–16, 49, 90, 91] Vüllers *et al.* [15] advanced the fabrication process introducing a sacrificial layer, and developed a thin nanofur, a polycarbonate nanofur foil with a thickness of approximately 200 µm. A PC foil with a thickness of 200 µm is fixed to the bottom plate of a hot embossing machine by hot embossing, using a cyclic-olefin-copolymer (COC) sacrificial layer between the PC and the bottom plate. After the subsequent hot pulling step, which is similar to the hot pulling technique introduced by Röhrig *et al.* [16], the sacrificial layer is removed from the backside of the PC nanofur. [15] The fabrication process of thin nanofur is illustrated in Fig. 2.13b. The surface of thin nanofur is similar to the surface of normal nanofur. An SEM image of the nanofur surface is shown in Fig. 2.13c.

PC nanofur is superhydrophobic and superoleophilic with a typical water contact angle (WCA) above 150° and an oil contact angle (OCA) close to 0°. Therefore, it selectively absorbs oil from oil/water mixtures. As discussed in Ch. 3, the hairy structure of nanofur not only causes superhydrophobicity, but also leads to an increased oil capacity, as the space between the hairs is available for oil absorption and retention. On top of that, multifunctional nanofur is self cleaning, [15] and can improve the efficiency of solar cells [15] or be utilized for underwater drag reduction [14].

This thesis focuses on nanofur for oil/water separation applications. Referring to this, the established hot pulling process possesses several issues. Heating and cooling of the mold during each executed hot pulling step leads to high energy consumption and long cycle

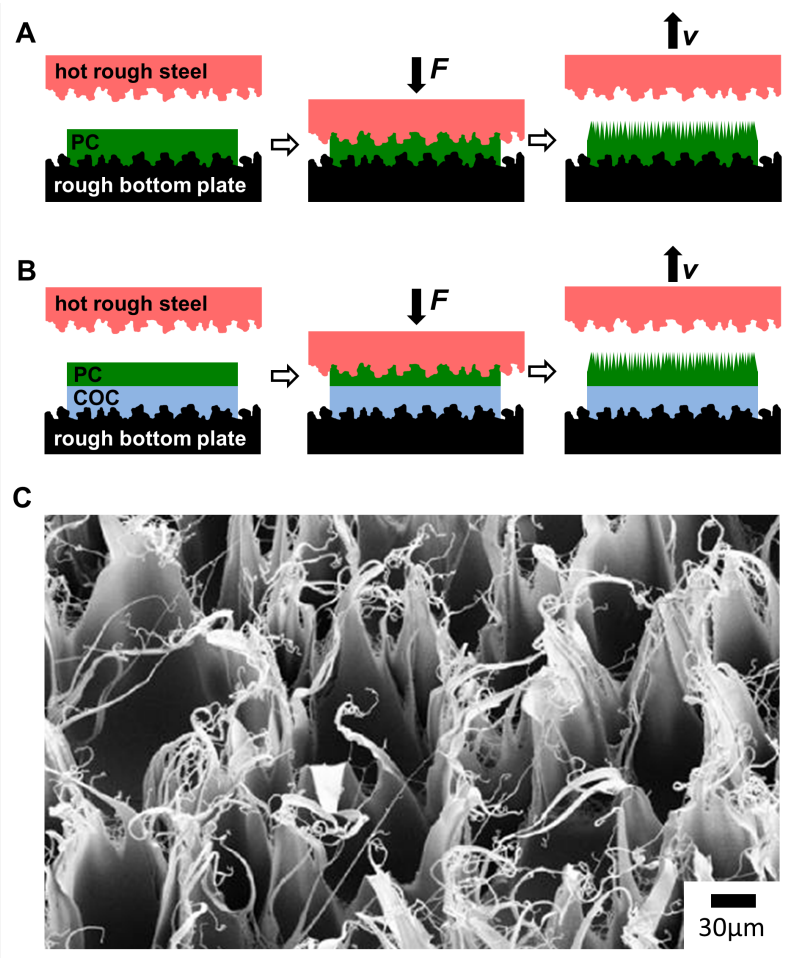

Figure 2.13: Fabrication of nanofur and thin nanofur by hot pulling. **A)** Nanofur fabrication process developed by Röhrig *et al.* [16]. A hot rough steel plate is pressed into the surface of a polymer foil and supsequently retracted, which leads to the elongation of the softened polymer and the formation of nanofur. **B)** Thin nanofur fabrication process described by Vüllers *et al.* [15]. A COC sacrificial layer between the polycarbonate foil and the rough bottom plate allows the fabrication of thin nanofur. **C)** SEM image of the resulting polycarbonate nanofur.

times. The sample size is limited by the maximum mold size. Also, nanofur as a single-use oil sorbent leads to an increased material consumption and an increased amount of waste to be disposed. These characteristics are addressed in this thesis and alternative solutions are presented in Ch. 4. This includes the introduction of a roll-to-roll nanofur fabrication process which allows the continuous fabrication of nanofur and leads to incomparably shorter fabrication times. This paves the way towards the industrial large-scale nanofur fabrication. Prior to this, the oil absorption by natural oil sorbents that serve as role model for nanofur is investigated in Ch. 3.

3. Superhydrophobic Plant Leaves as Oil Spill Cleanup Material

Biomimetics is the idea of applying biological principles to artificial materials or systems. Prior to the presentation of improvements of artificial, bioinspired nanofur material in Ch. 4 and 5, its role models (floating fern *Salvinia* and water lettuce *Pistia*) are studied in this chapter. The oil absorption capacity of four *Salvinia* species with different surface structures and of water lettuce (*Pistia stratiotes)* is quantified and compared to the oil absorption capacities of Lotus leaves *(Nelumbo nucifera)* and artificial oil sorbents. By comparing the oil absorption of leaves with trichomes (hairs) of *Salvinia* and *Pistia* to Lotus leaves with no trichomes, the influence of the presence and the morphology of trichomes on the amount of oil absorbed by their surfaces is examined. Specifically, the influence of the hair length and shape is analyzed by comparing different hair types ranging from single trichomes of *Salvinia cucullata* to complex eggbeater-shaped trichomes of *Salvinia molesta* in order to establish a basis for improving artificial bioinspired oil absorbents. Also, the influence of the oil density and viscosity on the oil absorption capacity is investigated.

3.1 Natural Oil Sorbents

The search for environmental friendly and efficient oil absorption materials is challenging, and the use of oil absorption methods inspired by nature or based on biological materials is a promising approach. [16, 35, 49–51] Biological materials commonly used for oil spill cleanup, such as saw dust, wheat straw, milkweed fibers or aquatic plants, however, absorb huge amounts of water in addition to the oil. [36, 92–99] In contrast, materials with superhydrophobic and superoleophilic special wetting properties (see Ch. 2.1) ensure selective absorption of oil from oil/water mixtures. The aquatic floating weeds *Salvinia molesta* and *Pistia stratiotes* gained interest as selective oil sorbents due to their superhydrophobic trichome-covered surface. [95, 96, 98, 99] Superhydrophobicity as a feature of many biological surfaces occurs from the combination of a hydrophobic surface chemistry (e.g. wax) and a hierarchical micro- and nanoscaled surface structure. In nature, surface coverage with hydrophobic wax protects plants from excessive water evaporation, microorganisms, mechanical damage, or degradation by water. [100] In addition, superhydrophobicity leads

to the retention of a stable air layer on the leaf surface, which ensures buoyancy and the survival of the plant when dragged underwater, and prevents the leaf surface from getting wet. [101] Lotus leaves are well known for their superhydrophobic and self cleaning properties, which originate from their two-level hierarchical surface structure (microbumps formed by convex papillae, covered by nanoscale wax crystals). *Salvinia* (see Fig. 3.1) and *Pistia* leaves are superhydrophobic, too, and have a more complex three-level hierarchical surface architecture. Their trichomes (hairs) are several hundred microns high, and contain microscale convex cells superimposed by nanoscale wax crystals. [35, 53]

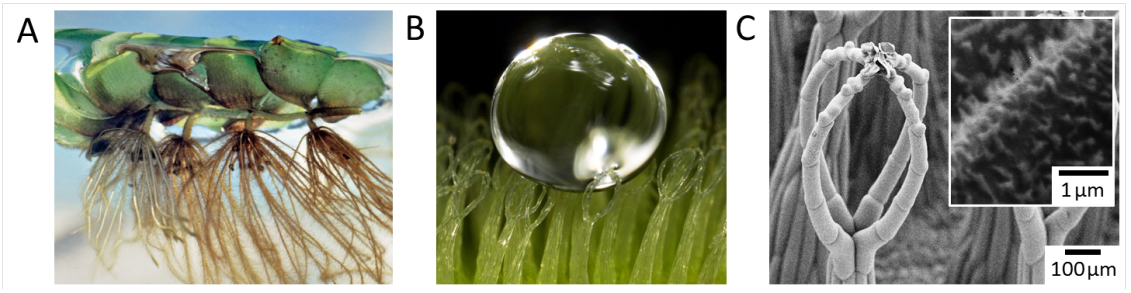

Figure 3.1: *Salvinia molesta* leaves and trichomes. **A)** Floating fern *Salvinia molesta* has two types of leaves: brown submerged root-like leaves and green floating leaves. **B)** Photograph of a water droplet on eggbeater-shaped superhydrophobic trichomes covering the upper side of floating *Salvinia molesta* leaves. The extreme water repellency of *Salvinia* leaves is caused by the hierarchical structure and the hydrophobic wax coverage. **C)** SEM images of the three-level hierarchical structure of *S. molesta*, consisting of several hundred micrometers high trichomes, microscale convex cells and nanoscale wax crystals (inset). These pictures were kindly provided by Prof. Dr. Wilhelm Barthlott, University of Bonn.

Salvinia molesta and *Pistia stratiotes* originate from South America and spread throughout the tropical and subtropical parts of the world where they proliferate and become a pest. [102–107] These pest plants found in abundance in nature are capable of removing inorganic contaminants such as heavy metals, nitrate, and phosphate from water. [108, 109] Besides water-repellency, the leaves exhibit an increased surface wetting with low surface tension liquids such as oils (superoleophilicity), and capillary action in the interstices between the trichomes. Due to this combination of properties, they are promising candidates to be used as a natural material for selective oil absorption. It has been previously shown that dried powdered leaves of *S. molesta* and *P. stratiotes* can serve as oil sorbents. [95, 98, 99] But dry powdered leaves with desiccated surface structures lose their superhydrophobicity and therefore absorb significant amounts of water in addition to oil. The effect of hierarchical trichomes (hairs) on the water-repellency of leaves is well known. [110, 111] The influence of the trichomes on the oil absorption capacity of the leaves is investigated in this chapter. An interesting example of oil absorption by hairy structures in nature are oil-collecting bees (see Fig. 3.2), which use energy-rich floral oil for larval nutrition. [112–114] With their hair-covered legs and abdomen, these highly specialized bees successfully collect large amounts of oil from oil flowers. [115–117] Therefore,

it can be assumed that the hierarchical hairy surface structures of *Salvinia* and *Pistia* not only cause the superhydrophobicity of the plant leaves, but also increase their ability to absorb oil.

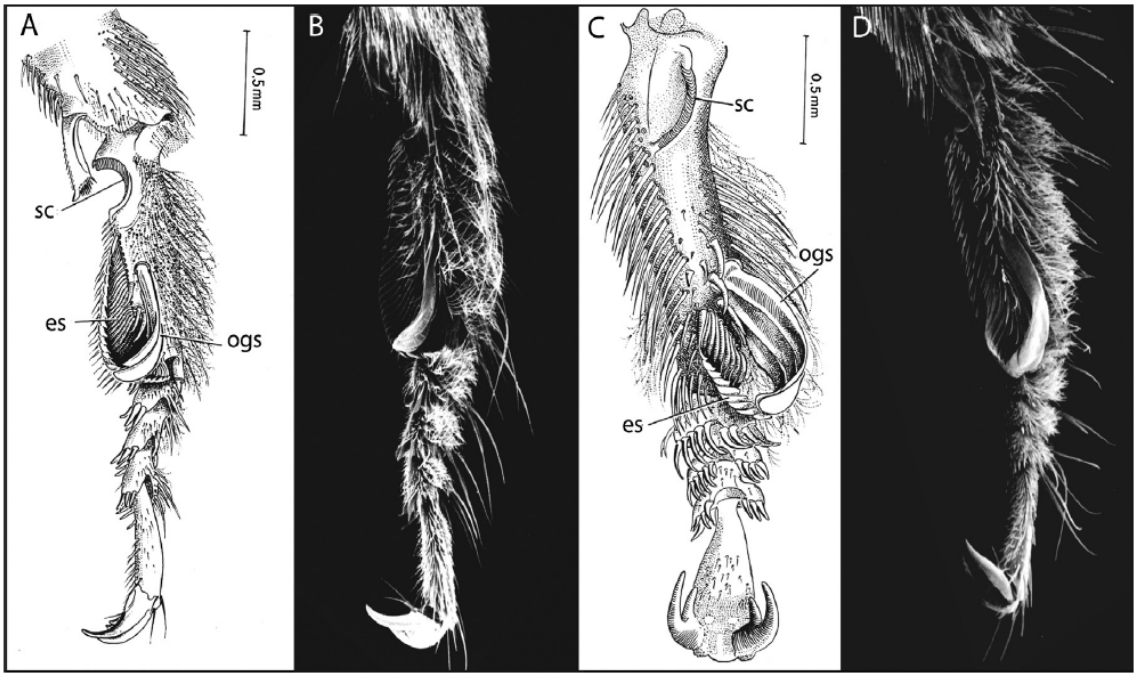

Figure 3.2: Drawings (A and C) and SEM images (B and D) of legs of oil collecting bees, showing their oil harvesting hairy structure. The bees collect oil from oily flowers using their hairy legs. Reprinted from [112]

Here, the oil absorption efficiency of the whole leaves of *Salvinia* and other plants is investigated. First, the influence of the physical properties of the oils such as density and viscosity on sorption capacity of *Salvinia molesta* leaves is studied. Next, the oil absorption capacities of fresh and dry leaves of the superhydrophobic plants *Salvinia molesta*, *Pistia stratiotes* (water lettuce), and *Nelumbo nucifera* (Lotus) (see Fig. 3.3a,e,f) are investigated to reveal the influence of the leaf surface structure on the oil absorption. Furthermore, the oil absorption efficiency of the plant leaves is compared to that of synthetic oil sorbents. Finally, the oil sorption capacity of four *Salvinia* species (*S. molesta*, *S. oblongifolia*, *S. minima*, and *S. cucullata*) is studied in order to compare the four different trichome types found in the genus (see Fig. 3.3a-d). [118] These results allow the exploration of the physical aspects of oil absorption by hairy surface architectures, and the investigation of the influence of hair morphology and size on the oil absorption capacity. In consequence, not only plants which have a great potential to be used as natural sorbents for the selective absorption of spilled oil from water are identified in this chapter. It also provides a basis for possible improvements of bioinspired artificial hairy oil absorbers. [16, 49]

3.2 Methods and Materials for Plant Leaves Characterization

The plants used for the following experiments were kindly provided by Prof. Dr. Wilhelm Barthlott and the Botanical Gardens of the University of Bonn: *Salvinia molesta* (BG BONN 14459), *Salvinia oblongifolia* (BG BONN 14457), *Salvinia minima* (BG BONN

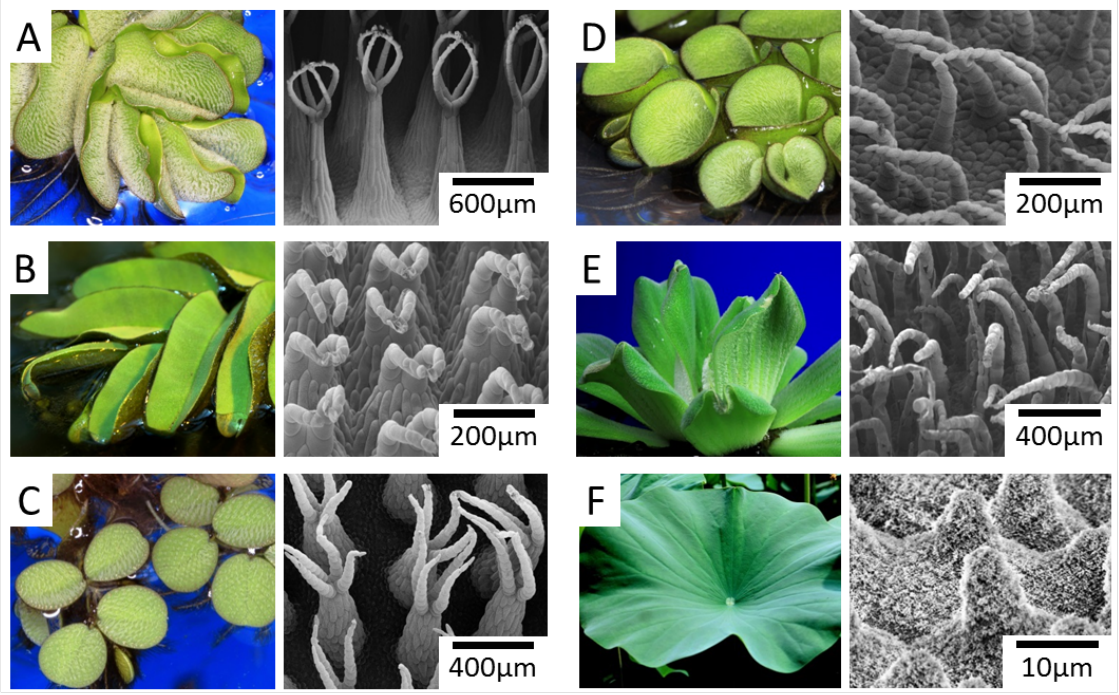

Figure 3.3: Photos and SEM images of leaves of four species of the floating fern *Salvinia* as well as water lettuce and Lotus. **A)** *Salvinia molesta* with eggbeater-shaped trichomes, **B)** *Salvinia minima* with tree-like trichomes, **C)** *Salvinia cucullata* with simple single standing trichomes, and **D)** *Salvinia oblongifolia* where tips of two trichomes are connected. **E)** Water lettuce *Pistia stratiotes* with single standing trichomes on both the dorsal and the ventral side of the leaves. **F)** Papillate *Nelumbo nucifera* (Lotus) leaves. These photos and SEM images were kindly provided by Prof. Dr. Wilhelm Barthlott, University of Bonn.

8595), *Salvinia cucullata* (BG BONN 18268), *Nelumbo nucifera* (BG BONN 14404), and *Pistia stratiotes* (BG BONN 1077). Fresh leaves from living plants were washed with tap water and used for the measurements immediately. For the oil sorption experiments of *Salvinia*, only their floating leaves (i.e. no root-like submerged leaves) were used. The keel-like aerenchyma was removed from *S. oblongifolia*. To produce vacuum-dried leaves, the leaves were washed with tap water and dried in vacuum at room temperature for 24 hours. For CPD-dried *S. molesta* leaves, leaves were dehydrated through a graded ethanol series (50% to 100% ethanol) and subsequently dried in a critical point drier (CPD 020, Balzers Union, Lichtenstein). The oil absorption capacity was quantified in two ways: per area in g/m^2 (oil/leaf surface) and per weight in mg/mg (oil/leaves).

To determine the surface area of the leaves, they were flattened by a glass slide and photographed on graph paper, and the corresponding area was measured by analyzing the photos with an image processing software. [119] As *Pistia stratiotes* leaves are covered with trichomes on the dorsal and ventral sides of the leaves, the measured surface area values for *Pistia* leaves were doubled. For oil absorption measurement, the samples were weighed and then immersed into oil for 30 seconds. The subsequent draining of the leaves by suspension (90 s) was used to remove excessive oil, and the drained leaves were weighed

again. The difference in weight before and after immersing the leaves in oil was determined as the amount of absorbed oil. Four different oils were used: artificial crude oil (Grüssing Roherdölersatz PAE15805, density $\rho = 0.805$ g/ml, kinematic viscosity $\nu \approx 4$ mm^2/s), hydraulic oil (Total Azolla ZS 10, $\rho = 0.839$ g/ml, $\nu \approx 21$ mm^2/s), and two types of crude oil (MiRO OK 679, $\rho = 0.856$ g/ml, $\nu \approx 6$ mm^2/s and MiRO EK 651, $\rho = 0.878$ g/ml, $\nu \approx 30$ mm^2/s, Mineraloelraffinerie Oberrhein, Germany). When not otherwise stated, hydraulic oil (Total Azolla ZS 10) was used for the oil absorption experiments. In addition to plant leaves, the oil sorption capacity of commercial oil sorbents (Öl-Ex Allwetter Typ III R [120] and Deurex Pure [121]) as well as of the nanofur was measured, following the same procedure as for the leaves. The experiments presented in this chapter were carried out in collaboration with the student apprentice Isabelle C. Rodrigues da Silva.

3.3 Results and Discussion

For an effective oil/water separation, a material that repels water and absorbs oil is beneficial. Floating leaves of water fern *Salvinia* fulfill this prerequisite: Due to their wax-covered hierarchical surface architecture, they are superhydrophobic and superoleophilic. [110, 118, 122, 123] In Fig. 3.4, the capability of *Salvinia molesta* to selectively absorb oil from water is demonstrated by dipping a *Salvinia molesta* floating leaf into a simulated crude oil spill. As can be seen, the crude oil is absorbed by the leaf within a few seconds. This basic experiment is the first indication of the great potential of *S. molesta* floating leaves as selective oil sorbents. Also, the experiments reveal that the maximum absorption is reached after less than 30 s and that the oil is retained by the leaves until the plant material starts to degrade after some days (see Fig. 3.5).

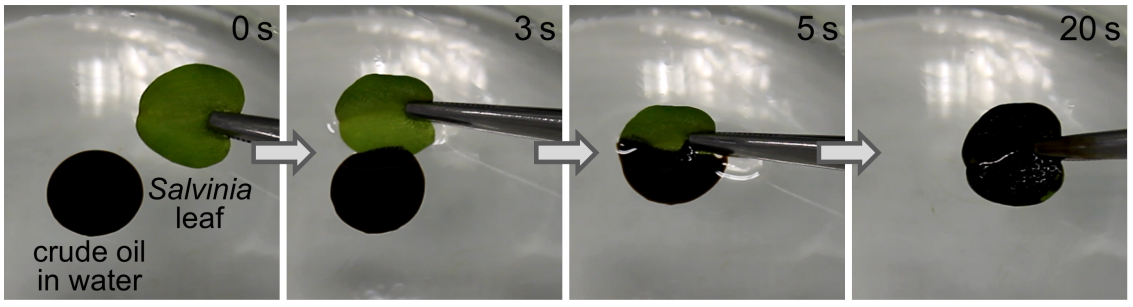

Figure 3.4: Demonstration of the fast and selective oil absorption by a *Salvinia molesta* floating leaf within 20 seconds. After dipping the leaf into a simulated oil spill on the water surface, the crude oil is absorbed quickly whereas the water is repelled by the superhydrophobic trichome structures on the upper side of the leaf.

The quantification of the oil absorption capacity of *Salvinia* leaves allows a comparison to other surfaces. Also, it helps explaining the mechanisms of oil absorption by different trichome types and to identify the most efficient absorbing architecture. First, sorption capacities of *Salvinia molesta* leaves (g/m^2) with four different oils were measured in order to study the influence of the physical oil properties on the absorption capacity. Artificial crude oil (PAE15805, number of sample leaves $n = 10$), hydraulic oil (Total

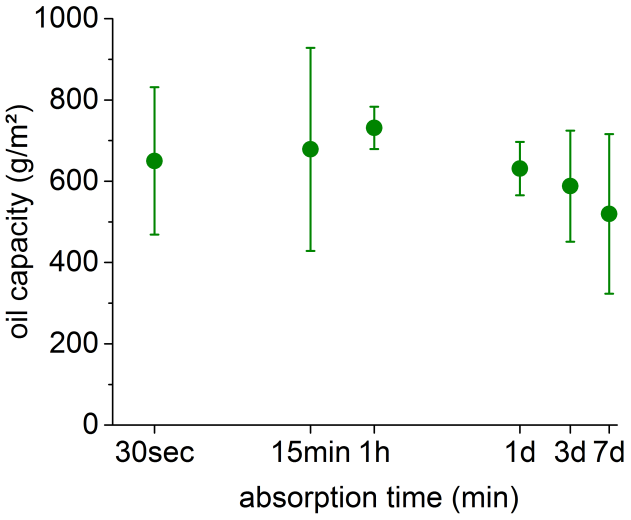

Figure 3.5: Oil absorption time of *Salvinia molesta* leaves. The leaves absorb huge amounts of oil within seconds. After 30 s there is no more significant increase in oil absorption. As the leaves degrade after few days, the measured weight decreases. A logarithmic scale is used for the time axis.

Azolla ZS 10, $n = 10$), and two types of crude oil (MiRO OK 679 and MiRO EK 651, $n = 5$ leaves each) were used for these measurements. The results depicted in Fig. 3.6a indicate that a higher oil density leads to a higher oil absorption capacity. For a better comparison of the measured values, the influence of the oil density on the measurement was eliminated by converting the values from g/m^2 to ml/m^2: *Salvinia molesta* absorbs on average 630.0 ml/m^2 of artificial crude oil, 774.8 ml/m^2 of hydraulic oil, 989.3 ml/m^2 of crude oil OK 679, and 1099.6 ml/m^2 of crude oil EK 651. As artificial crude oil has the lowest viscosity of all oils used in this experiments, and EK 651 has the highest, it can also be deduced that a higher oil viscosity can lead to a higher oil uptake (see Fig. 3.6b). Though hydraulic oil is more viscous than crude oil OK 679, the crude oil consists of multiple chemical components which might influence the absorption and therefore result in higher oil absorption capacity values. In general, these results show that *Salvinia* leaves absorb and retain different types of oil, and that its absorption capacity depends on the physical properties of the oil.

The effect of the presence of the trichomes (hairs) on the leaf surface on the oil absorption capacity was studied by comparing the absorption of trichome-covered leaves (with intact trichomes and trichomes desiccated by drying) with non-hairy plant leaves. Photos and SEM images of sorbents and their structures are shown in Fig. 3.3 (plant leaves) and Fig. 3.7 (artificial materials), and include complex hairy *Salvinia molesta* leaves, simple hairy leaves of *Pistia stratiotes*, papillate leaves of *Nelumbo nucifera*, and artificial sorbents. The measured oil absorption capacities of fresh and vacuum-dried hairy *Salvinia molesta* and *Pistia stratiotes* leaves are compared to the capacity of non-hairy *Nelumbo nucifera* leaves covered with hierarchical wax structures in Fig. 3.8 (number of samples: $n = 14$ (vacuum-dried *Salvinia*), $n = 10$ (fresh *Salvinia*, CPD-dried *Salvinia*, and fresh and dry *Nelumbo nucifera*), $n = 3$ (*Pistia stratiotes* and all artificial sorbents)). The results shown in

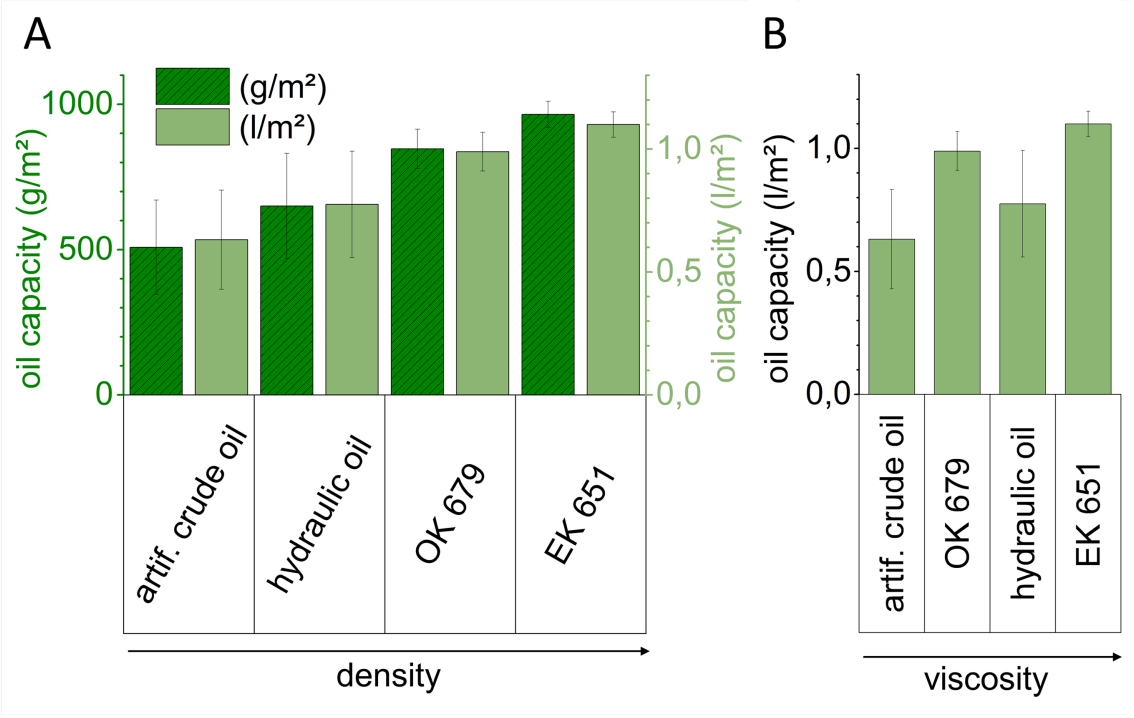

Figure 3.6: Correlation of the oil absorption capacity of *Salvinia molesta* and the oil density respectively viscosity. **A)** Oil absorption capacity per leaf surface of *Salvinia molesta* (fresh floating leaves), measured for four different oils: artificial crude oil, hydraulic oil, and two types of crude oil (OK 679 and EK 651). The oil density increase is marked with an arrow, with artificial crude oil having the lowest density. In order to eliminate the possible influence of the oil density on the measurement, oil absorption (g/m^2) was also converted to l/m^2. **B)** Oil absorption capacity per leaf surface (l/m^2) of *Salvinia molesta* (fresh floating leaves), measured for four different oils: artificial crude oil, hydraulic oil, and two types of crude oil (OK 679 and EK 651). The oil viscosity increase is marked with an arrow, with artificial crude oil having the lowest viscosity.

Fig. 3.8a indicate that both fresh and vacuum-dried *Salvinia molesta* and *Pistia stratiotes* leaves absorb more oil per area (g/m^2) than *Nelumbo nucifera* leaves. For dry plant leaves, there is absorption within the inner tissue of the plants (bulk material) in addition to the absorption by the surface structure. This explains the higher absorption of the CPD dried *Salvinia molesta* leaves compared to the fresh leaves. When *S. molesta* and *P. stratiotes* leaves are dried in vacuum, the trichomes become partially deformed and wrinkled, whereas they are perfectly conserved when CPD dried. This results in a lower absorption capacity (g/m^2) of the vacuum-dried leaves, and emphasizes the importance of the trichomes on the leaf surface for the high oil uptake.

The oil absorption capacities of leaves of the two plants with trichomes (*Pistia stratiotes* and *Salvinia molesta)* are similar in uptake per m^2, but *P. stratiotes* has a lower capacity per weight (mg/mg) as its leaves are thicker and heavier than *S. molesta* leaves (Fig. 3.8b). In general, dry leaves of all plants tested absorb more oil than fresh ones, which is a result of the decreased weight after water loss (e.g. the weight loss of *Salvinia molesta* through

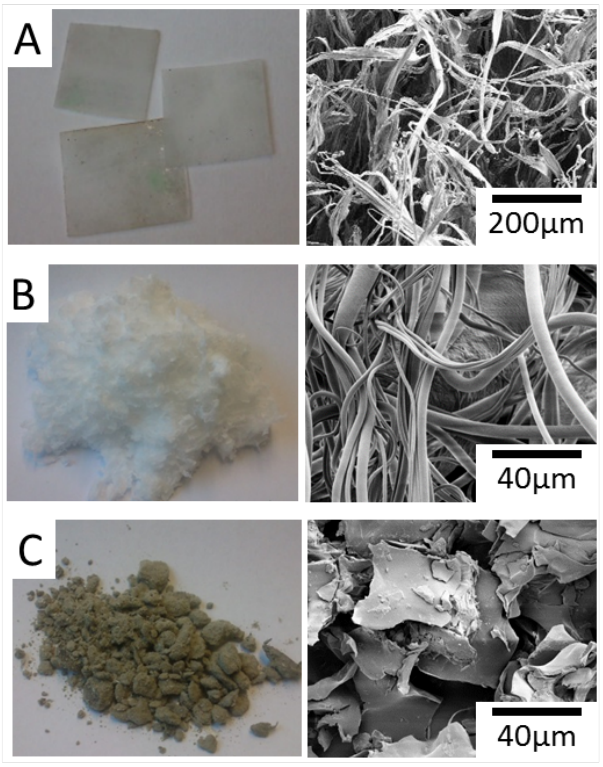

Figure 3.7: Photos and SEM images of the artificial oil absorption materials nanofur **(A)**, Deurex Pure **(B)**, and Öl-Ex **(C)**. Nanofur and Deurex Pure are hairy materials, Öl-Ex **(C)** is a granular material.

drying is ∼87 %). Together with the high absorption by the surface structure and the bulk material, this leads to CPD-dried *Salvinia molesta* leaves having a one order of magnitude higher sorption capacity compared to other samples.

The oil absorption capacities of plant leaves were compared to two commercial oil sorbents (Deurex Pure and Öl-Ex) and to polymeric hair-covered nanofur. Comparable to leaves with trichomes, the artificial oil sorbents with hair-like morphology (Deurex Pure and nanofur) absorb a larger amount of oil than the non-hairy sorbent (Öl-Ex) (see Fig. 3.8). In general, the comparison shown in Fig. 3.8 indicates that hairy superhydrophobic structures (*Salvinia molesta* and *Pistia stratiotes*), where capillary interstices between the trichomes are available for oil absorption, absorb significantly more oil than non-hairy papillate superhydrophobic structures (*Nelumbo nucifera*). Additionally, the deformation of the trichomes reduces the oil absorption capacity of the leaves. This result proves that the trichomes (hairs) play a key role not only in the special wetting properties of the leaves, but also in increasing their oil absorption capability.

The dry leaves of the aquatic plants *Salvinia molesta* and *Pistia stratiotes* have a higher oil absorption capacity than the commercial synthetic oil sorbents tested here. As a consequence, the leaves have a great potential to be used as natural, biodegradable oil sorbents. Air-dried leaves have similar properties as the vacuum-dried samples, so leaves can be dried cost-efficiently and in large amounts. For selective oil absorption from oil/water mixtures, however, the dry leaves of *Salvinia* are inefficient as only the dorsal side of the leaves,

which is covered with trichomes, has superhydrophobic properties when dry. The ventral side of the dry *Salvinia* leaves, in contrast, absorbs water, which significantly increases the weight of waste to be disposed, and drastically decreases the economic efficiency. Dried leaves of *Pistia stratiotes*, in contrast, remain water repelling, as both sides of the leaves are covered with superhydrophobic trichomes. This leads to an increased selectivity and therefore a higher efficiency of the oil/water separation.

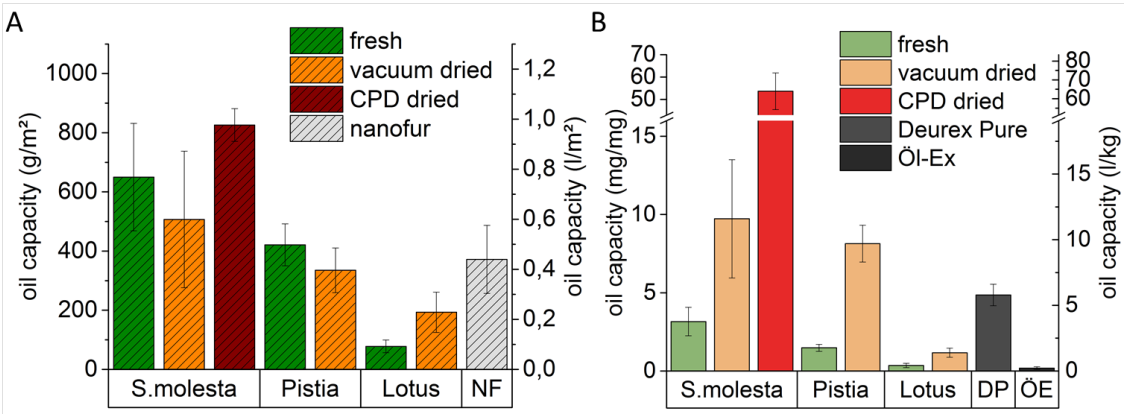

Figure 3.8: Comparison of different oil sorbents and their oil absorption capacities. **A)** Hydraulic oil absorption capacity per leaf surface of fresh and dried *Salvinia molesta*, *Pistia stratiotes* and *Nelumbo nucifera* leaves. Fresh and vacuum dried leaves of all plants were used, and additionally *Salvinia molesta* leaves were dried in a critical point dryer (CPD). The typical oil capacity of nanofur (NF) is also illustrated in this graph. **B)** Oil absorption capacity per weight of fresh and dried *Salvinia molesta*, *Nelumbo nucifera* and *Pistia stratiotes* leaves, and of two commercial oil sorbents (Deurex Pure (DP) and Öl-Ex (ÖE)).

Four different *Salvinia* species possessing trichomes with different shapes were tested to investigate the influence of the particular trichome morphology on the oil absorption capacity of the leaves: *S. molesta*, *S. minima*, *S. cucullata*, and *S. oblongifolia*. [118,122] All *Salvinia* species have a complex three-level hierarchical leaf surface architecture, providing trichomes that consist of convex cells with superimposed wax crystals. [53] The structural parameters of the different types of *Salvinia* trichomes are summarized in Tab. 3.1, SEM images of the trichomes are shown in Fig. 3.3. Solitary single-standing Cucullata type trichomes are slightly bent and are on average 558 µm high. On *Salvinia minima* leaves, trichomes of Natans type form groups of four and are ∼919 µm high. Oblongifolia type trichomes all bend in the same direction and the terminal ends of two trichomes are connected. With an average height of 310 µm, they are shorter than the other types. Molesta type trichomes are the highest trichomes with a height of ∼2629 µm, on which groups of four trichomes with fused ends, sitting on one emergence, form an eggbeater-like shape. [101] The comparison of the oil absorption capacities by fresh leaves of *S. molesta*, *S. minima*, *S. cucullata*, and *S. oblongifolia* is presented in Fig. 3.9a. *Salvinia molesta* has the highest sorption capacity per leaf surface and absorbs 650 g/m^2 of oil, *S. oblongifolia* absorbs 441.1 g/m^2 oil, *S. cucullata* and *S. minima* absorb 313.5 g/m^2 and 319.3 g/m^2 (Tab. 3.1). The number of samples was $n = 7$ for *S. minima* and $n = 10$ for all other

species.

	S. molesta	*S. minima*	*S. cucullata*	*S. oblongifolia*
Typical trichome height, µm from Ref. [101]	2629 ± 285	919 ± 107	558 ± 143	310 ± 41
Trichome type from Ref. [118]	Molesta type: groups of four sitting on one emergence, ends fused, egg-beater shape	Natans type: groups of four sitting on one emergence, ends separated	Cucullata type: solitary trichomes	Oblongifolia type: groups of two, ends connected
Leaf size, mm^2	256 ± 73	23 ± 3	156 ± 31	543 ± 178
Leaf mass per area, g/m^2	207 ± 18	76 ± 30	118 ± 17	387 ± 95
Oil capacity, g/m^2	650.0 ± 181.4	319.3 ± 72.6	313.5 ± 76.9	441.1 ± 145.5
Oil capacity, mg/mg	3.2 ± 0.9	4.5 ± 1.4	2.6 ± 0.4	1.2 ± 0.3

Table 3.1: Comparison of four different *Salvinia* species: trichome height and type, leaf size and normalized mass, oil absorption capacity. For the absorption capacity measurements, fresh floating *Salvinia* leaves were used, the keel-like aerenchyma was removed from *S. oblongifolia*.

Mayser *et al.* [101] measured the volume of air retained by the hairy structures of the different *Salvinia* types when submerged under water, and showed that *S. molesta*, which has the longest trichomes of all tested *Salvinia* species, retains the largest air volume per surface area. *S. oblongifolia*, on the other hand, has the shortest trichones and retains the smallest air volume. For the oil absorption capacity (Fig. 3.9), the trichome height also plays a key role. *S. molesta* both has the longest trichomes and the highest oil sorption capacity. But contrary to the expectations derived from the studies of Mayser *et al.*, the trichome height and the volume available between the trichomes are not the only crucial criteria determining the sorption capacity. *Salvinia oblongifolia* has the second highest oil sorption capacity per area, while it retains the lowest air volume [101] and its hairs are the shortest of all four species (see Tab. 3.1). [118] As the oil absorption by *Salvinia* species does not exclusively correlate with the trichome height or the cavity volume between the trichomes, the influence of the trichome architecture on the absorption was studied. The common characteristic of the two species with the highest oil sorption (*S. molesta* and *S.*

oblongifolia) is that the ends of their trichomes are connected, as can be seen from the SEM images in Fig. 3.3. In contrast, the trichomes of the other two species with a lower capacity are separated.

The conclusion that the fusion of the tips of the trichomes increases the absorption and retention of oil is additionally supported by the microscopy images of the leaf cross sections after oil absorption shown in Fig. 3.9b. The trichomes of *S. minima* and *S. cucullata* bend, cluster together or stick out from the oil after absorbing it, which decreases the volume available for oil sorption in two ways as indicated in Fig. 3.9c. First, when the surface area of a single standing trichome touching the oil/air interface is too small and the surface tension of the oil is too low to provide an oil/air interface which can be supported by the trichome tip, the tip breaks through the interface and the volume available for retaining oil is reduced by the part of the trichome sticking out. This phenomenon was commonly observed in *S. minima* trichomes, which have the highest stiffness per trichome group of all trichome types [124], and was occasionally observed in more elastic *S. cucullata* trichomes. On the other hand, single bent trichomes provide a larger surface area touching the oil/air interface, and do not break through the surface. But in this case the volume available for retaining oil is reduced due to the reduced height of the bent trichomes. In particular, trichomes of *S. cucullata* have the lowest stiffness of all trichome types [124], which leads to a significantly decreased oil sorption capacity due to trichome bending. In contrast, the complex shape and lower elasticity of the connected trichomes of *S. molesta* and *S. oblongifolia* lead to upright-standing trichomes with only the terminal trichome ends being bent. The stiffness of the trichomes prevents a decrease in the trichome height by extreme bending, which would result in a decrease in the volume available for oil absorption. Also, a large surface area of the trichome tip touches the oil/air interface, ensuring a proper interface support. As a result, the spaces between the trichomes of *S. molesta* and *S. oblongifolia* can serve as oil retaining spaces over the entire trichome height, whereas the volume available for retaining oil between the trichomes of *S. minima* and *S. cucullata* is decreased.

Fabricating hierarchical artificial hairy structures for absorbing oil, which are inspired by these results, would allow achieving a higher oil sorption capacity. The oleophilic and hydrophobic surface chemistry and the hierarchical nature of the micro- and nanostructured hairs with capillary interstices ensure an effective and selective oil absorption. Intuitively and as a result from the studies presented in this chapter, long hairs provide higher sorption capacities than short hairs. However the hair length is not the only crucial factor; additionally, the ends of rigid hairs should be connected and/or bent down to provide a sufficient support of the oil/air interface. This ensures that the spaces between the hairs are available for oil absorption, resulting in a high oil absorption capacity. In the case of non-connected straight hairs, inelastic hairs provide no support for the oil/air interface, whereas an extreme deformation occurs when the elasticity of hairs is high. In both cases the oil absorption capacity is decreased. In contrast, a moderate elasticity of the hairs or rigid hairs with elastic tips ensure an appropriate bending of hairs and therefore high oil absorption capacities.

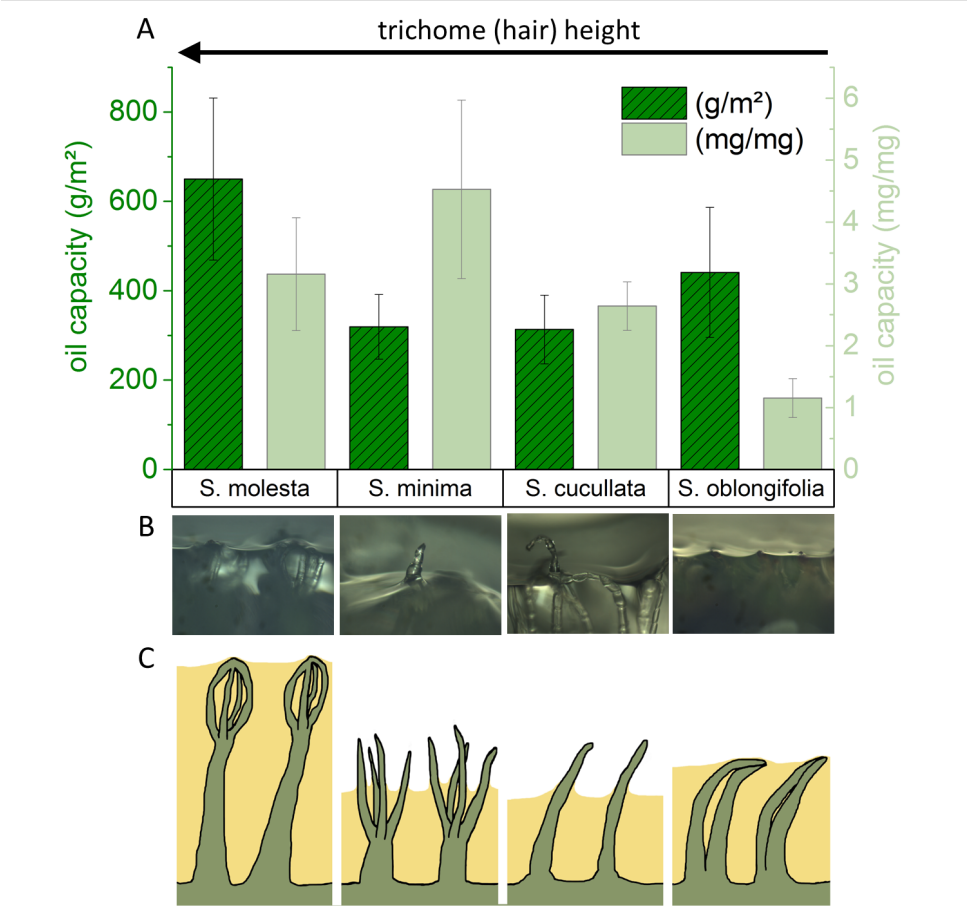

Figure 3.9: Influence of the trichome type on the oil absorption capacity of *Salvinia* floating leaves. **A)** Hydraulic oil absorption capacity of leaves of four different *Salvinia* species: *Salvinia molesta*, *Salvinia minima*, *Salvinia cucullata*, and *Salvinia oblongifolia*. The trichome height increase is indicated with an arrow, with *S. molesta* having the highest trichomes. **B)** Microscopy images show the cross section of *Salvinia* leaves with visible trichomes after oil absorption. *S. molesta* and *S. oblongifolia* possess trichomes with connected tips; the space between the trichomes is full to the tips with oil. In contrast, trichomes of *S. minima* and *S. cucullata* are not connected and some stick out of the oil/air interface or bend and cluster together. The space between the trichomes is not completely filled with oil. The sketch below the microscopy images **(C)** illustrates these findings.

3.4 Conclusions on Superhydrophobic Plant Leaves for Oil Spill Cleanup

Leaves of the invasive and fast growing floating plants *Salvinia molesta* and *Pistia stratiotes* achieve superhydrophobic and superoleophilic properties through their wax-covered surface and their complex hierarchical surface architecture. Therefore, they can be used to selectively absorb oil from the water surface. The results presented in this chapter demonstrate that *Salvinia molesta* absorbs oil within seconds with a sorption capacity dependent on the physical properties of the oil. When used for oil absorption from oil/water mixtures, the fresh leaves of all tested aquatic plants are water repellent and can selectively absorb oil. Dry *Salvinia* leaves, however, are superhydrophobic only on the trichome-covered top side of the leaves, and the bottom side absorbs water in addition to oil. In contrast, dry leaves of *Pistia stratiotes* are water-repellent, as both sides of the leaves are covered with trichomes. The comparison of the oil sorption capacity of the leaves of *Salvinia molesta*, *Pistia stratiotes*, and *Nelumbo nucifera* (Lotus) reveals that the complex hierarchically structured hairy surfaces of *Salvinia molesta* and *Pistia stratiotes* leaves absorb more oil than the simpler structured papillate superhydrophobic surfaces of *Nelumbo nucifera* leaves. In addition, the influence of the trichome morphology on the oil absorption was investigated by comparing the oil uptake of different *Salvinia* species (*S. molesta*, *S. minima*, *S. cucullata*, and *S. oblongifolia*). Contrary to the intuitive assumption, the experiments show that not only the trichome height plays a role in oil absorption capacity, but also the architecture of the trichomes. Due to the larger volume available for oil absorption, *Salvinia* species with fused trichomes (*S. molesta* and *S. oblongifolia*) achieve higher oil sorption capacities than those with separated trichomes (*S. cucullata* and *S. minima*). It follows that artificial oil sorbents can benefit from having a hair-like complex hierarchical surface, as this combines superhydrophobic properties of hierarchical surface architectures and the high oil sorption capacity of hairy structures. For achieving a high absorption capacity, hairs should not only be long, but also feature bent and/or fused tips. This ensures the sufficient support of the oil/water interface. Therefore the spaces between the hairs can fill to the tip with oil. These results confirm that living organisms have developed in more than 420 million years of evolution the most complex and sophisticated mechanisms for the interaction with liquids and that it is worth considering these surfaces as role models for biomimetic technical applications. [4]

A shortened version of this chapter was published as the article "Microstructures of superhydrophobic plant leaves - inspiration for efficient oil spill cleanup materials". Claudia Zeiger, Isabelle C. Rodrigues da Silva, Matthias Mail, Maryna N. Kavalenka, Wilhelm Barthlott, Hendrik Hölscher: Bioinspir. Biomim., 2016, ***11****, 056003.*

4. Nanofur for Selective Oil Absorption

Inspired by natural superhydrophobic surfaces such as *Salvinia* and *Pistia* leaves (see Ch. 3), polymeric nanofur was developed (see Ch. 2.2.5). [16] It has superhydrophobic and superoleophilic special wetting properties which ensures the selective absorption of oil from oil/water mixtures. However, the state of the art nanofur and its fabrication process have several issues. First, the discontinuous fabrication of nanofur in a hot embossing machine is restricted by long cycle times, and the sample size is limited by the maximum mold size. Also, nanofur as a single use oil sorbent generates significant amounts of waste and leads to an enormous material input and to increased waste disposal costs. Besides that, several applications require polymeric materials with specific properties, and the nanofur material range is limited. Solutions to these issues are presented in this chapter. This includes an introduction of a roll-to-roll nanofur fabrication process which leads to the continuous fabrication of nanofur and therefore to incomparably shorter fabrication times. This paves the way towards the industrial large-scale nanofur fabrication. Also, the nanofur fabrication process is transferred to other polymers such as polyethylene and polypropylene. Furthermore, an extra level of hierarchy is added to the hierarchically micro- and nanostructured nanofur by nanothermoforming. To enhance the environmental sustainability, a reusable nanofur material is presented. Reusability includes removing the absorbed oil by washing the oil-soaked nanofur with solvents, as well as nanofur from a shape memory polymer. The latter allows the mechanical squeezing out of the absorbed oil. Subsequently, the nanofur structure is recovered and can be reused. Also, an alternative nanofur fabrication technique is introduced which is less sensitive to the variation of process parameters. This cold pulling process is first executed on a hot embossing machine and then transferred to a roll-to-roll process. This allows the upscaling of nanofur fabrication to the large-scale fabrication of nanofur in a continuous process and reveals the possibility of an industrial fabrication of nanofur.

4.1 Increased Material Diversity

Depending on the actual application, the use of nanofur from other polymers than PC can be advantageous due to the specific polymer properties. PC has a high softening

temperature, which on the one hand leads to a high thermal stability of the nanofur foils. On the other hand, a high process temperature is required for the hot pulling process, which leads to an increased energy consumption for heating up the mold and to increased cycle times. Also, the choice of the hot embossing machines is limited, as not all machines can reach temperatures above 200°C. Due to the material properties, PC nanofur foils are comparably hard and stiff, and chemically unresistant to various solvents, including some oils such as chloroform. This limits the usability of PC nanofur in oil/water separation applications. The fabrication of nanofur from a bigger variety of polymers can therefore increase the application diversity and decrease the fabrication costs. In this chapter, nanofur surfaces fabricated from low density polyehtylene (LDPE), high density polyethylene (HDPE), polypropylene (PP), orientated polypropylene (OPP), polyamide 6 (PA6), and polymethylmethacrylate (PMMA) are presented.

Experimental

For the fabrication of nanofur from LDPE, HDPE, PP, OPP, PA6, und PMMA, the fabrication process is similar to the hot pulling process introduced by Röhrig *et al.* [16] and described in Ch. 2.2.5, but is executed with adapted process parameters. The pulling temperature depends on the choice of the material and is about 180°C (HDPE), 140°C (PMMA), 135°C (LDPE), 200°C (PP), 262°C (OPP), and 210°C (PA6). The nanofur from PA6 was pulled with a retraction speed of 5000 mm/min, all other materials at 1000 mm/min. These experiments were carried out in collaboration with Alexander Storz, who analyzed aspects of the nanofur fabrication in his master's thesis. [125]

Results and Discussion

The nanofur surfaces from all mentioned polymers consist of a cratered structure, more or less densely covered with micro- and nanohairs, as can be seen in the SEM images in Fig. 4.1. The PMMA nanofur consists of big craters with high crater walls and a few long hairs with accurate tips. PA6, LDPE, PP, and OPP nanofur craters are less high with fewer, shorter, and less accurate hairs. HDPE nanofur in contrast consists of long, thin hairs elongated from the surface. LDPE, HDPE, PP, and OPP nanofur are superhydrophobic in air, as indicated in Fig. 4.2. The PMMA nanofur water contact angle (WCA) is 148°, which is due to the big hair diameter and the surface being structured in micrometer range rather than in nanometer range. The WCA of PA6 nanofur is 140°, but as the intrinsic WCA of the flat PA6 is close to 65°, the increase in WCA caused by the nanofur structure is remarkable. This result also confirms the theory that any structure added to polymers with an intrinsic WCA $> 65°$ increases the WCA, as discussed in Ch. 2.1.

In Fig. 4.3, the oil absorption capacities of nanofur from LDPE (106 g/m^2), HDPE (151 g/m^2), PP (300 g/m^2), and OPP (291 g/m^2) are illustrated and compared to the unstructured surfaces of the same materials. These results reveal that the nanofur surfaces from all of these materials can selectively absorb significant amounts of oil. All mentioned polymers have a lower softening temperature than PC, which on the one hand leads to a lower thermal stability, and on the other hand to a lower fabrication temperature and therefore to shorter fabrication cycle times. LDPE, HDPE, PP, and OPP are more resistant

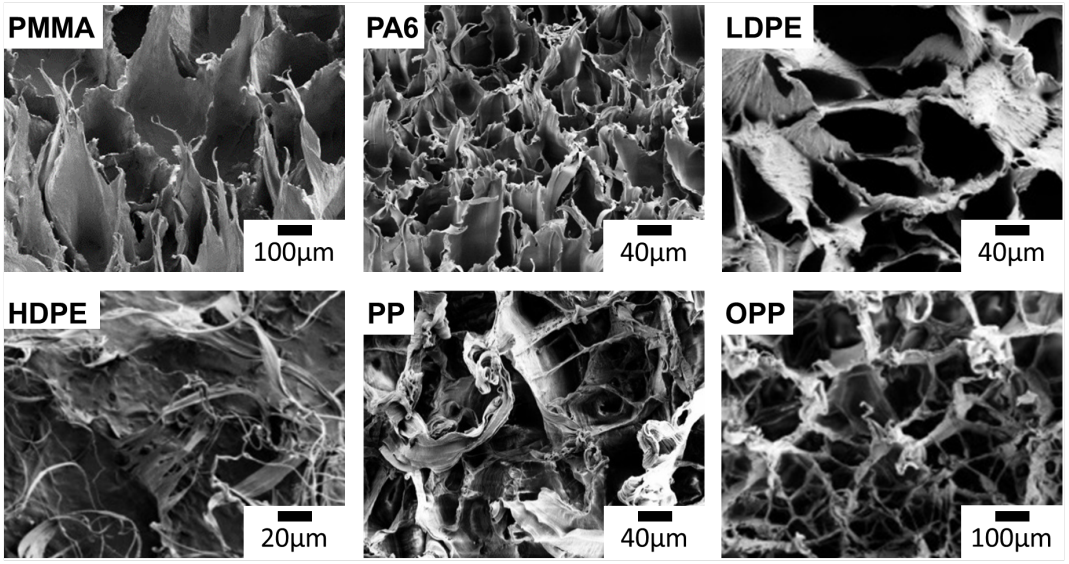

Figure 4.1: SEM images of nanofur made from polymethylmethacrylate (PMMA), Polyamide 6 (PA6), low-density polyethylene (LDPE), high-density polyethylene (HDPE), polypropylene (PP) and oriented polypropylene (OPP).

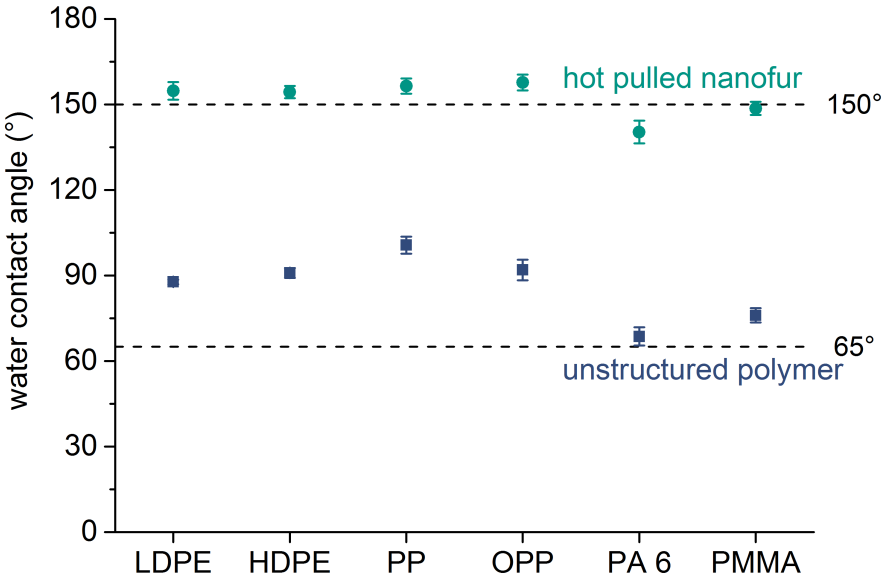

Figure 4.2: Water contact angles of nanofur from various polymers. Hot pulled nanofur made from polyamide 6 (PA6) and PMMA is hydrophobic in air, nanofur from low-density polyethylene (LDPE), high-density polyethylene (HDPE), polypropylene (PP), and oriented polypropylene (OPP) is superhydrophobic in air with WCAs higher than 150°. Contact angles of all structured materials are significantly higher compared to the respective flat surfaces (between 65° and 100°).

to solvents, and they are softer and more flexible compared to PC. PMMA dissolves well in anisole (methoxymenzene), so PMMA can be spincoated on the surfaces of other materials. In summary, the extension of the material variety allows the selection of the nanofur material according to the application-specific needs. The further extension to other polymers is possible with an adequate adaption of the process parameters.

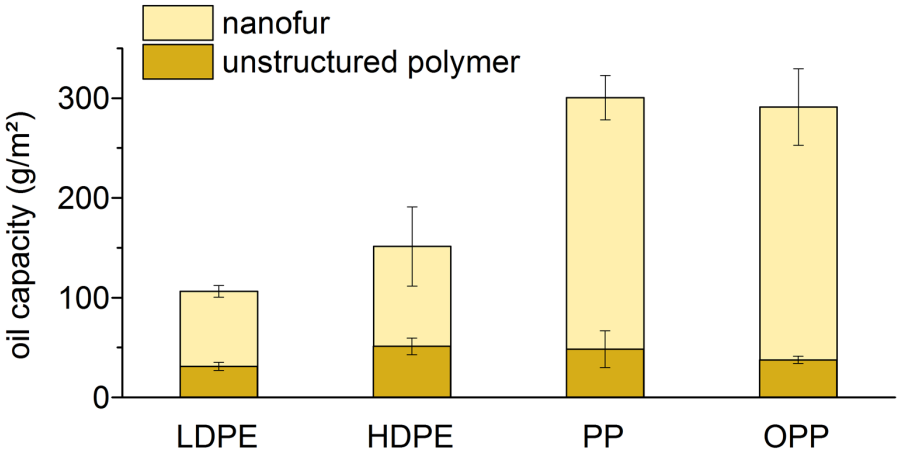

Figure 4.3: Oil absorption capacity of nanofur from low-density polyethylene (LDPE), high-density polyethylene (HDPE), polypropylene (PP), and oriented polypropylene (OPP) is compared to the oil absorption capacity of unstructured surfaces of the same materials. LDPE nanofur absorbs 106 g/m^2 (unstructured LDPE: 31 g/m^2), HDPE nanofur absorbs 151 g/m^2 (unstructured: 51 g/m^2), PP nanofur absorbs 300 g/m^2 (unstructured: 48 g/m^2), and nanofur from OPP absorbs 291 g/m^2 hydraulic oil (unstructured: 38 g/m^2).

4.2 Advanced Nanothermoforming Techniques

For some applications, it can be beneficial to add an additional level of hierarchy to two-level hierarchically structured surfaces. In nature, rice leaves are known to possess a three-level (macro/micro/nano) hierarchical structure. It consists of macrogroves in the sub-millimeter range, superimposed by a superhydrophobic micro/nanostructure. [126,127] According to Bixler and Bhushan [127] the so-called rice leaf effect causes under water drag reduction. It is a combination of the shark skin effect and of drag reduction by an underwater air layer. Shark skin possesses millimeter-range riblets, aligned in the direction of the water flow. This reduces the underwater drag by several percent. [9, 128] An air layer between the superhydrophobic solid surface and the water reduces the solid-water contact surface and therefore reduces the underwater drag. [14, 110] The combination of both effects is expected to lead to an increased drag reduction. [11,129,130] On top of that, adding an extra hierarchy level to a nanofur surface can increase the oil absorption capacity per area, and therefore increase the efficiency of nanofur as an oil sorbent material.

Nanothermoforming is a replication technique that utilizes the shape memory effect of shape memory polymers to combine a primary (typically µm range) with a secondary (typically nm range) surface structure. [88] Both structures are fabricated by hot embossing. The nanothermoforming process is regularly applied to fabricate two-level hierarchical

sophisticated optical structures. In this chapter, the fabrication of three-level hierarchical structures by nanothermoforming is presented. First, an extra level of hierarchy is added to the original two-level nanothermoforming process which is described in Ch. 2.2.4. Next, the nanothermoforming process is combined with hot pulling to fabricate nanothermoformed nanofur. As nanofur has a hierarchical micro- and nanostructure which consists of microcraters and nanohairs, the nanothermoforming adds a third level of hierarchy to the surface structure.

4.2.1 Nanothermoformed Three-Level Hierarchical Structure

The nanothermoforming process as introduced in Ch. 2.2.4 and illustrated in Fig. 2.10 [88] utilizes the shape memory effect of shape memory polymers (SMP) to combine a primary (often micrometer size) structure with a secondary (often nanometer size) structure that superimposes the primary structure. Nanothermoforming is a five step process that contains of three hot embossing steps plus one spincoating step and one heating step. A shape memory polymer is used as an active mold, which adds a primary structure to a secondarily structured polymer foil. In the first hot embossing step, the primary structure is embossed into a shape memory polymer foil at a temperature $T > T_{\text{hard}}$. This process step defines the primary structure as the permanent shape of the SMP. After that, the permanent structure is temporarily flattened in a second hot embossing step at $T < T_{\text{hard}}$. Third, a thin polymer foil is spincoated on the surface of the temporarily flattened SMP. After complete drying, a secondary structure is embossed into the spincoated foil (fourth step). Here, the applied embossing temperature needs to be below T_{trans} of the SMP to preserve its permanent shape. At the same time, it has to be high enough to allow structuring the spincoated polymer. In the last step, the SMP with the spincoated, structured foil on top is heated up to a temperature that triggers the recovery of the permanent structure of the SMP. This leads to a deformation of the nanostructured polymer foil and results in a hierarchically micro- and nanostructured surface. As no demolding step is required after the last step, structures with undercuts can be fabricated using this technology. Here, an extra level of hierarchy is added by using two shape memory polymers instead of only one. The schematic of the three-level nanothermoforming process is presented in Fig. 4.4.

The shape memory polymers Tecoflex® (TFX) and Tecoplast® (TP) presented in Ch. 2.2.2 are both thermoresponsive and respond to unequal temperature ranges. Therefore, they can be combined for the fabrication of a two-level hierarchical structure. The third level is achieved by adding an additional structured layer of PMMA, as in the normal two-level nanothermoforming. A millimeter range primary structure is embossed into the TP foil, which has a higher T_{hard} and T_{trans} compared to TFX, at $T = 190°\text{C}$, then the TP foil is temporarily flattened at $T = 85°\text{C}$. On top of the flattened TP, a TFX foil is spincoated (TFX in chloroform, 2.5 %, 2500 rpm, 3 layers). As chloroform has a negative effect on the shape memory effect of TP, a protection layer (PMMA in xylene, 2 %, 2500 rpm) is spincoated on the flattened TP prior to the TFX. Next, a secondary micro-range structure is embossed into the TFX as a permanent structure ($T = 85°\text{C}$) and temporarily flattened ($T = 45°\text{C}$). A PMMA layer is spincoated on the flattened TFX surface. Potential dissolvents for the spincoating of PMMA are xylene (dimethylbenzene) and anisole (methoxybenzene). PMMA dissolved in xylene allows the deposition of a thin PMMA film and does not negatively influence the shape memory effect of TP.

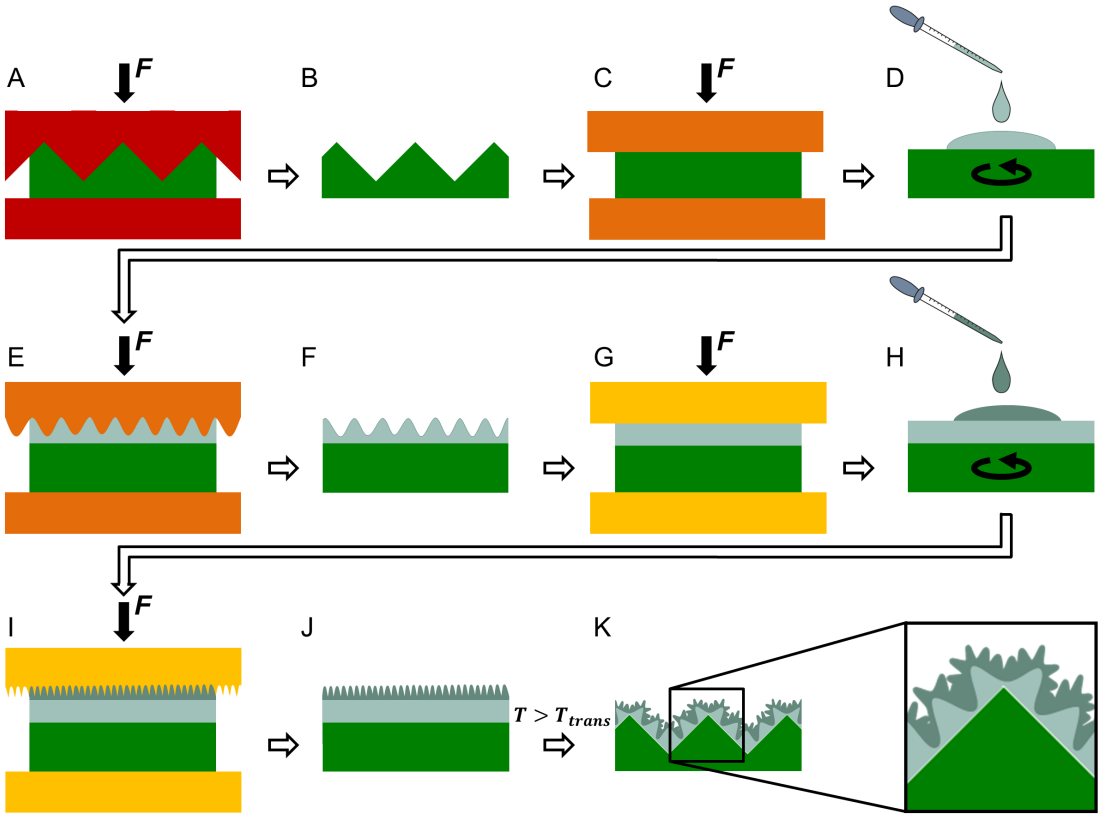

Figure 4.4: Schematic of a three-level hierarchical structure fabricated by nanothermoforming, which allows one extra level of hierarchy compared to classical nanothermoforming shown in Fig. 2.10. **A)** A primary structure is replicated into the shape memory polymer TP as permanent structure (**B**) and temporarily flattened (**C**). **D)** Next, a TFX layer is spincoated on top of the TP and a secondary structure is embossed as permanent structure in TFX (**E, F**). **G)** TFX is temporarily flattened and **H)** PMMA is spincoated on top. **I)** Tertiary structure (**J**) is embossed into PMMA. **K)** Heat triggers the shape memory effect of TP and TFX and causes the recovery of the permanent structures. The result is a three-level hierarchical structure.

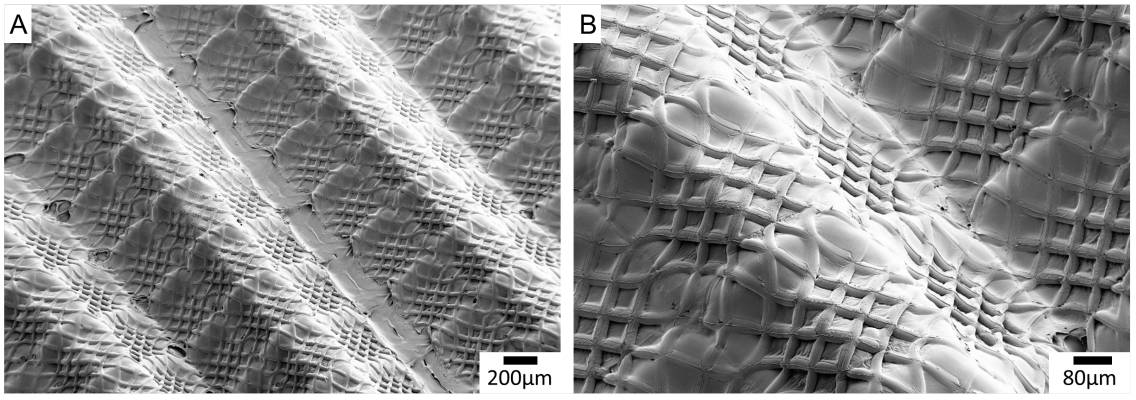

Figure 4.5: SEM images of a three-level hierarchical surface structure fabricated by nanothermoforming. **A)** Primary 1 mm grove structure with triangular shape is superimposed by secondary 300 µm well structure and tertiary 80 µm hole structure. **B)** Detailed view on secondary and tertiary structure.

However, as the solubility of PMMA in xylene is low, only a low concentration solution of about 2 % can be used for spincoating, which leads to an insufficient foil thickness or requires numerous spincoating steps. A solution of PMMA in anisole in contrast allows the spincoating of thicker layers, as a higher PMMA concentration is possible (8 % solution is used successfully), but anisole has a negative influence on the shape memory effect. This challenge can be solved by introducing a multi-step spincoating process. All spincoating steps are performed at 2500 rpm. First, a protection layer using PMMA dissolved in xylene is spincoated on the SMP, and subsequently a thicker layer of PMMA dissolved in anisole is spincoated on the first PMMA layer. After drying, a tertiary structure is embossed into the PMMA layer at $T = 50°C$. Subsequently, the shape memory effect is triggered on a hot plate at $T = 100°C$. Both TP and TFX recover their permanent shapes and deform the structured PMMA. The resulting three-level hierarchical structure is presented in Fig. 4.5. This advanced nanothermoforming technique allows the fabrication of more complex micro- and nanostructures compared to the normal two-level nanothermoforming. However, the fabrication process which consists of five embossing steps, several spincoating steps, and a final heating step is complex and time consuming. An alternative approach for the fabrication of three-level hierarchical structures is presented in the following section.

4.2.2 Nanothermoformed Nanofur

Nanofur is a hierarchical structure which consists of micrometer-range craters and hairs with a diameter in the nanometer range. A combination of nanofur and a micro-range structure by nanothermoforming, therefore leads to a three-level hierarchical structure. In contrast to the three-level nanothermoforming, the complexity of the fabrication process of nanothermoformed nanofur is equal to the normal two-level nanothermoforming as described in Ch. 2.2.4. For the nanothermoformed nanofur, however, an embossed structure is combined with a hot pulled nanofur structure rather than with another hot embossed structure. As the hot pulling process is critical in regard to the process parameters, the nanothermoforming of nanofur requires an adequate combination of SMP and the spincoated polymer. As a high T_{hard} of the SMP allows high temperatures for the replication of the secondary structure, TP is used to nanothermoform the nanofur rather than TFX. Furthermore, the spincoated polymer needs to fulfill the following prerequisites and to possess these properties:

- The polymer needs to be hot-pullable, i.e., suitable for the fabrication of nanofur. Not all polymers fulfill this requirement, but besides PC all polymers mentioned in Ch. 4.1 do: PE, PP, PMMA, and PA6
- The hot pulling temperature needs to be low enough in comparison to the T_{trans} of the SMP to ensure that the permanent shape of the SMP is not redefined during the hot pulling process.
- The softening temperature of the polymer, on the other hand, needs to be high enough to avoid the melting of the nanofur hairs while triggering the shape memory effect of the active mold by heating up the foil.
- The polymer must be spincoatable, i.e. it must dissolve in a dissolvent and produce an evenly thin film when spincoated.

- As some SMPs are sensitive to certain chemicals, only dissolvents that do not affect the SMP and the shape memory effect can be used for spincoating.
- After spincoating and drying, the spincoated foil must adhere to the active mold to enable the hot pulling and the subsequent nanothermoforming of the nanofur.
- The thickness of the spincoated polymer foil must be sufficiently high for hot pulling.

Due to these requirements, PMMA is the only one of all tested materials that can potentially be used for the fabrication of nanothermoformed nanofur. In contrast, the softening temperature of PC is too high and materials such as PE and PP hardly dissolve in any common solvent that allows spincoating and does not influence SMP. Potential dissolvents for spincoating of PMMA are xylene (dimethylbenzene) and anisole (methoxybenzene). As discussed in Ch. 4.2.1, a multi-step spincoating process is required for the fabrication of a sufficiently thick PMMA layer without influencing the shape memory effect. First, a protection layer is spincoated on the SMP, using PMMA dissolved in xylene, and subsequently a thicker layer of PMMA dissolved in anisole is spincoated on the first PMMA layer. Another issue is that the hot pulling temperature of PMMA is higher than T_{hard} of TP. Therefore, the hot pulling process has to be adapted for the fabrication of nanothermoformed nanofur. In contrast to hot embossing, hot pulling does not allow to compensate a decreased process temperature by an increased embossing force. Therefore, the regular hot pulling temperature was chosen, and the contact time between the sandblasted mold and the polymer surface was minimized. The low thermal conductivity of polymers allows the softening and hot pulling of the thin spincoated PMMA foil without influencing the permanent shape of the TP.

For the fabrication of the nanothermoformed nanofur as illustrated in Fig. 4.6, a permanent shape of the TP is embossed at $T \approx 190°\text{C}$ using a hot embossing machine. The permanent structure consists of grooves with a triangular profile and a periodicity of approximately 1 mm. This permanent SMP structure is temporarily flattened by hot embossing using a flat mold at $T \approx 85°\text{C}$. PMMA is spincoated in a three step spincoating process. For the fabrication of a protection layer, two layers of PMMA dissolved in xylene (2 %) were spincoated on the temporary flat TP at 2500 rpm with 2 minutes drying time in between. Subsequently, a thicker PMMA layer was spincoated from a solution of PMMA in anisole (8 %) at 2500 rpm. After drying at air temperature for 24 hours, nanofur was hot pulled from the PMMA surface at $T \approx 155°\text{C}$ with a sandblasted steel plate serving as a mold. The mold was sandblasted in a two step process (coarse aluminum silicate clinker (0.2 mm - 1.4 mm), and fine-grained aluminium oxide F400). To minimize the contact time between the hot sandblasted mold and the polymer surface, the hot pulling process was slightly adapted. When the mold touches the surface, it is quickly pressed into the polymer surface and retracted immediately, with no waiting time. The last step of the nanothermoforming process is triggering the shape memory effect of the TP by putting the foil on a hot plate at $T = 100°\text{C}$ for 30 seconds. The TP recovers its permanent shape and the nanothermoformed nanofur is generated.

Nanothermoformed nanofur was successfully fabricated from PMMA using the shape memory polymer TP as an active mold. In Fig. 4.7, an SEM image of the nanothermoformed nanofur is shown. The primary structure is a groove structure with a triangularly

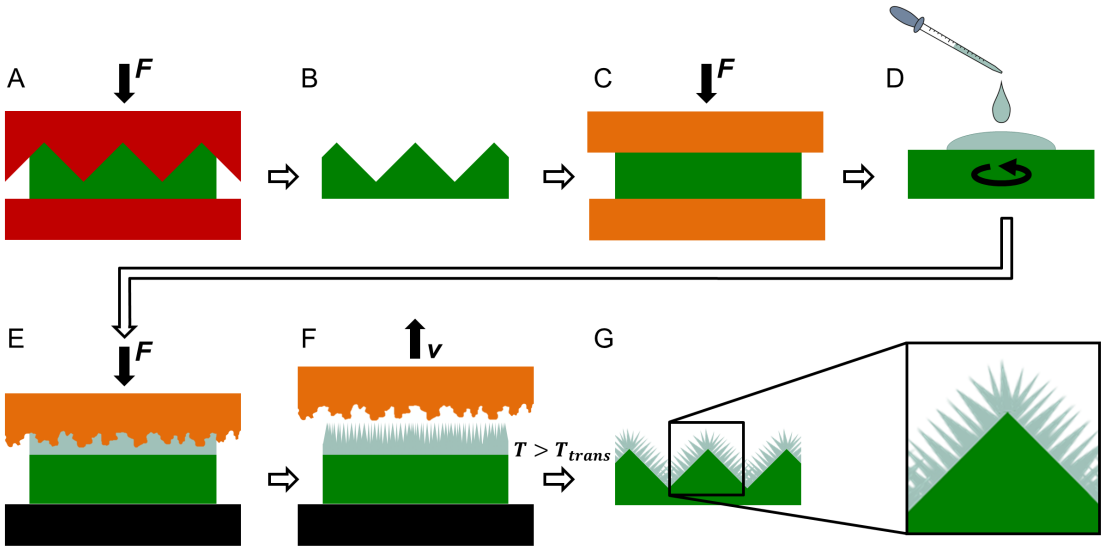

Figure 4.6: Schematic of fabrication of nanothermoformed nanofur. **A)** Primary structure is replicated into TP as permanent structure (**B**) and temporarily flattened (**C**). **D)** PMMA layer is spincoated on top of TP and **E)** nanofur is fabricated as secondary structure (**F**) by hot pulling. **G)** Heat ($T > T_{\text{trans}}$) triggers shape memory effect of TP and causes the recovery of the permanent structure. The result is a three-level hierarchical nanothermoformed nanofur structure.

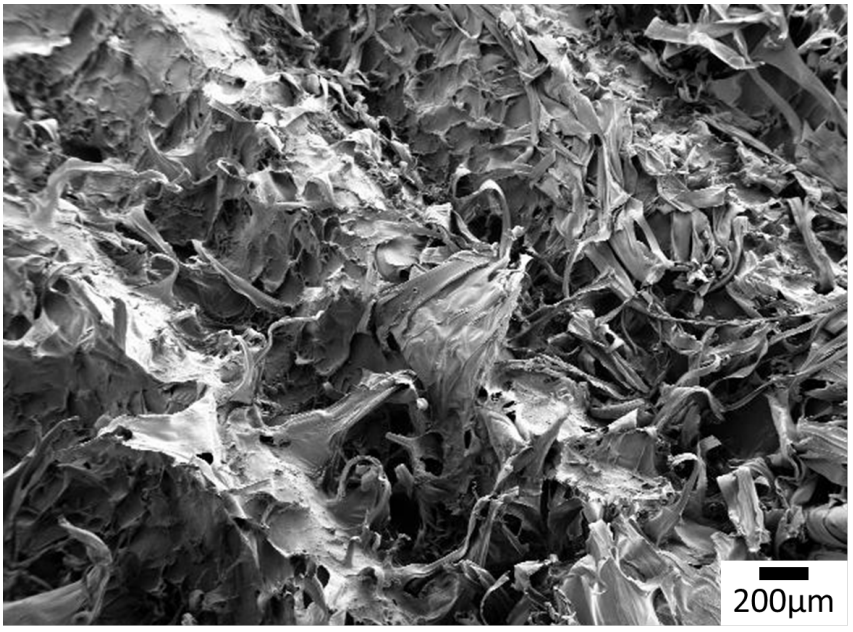

Figure 4.7: Nanothermoformed nanofur from PMMA fabricated with an active mold from TP. The primary structure consists of grooves with a triangular cross section and a periodicity of approximately 1 mm. The secondary structure is nanofur. The SEM proves the successful fabrication of nanothermoformed nanofur, but also shows that the diameter of the nanofur hairs is comparably thick.

shaped cross section and a periodicity of ∼1 mm. The secondary structure is the nanofur from PMMA. Due to the specific hierarchical surface structure, the quantification of the contact angle is challenging. Water droplets put on the surface remain in a spherical shape but adhere to the surface, which indicates a hydrophobic wetting behavior. However, the surface does not show a superhydrophobic wetting behavior in the Cassie-Baxter state with a low rolloff angle, as the nanofur from PC and other materials does. This is due to the fact that the PMMA nanofur has bigger hairs and a lower contact angle compared to nanofur from other materials. Also, the primary structure with a periodicity of ∼1 mm offers a large contact surface area for water droplets and enhances droplets to stick to the surface. Due to the lack of superhydrophobicity, the oil absorption capacity was not tested. Still, these promising results supply a basis for the future research on nanothermoformed nanofur with other material combinations.

4.3 Reusable Nanofur

As already mentioned, nanofur is a superhydrophobic and superoleophilic material, introduced by Röhrig *et al.* [16], that selectively absorbs oil from oil/water mixtures. Superhydrophobicity leads to a high oil absorption efficiency of the nanofur, as no water is absorbed in addition to oil. However, the oil absorption by nanofur leads to huge amounts of waste when it is used as a one-way sorbent. The reusability of nanofur, in contrast, reduces waste and increases the environmental sustainability. In this section, two approaches of reusing nanofur are presented. Reusing nanofur requires removing the oil after absorption without destroying the structure, or with the subsequent recovery of the structure. The first is achieved by washing the nanofur with a solvent, the latter by fabricating the nanofur from a shape memory polymer. The experiments presented in this section were carried out in collaboration with Alexander Storz in the context of his master's theses [125] (reusing nanofur by washing) and Hanna Wund in the context of her bachelor's thesis [131] (nanofur from Tecoflex®).

4.3.1 Reusing Nanofur by Washing

One approach that allows to use nanofur several times, is washing it with a solvent that removes the oil from the nanofur surface. Tests were executed with PP nanofur after hydraulic oil absorption. The initial water contact angle on dry PP nanofur in air is around 150° and the oil absorption capacity is 300 g/m^2. The oil contaminated nanofur samples were washed with isopropanol twice using a shaker (IKA, RCT basic) for 5 min at 200 rpm and were subsequently allowed to dry for at least twelve hours. Five cycles of oil absorption and washing were executed with PP nanofur samples. As can be seen in Fig. 4.8, there is no significant change of the oil absorption capacity and the water contact angle over the cycles. These results indicate that nanofur can be reused after removing the oil by washing.

4.3.2 Reusable Nanofur from Shape Memory Polymer

The second approach of resuing nanofur requires the shape memory effect of shape memory polymers. The nanofur is fabricated as a permanent shape from the shape memory polymer Tecoflex EG-72D® (TFX) (see Ch. 2.2.1). After oil absorption, the nanofur is

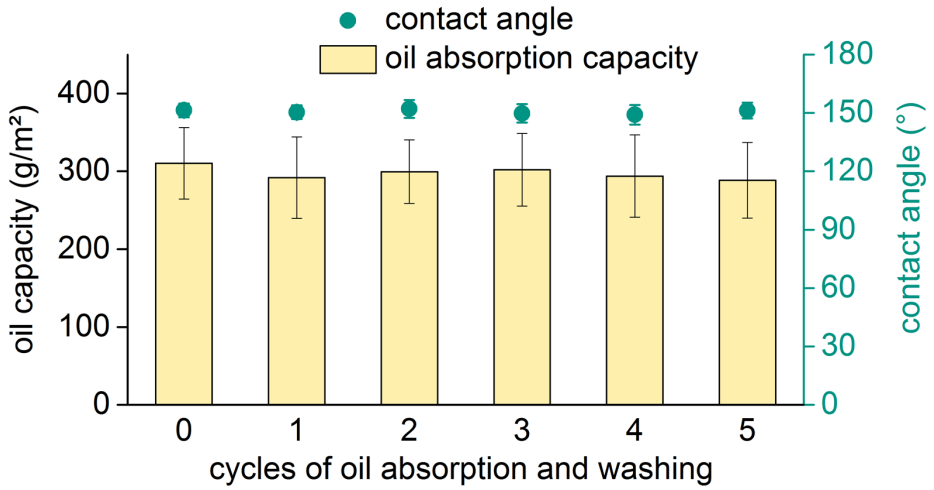

Figure 4.8: Reusing nanofur by washing. Water contact angle and oil absorption capacity of initial PP nanofur and after washing and reusing. There is no significant change of the WCA or the oil absorption capacity over five cycles of washing and reusing.

temporarily flattened, which temporarily destroys the surface structure and squeezes the oil out. The advantage of this method is that, in contrast to washing the nanofur, the absorbed oil is not mixed with a solvent and can be collected and reused, or disposed. After removing the oil, the flattened nanofur is heated up to trigger the shape memory effect which recovers the permanent nanofur shape.

4.3.2.1 Experimental

The nanofur from the shape memory polymer TFX is fabricated similar to the fabrication process introduced by Röhrig *et al.* [16] with adapted process parameters. The mold was sandblasted in a two step process, first with aluminium silicate clincer 0.2 mm - 1.4 mm and subsequently with fine-grained aluminium oxide F320. A TFX foil with a thickness between 0.5 mm and 1 mm was fixed on the bottom plate by hot embossing at $T \approx 125°C$ with 5 MPa. The mold temperature for hot pulling is 120°C. The rough hot mold is pressed into the polymer surface, where it remains for 5 s. Next, the mold is pressed into the polymer with 3 MPa and subsequently retracted with 0.35 mm/min. During the hot pulling process, the mold temperature rises to 130°C. The permanent nanofur surface structure is temporarily flattened by hot embossing ($T = 60°C$, pressure $p = 2.8$ MPa) and cooled to 25°C before releasing the pressure. The flattened nanofur structure is recovered by heating up the sample in an oven ($T = 60°C$ for 10 minutes). The cycle of temporarily flattening and subsequently recovering the TFX nanofur is illustrated in Fig. 4.9.

4.3.2.2 Characterization and Results

The surface of the as-prepared TFX nanofur is characterized by SEM and is compared to the surface after three cycles of flattening and recovering. The comparison of the SEM images is shown in Fig. 4.10 and reveals that the as-prepared TFX nanofur contains of a cratered structure with few short hairs. After three cycles of flattening and recovering,

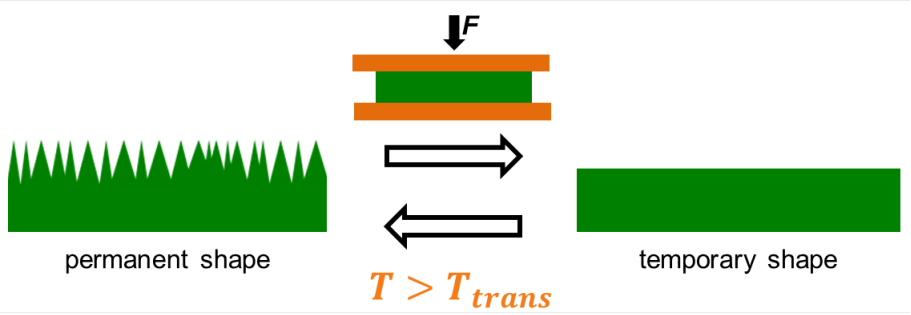

Figure 4.9: Reusable nanofur from a shape memory polymer. Nanofur is the permanent shape and can be temporarily flattened. Heat triggers the shape memory effect and recovers the nanofur structure.

the cratered structure is still visible, although the hairs of the nanofur structure are less accurate and stick together. In addition, the TFX nanofur surface is characterized by measuring the oil absorption capacity and the water contact angle in air. Both properties were tested for the TFX nanofur over ten cycles.

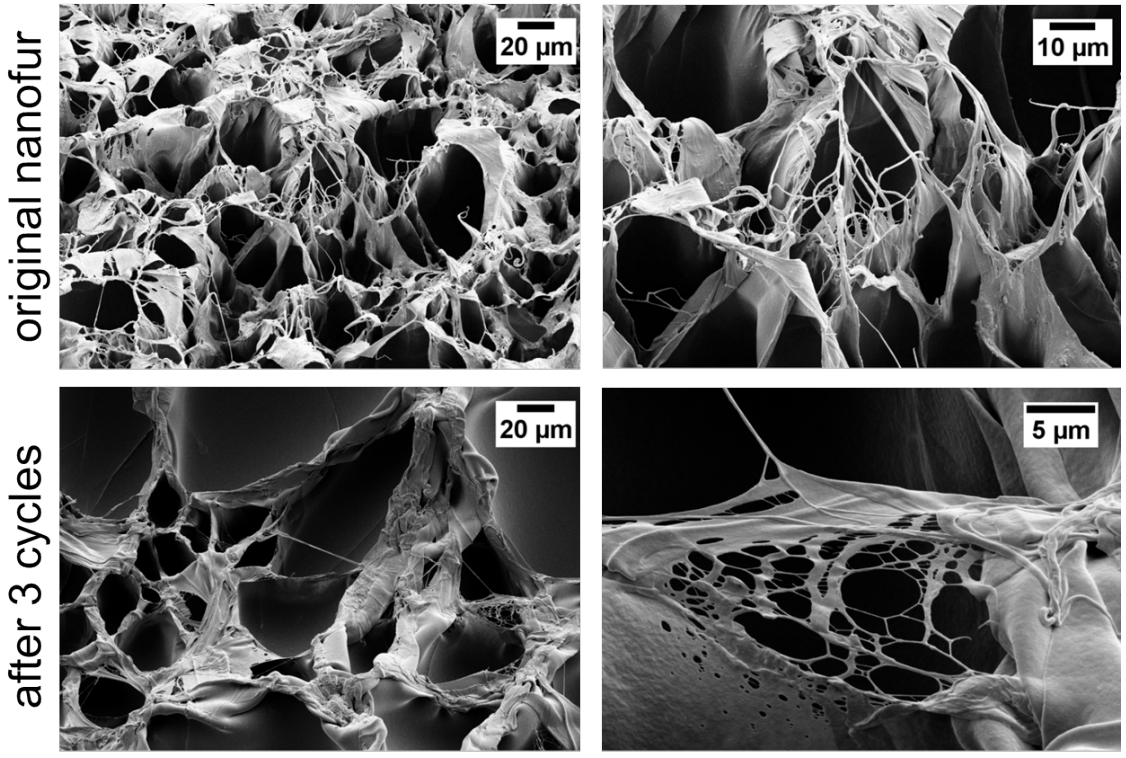

Figure 4.10: SEM images of reusable nanofur from a shape memory polymer. The cratered structure of the original, as-prepared TFX nanofur is similar to the structure after three cycles of flattening and raising up. Some hairs, however, stick together after three cycles.

Contact Angle

For the quantification of the surface wetting properties, the water contact angle was measured on the original TFX nanofur (5 µL droplets of distilled water, dosing speed 0.1 µL/s). After each cycle of flattening and recovering the nanofur structure, the water

contact angle was measured again and compared to the initial CA. In addition, the WCA on the flat structure was checked on a random basis. For each measurement, the contact angle was measured on five arbitrarily chosen spots of each nanofur sample.

The results of the contact angle measurements are presented in Fig 4.11. Flat TFX is hydrophilic with WCA $\approx 84°$. The as-prepared TFX nanofur is hydrophobic with a water contact angle around 138°. The CA of the nanofur surface decreases during the first three cycles and remains constant over the following seven cycles. After ten cycles, the surface is still hydrophobic (CA $\approx 126°$). The flattening and recovering can be repeated more than ten times, as shown by Schmidt *et al.*, who examined the shape memory effect of TFX over 50 cycles. [132] By temporarily flattening the nanofur, the WCA of the flat TFX (CA $\approx 84°$) is almost reached. However, the measured CA of the temporary flat surface varies between 80° and 95°. This is due to the partly recovery of the surface structure after flattening and before measuring the contact angle. The recovery can be avoided by cooling down the sample to a temperature $\leq 20°C$ during the flattening process and storing it at a similar temperature. For the oil/water separation, however, this is non-relevant. In summary, these results reveal that the nanofur from TFX is hydrophobic both when it is new and after ten cycles of flattening and recovering, and therefore absorbs only oil and no water.

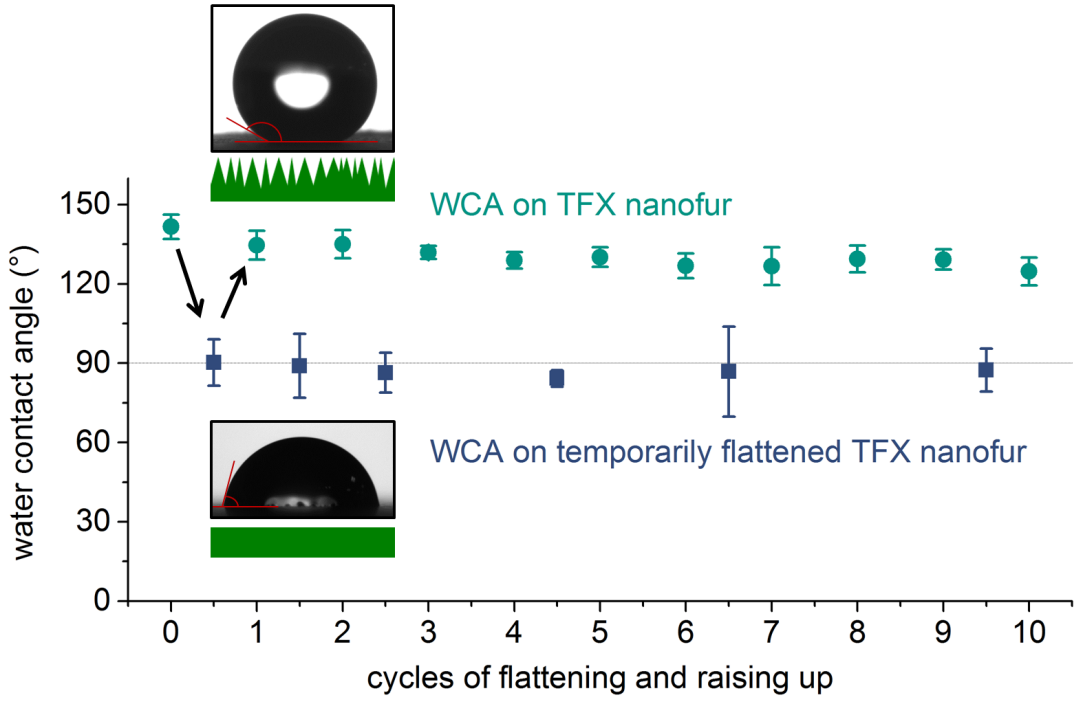

Figure 4.11: Contact angle of reusable nanofur made from a shape memory polymer. Nanofur from Tecoflex® is temporarily flattened and subsequently recovered ten times. Nanofur (green circles) is almost superhydrophobic with a CA close to 150°, the flattened surface (blue squares) is hydrophilic with an average CA below 90°. Over ten cycles, the contact angle of nanofur decreases from 138° to 126°.

Oil Absorption

The oil absorption capacity per surface area of five samples was measured over ten cycles. To determine the surface area of the nanofur samples, they were photographed on a graph paper, and the corresponding areas were measured by analyzing the photos with an image processing software [119]. The samples were weighed and then immersed into hydraulic oil (Total Azolla ZS 10) for 60 seconds. The subsequent draining of the samples by suspending (60 s) and wiping off the backside removed excessive oil, then the samples were weighed again. The difference in weight before and after immersion in oil was determined as the amount of absorbed oil. The samples were subsequently flattened by hot embossing as described in Sec. 4.3.2.1. The oil was squeezed out and collected. The samples were weighed again and the difference in weight before and after flattening was determined as the amount of removed oil. The difference between absorbed oil and removed oil was determined as residual oil that could not be removed from the sample by temporarily flattening the nanofur surface. Oil absorption, removing oil by flattening, and recovering nanofur by heating up were repeated ten times.

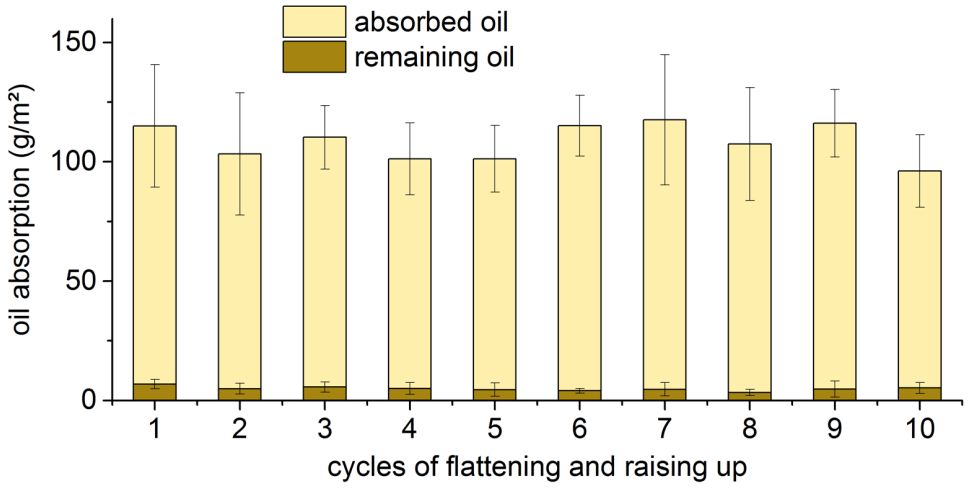

Figure 4.12: Oil absorption capacity of reusable nanofur from a shape memory polymer. Nanofur from Tecoflex® absorbs 108 g/m^2 hydraulic oil on average. By temporarily flattening the nanofur structure, 95% of the absorbed oil is removed. Absorption, flattening and recovering of the nanofur structure are repeated ten times with no significant change in the absorption capacity.

The as-prepared TFX nanofur absorbs 115 g/m^2 on average. This is more than 280 % of the oil absorption capacity of unstructured TFX (∼40 g/m^2). The results of the oil absorption experiments are illustrated in Fig. 4.12. The oil absorption is constant over ten cycles and is on average 108 g/m^2, i.e. there is no significant decrease in oil absorption capacity. 95% of the absorbed oil is removed by the temporary flattening of the nanofur structure. An average of 5 g/m^2 oil remains on the surface.

Application and Outlook

The results presented here reveal that TFX nanofur is hydrophobic, and that it remains hydrophobic with a decrease in WCA from 138° to 126° after ten cycles of flattening and

recovering the nanofur structure. The measured WCA of the temporary flat surface is higher than the WCA of the flat TFX. This is due to processing issues and could be avoided by an improved cooling and storage. The increase of the WCA of the temporarily flattened structure before recovering has no negative influence during the usage of the TFX nanofur as a reusable oil absorption material. The oil absorption capacity remains constant over ten cycles of absorbing oil, squeezing the oil out by flattening the nanofur structure, and recovering the nanofur structure. The average absorption capacity is 108 g/m^2. This qualifies the nanofur from TFX as a reusable material for oil absorption.

A possible setup for the oil/water separation with nanofur from a shape memory polymer is illustrated in Fig. 4.13. The reusable nanofur foil is fixed on a roll that touches the surface of an oil/water mixture. The oil is selectively absorbed from the water surface and retained in the nanofur structure. A second roll flattens the nanofur structure in a roll-to-roll-like process, the oil is squeezed out of the surface and can be collected. Subsequently, the temporarily flattened surface of the shape memory polymer is heated up and the nanofur structure is recovered.

A patent application was submitted that refers to oil/water separation in a continuous process using reusable nanofur from SMPs. Claudia Zeiger, Maryna Kavalenka, Matthais Worgull, Hendrik Hölscher: WO2016096142 A1 (DE102014119183 A1)

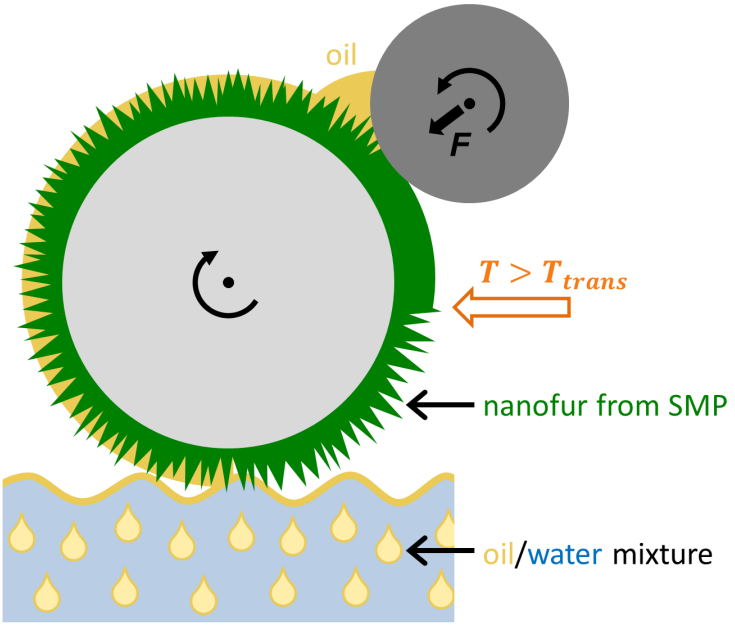

Figure 4.13: Oil/water separation with reusable nanofur from a shape memory polymer. In this setup, reusable nanofur from a shape memory polymer is fixed on a roller which touches the surface of an oil/water mixture. Oil is selectively absorbed by the nanofur and transported by the rotation of the roller. A second roller presses on the nanofur structure to temporarily flatten it and to squeezes oil out. The oil can be collected. The surface of the shape memory polymer on the roller is heated up to trigger the shape memory effect and recover the nanofur structure before the polymer surface touches again the oil/water mixture.

4.4 Cold Pulling as a New Nanofur Fabrication Technique

In the hot pulling process for nanofur fabrication, any variability in the mold temperature is fatal for the success of the fabrication of the structure. This is detrimental for the production of nanofur in a serial production process and inhibits transferring the hot pulling process to a continuous roll-to-roll large-scale fabrication process. In this section, an alternative approach for nanofur fabrication is presented. In a normal hot pulling process, the mold temperature at the moment of touching the polymer surface and during the pulling process is approximately the same, and in the range of or above the softening temperature of the pulled polymer. In contrast, in the newly developed cold pulling process, pulling is executed at a temperature which is significantly lower than the softening temperature of the polymer. This cold pulling process was developed in collaboration with Alexander Storz as part of his master's thesis. [125]

4.4.1 Cold Pulling Fabrication Process

For the cold pulling fabrication of nanofur, a steel mold is sandblasted similar to the sandblasting process for hot pulling as described in Ch. 2.2.5 [14–16, 49, 90]. The cold pulling process is illustrated in Fig. 4.14. A polymer foil with a thickness of ∼1 mm is placed between the sandblasted mold and a flat counter steel plate. The mold is heated to a temperature above the softening temperature of the polymer (process temperature is 130°C for HDPE and 165°C for PP) and pressed into the polymer foil. The polymer surface melts and floats into the cavities of the rough mold. In contrast to hot pulling, where the hot mold is retracted, the mold is cooled at a constant pressure for cold pulling. When a temperature significantly lower than the softening temperature is reached, the tool is opened and the polymer foil sticks to the rough surface. Subsequently, the polymer foil is manually pulled from the rough steel, which results in the elongation of the polymer and the formation of a polymer surface covered with nanohairs. With this cold pulling technique, nanofur was successfully fabricated from PE and PP. The pulling temperatures varied between 60°C and room temperature with no significant influence on the resulting surface. SEM images of the resulting cold pulled nanofur and the results of the contact angle measurements are presented in the following section, the advantages and issues of hot pulling and cold pulling are discussed.

Figure 4.14: Cold pulling fabrication process. A polymer foil is pressed into a sandblasted steel plate by hot embossing. After cooling down the mold and opening the tool, the polymer foil is manually pulled from the rough mold surface, which results in elongation of the polymer and the formation of nanohairs.

4.4.2 Characterization of Cold Pulled Nanofur

The structure fabricated by cold pulling is similar to hot pulled nanofur. As can be seen in Fig. 4.15, the cold pulled nanofur from HDPE consist of micro- to nanoscaled hairs, densely covering the foil surface. The cold pulled nanofur from PP consists of less densely packed, thicker hairs. The water contact angles of both HDPE and PP nanofur are around 150°, and equal to the WCAs of hot pulled nanofur from the same materials.

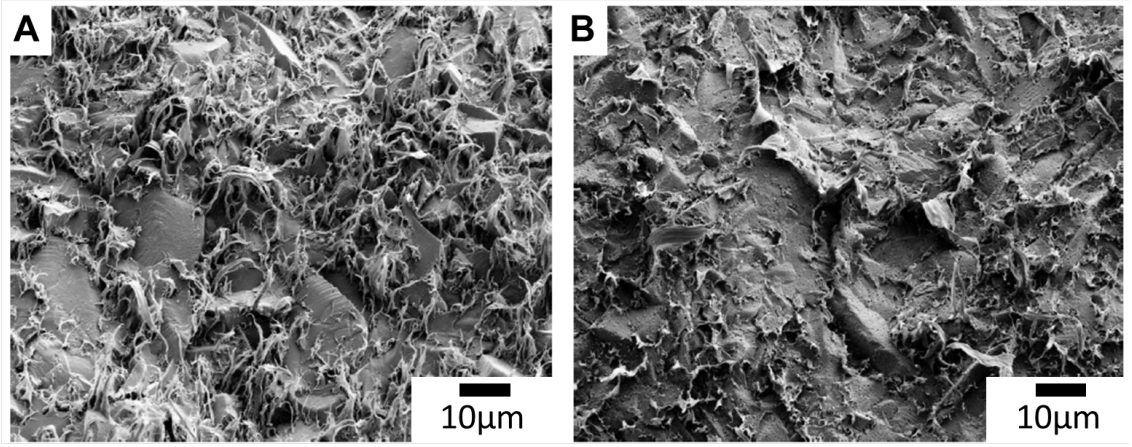

Figure 4.15: SEM images of cold pulled nanofur from HDPE **(A)** and PP **(B)**. They reveal that a hairy nanofur structure was succesfully fabricated by cold pulling from both materials. The process temperature was 130°C for HDPE and 165°C for PP. Cold pulling was executed at room temperature.

Compared to hot pulling, the process temperature range of the cold pulling process is significantly larger. In the hot pulling process, a change by a few degrees Kelvin can lead to the failure of the nanofur fabrication process. In contrast, a temperature variation between 60°C and room temperature did not significantly influence the resulting surface structure fabricated by the cold pulling process. This improves the feasibility of nanofur fabrication and allows a simple upscaling to bigger areas. An advantage of hot pulling is that the material range is bigger compared to the cold pulling process. The cold pulled nanofur was only fabricated from PE and PP, and the cold pulling of other polymers requires further research. While the mold needs to be sandblasted or cleaned after every hot pulling step, molds used for cold pulling can be reused. This is due to the fact that less polymer residues remain in the cavities of the mold after cold pulling in the first place. Additionally, residues remaining on the rough mold will melt into the surface of the polymer foil in the following cold pulling process. As a consequence, cold pulling is more efficient compared to hot pulling, as sandblasting prior to each pulling process is not required. These advantages of the cold pulling process even allow the fabrication of a polymer foil with nanofur on both sides. The double-sided nanofur fabrication is presented in the following section. Also, the cold pulling process is highly scalable and allows the fabrication of a nanofur surface on bigger areas, which are only limited by the size of the mold and the mold size restrictions of the hot pulling machine. To overcome these limitations, the cold pulling fabrication process is transferred to a roll-to-roll process, which is presented in Ch. 4.5.

4.4.3 Double Sided Nanofur

The combination of hot pulling and cold pulling enables the fabrication of a double sided nanofur, which is a polymer foil with a nanofur structure on both top and bottom side of the foil. First, a polymer foil is fixed on a sandblasted steel plate by hot embossing (Fig. 4.16a). The sandblasted steel plate serves as a counter plate for the hot pulling, and as a mold for the subsequent cold pulling. Therefore, this steel plate is sandblasted in a two step process similar to the sandblasting process of the mold for hot pulling. Second, the hot pulling is executed on the polymer foil with a second sandblasted steel plate. Finally, the polymer foil with the hot pulled nanofur on one side is removed from the rough counter plate by manually pulling (Fig. 4.16b). With this cold pulling step, nanofur is fabricated on the other side of the polymer foil. In summary, the double sided nanofur foil was fabricated by hot pulling on the top side of the polymer foil and subsequent cold pulling on the bottom side. This process was successfully executed with both PE and PP foils. The contact angle was equal on both sides and around 150° for both materials. In contrast to normal one-sided nanofur, the double-sided nanofur is superhydrophobic on both sides. This is beneficial for the oil/water separation and for other applications that require water repellency. As nanofur has an improved oil absorption capacity compared to the flat material, the double sided nanofur has a higher oil absorption efficiency than one-sided nanofur, as the oil capacity per square meter of the polymer foil is up to twice as high.

A patent application was submitted that refers to large area fabrication of nanofur by cold pulling and roll-to-roll fabrication of nanofur. Claudia Zeiger, Alexander Storz, Andreas Striegel, Maryna Kavalenka, Matthais Worgull, Hendrik Hölscher: 102018004339.9

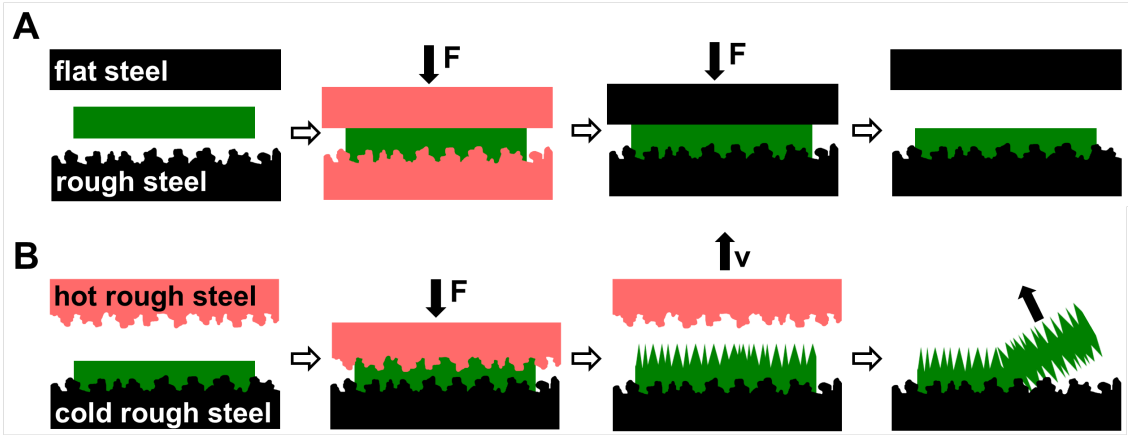

Figure 4.16: Cold pulling fabrication process. **A)** A polymer foil is fixed on a rough bottom plate by hot embossing. The rough bottom plate serves as a counter plate for the hot pulling step of the top side of the polymer foil and subsequently as a mold for the cold pulling of the backside. **B)** The hot pulling process with the top plate results in a nanofur surface on the top side of the polymer foil. Subsequent cold pulling by manually pulling the nanofur from the bottom plate results in nanofur on the other side of the polymer foil and therefore in a double sided nanofur.

4.5 Roll-to-Roll Large Scale Fabrication of Nanofur

Fabricating nanofur on a larger scale is challenging and the simple upscaling of the hot pulling process is restricted by the maximum mold size of the hot embossing machine and by an unequal temperature distribution within the mold. Therefore, the typical size of the nanofur samples is a few square centimeters. Also, the batch fabrication of the hot pulled nanofur is restricted by long cycle times. The development of cold pulling as an alternative fabrication method for nanofur now opens up the possibility to transfer the nanofur fabrication process to a roll-to-roll machine. However, some adaptions of the process are required. Cold pulling in a batch process using a hot embossing machine requires a change of the mold temperature. For the first step of the cold pulling process (fixing polymer foil to a rough steel plate), the mold is heated up above the softening temperature of the polymer. In the second step (the actual cold pulling step), the polymer foil is pulled and removed from the mold with a lower mold temperature. The roll-to-roll process (see Ch. 2.2.3), in contrast, features a constant mold temperature due to the continuous character of the fabrication process. Therefore, the fabrication process needs to be adapted. As can be seen in Fig. 4.17, a pre-heater is installed prior to the roll-to-roll feed. The surface of the polymer foil is heated up by the preheater to the highest possible temperature without risking the complete destabilization of the polymer foil by melting. The polymer foil with the softened surface is fed into the roll-to-roll machine. The top roll is roughened by sandblasting in a two step process, similarly to the sandblasting of molds for cold pulling on a hot embossing machine. The flat counter roll presses the softened polymer foil into the cavities of the top roll. Similar to batchwise cold pulling, the polymer foil is subsequently pulled manually from the rough roll, which elongates the polymer surface and forms the nanofur.

Nanofur from PP was fabricated in a roll-to-roll process with a preheater temperature of 235°C and a roller temperature of 75°C at a roller speed of 2.2 m/min. SEM images of the PP nanofur fabricated by the roll-to-roll process are presented in Fig. 4.18. The fabricated surface is similar to cold pulled nanofur, with micro- and nanosize hairs covering the polymer surface. Although further improvement and refining of the process parameters are required to fabricate nanofur in high quality and in industrial range, these results reveal that the large area fabrication of nanofur in a continuous process is possible.

A patent application was submitted that refers to large area fabrication of nanofur by cold pulling and roll-to-roll fabrication of nanofur. Claudia Zeiger, Alexander Storz, Andreas Striegel, Maryna Kavalenka, Matthais Worgull, Hendrik Hölscher: 102018004339.9

4.6 Conclusions on Nanofur as Improved Oil Absorbing Material

Nanofur fabricated by hot pulling possesses various issues which were addressed in this chapter. The batch fabrication of nanofur in a hot embossing machine is restricted by long cycle times and the sample size is limited by the maximum mold size. Also, heating and cooling of the mold for every hot pulling step leads to a high energy consumption. Furthermore, nanofur as a single-use oil sorbent leads to a high material consumption and to high disposal costs. Also, some applications require a polymer material with special

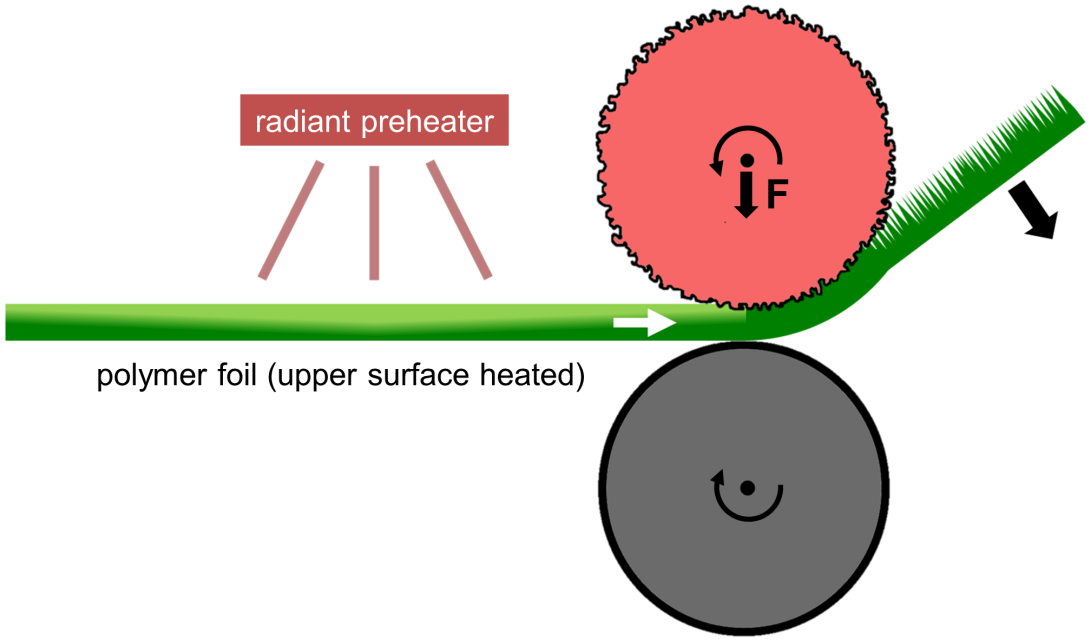

Figure 4.17: Roll-to-roll nanofur fabrication process. The top roller is roughened by sandblasting, the bottom roller is smooth. The polymer foil is preheated using a radiant heater to ensure softening of the upper polymer foil surface. A warm top roller is pressed into the polymer surface and analogously to cold pulling, the polymer flows into the cavities of the rough mold. The mold temperature is slightly below T_s of the polymer, and the softened polymer is solidified when in contact with the mold. The polymer adheres to the mold and is pulled from the mold surface, comparably to the cold pulling process.

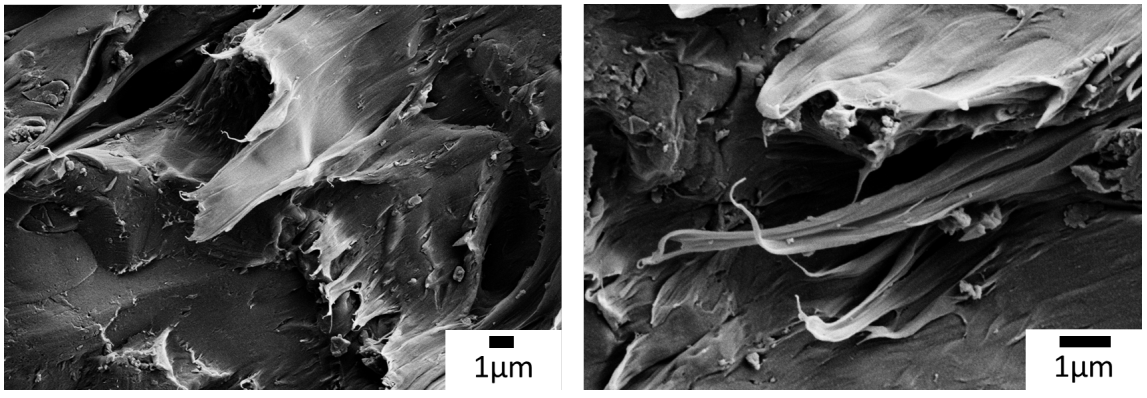

Figure 4.18: SEM images of nanofur fabricated on a roll-to-roll machine. The nanohairs indicate that roll-to-roll cold pulling of PP was successful and serve as a proof of principle. Even though the structure looks different from nanofur fabricated on a hot embossing machine, the surface is superhydrophobic with a WCA above 150°.

properties, which can only be reached if the material diversity is increased. Possible solutions to these issues were presented in this chapter.

The nanofur hot pulling process is adapted to the thermoplastic polymers polyethylene (PE), polypropylene (PP), polyamide (PA6), and polymethylmethacrylate (PMMA) by adapting the process parameters. Nanofur surfaces from all tested polymers possess an increased hydrophobicity or are superhydrophobic with WCAs around 150°, which is in agreement with the theory. By combining hot pulling with the nanothermoforming technique, an extra level of hierarchy is added to the nanofur. The reusability of nanofur was implemented in two ways: Oil-soaked nanofur was washed with solvents after oil absorption to remove the absorbed oil, with no significant change in the absorption capacity over five cycles of washing and reusing. This increases the environmental sustainability and economic efficiency of the nanofur as an oil sorbent material, as it decreases both the material input and the amount of waste to be disposed per amount of absorbed oil. The second approach takes advantage of the shape memory effect. Shape memory polymers are capable of recovering a pre-defined permanent shape as a reaction to a specific trigger after having been deformed. The nanofur structure is hot pulled from the shape memory polymer Tecoflex® and defined as its permanent shape. After oil absorption, the nanofur structure is temporarily flattened, and the oil is squeezed out. Subsequently, the flattened nanofur is heated up in order to trigger the recovery of the nanofur by the shape memory effect. Advantages of this approach are that no solvents are needed to remove the oil from the nanofur surface and that the absorbed oil can be collected. It is not mixed with water nor solvents. Experiments reveal only a small decrease in the WCA and no significant change in the absorption capacity over ten cycles of reusing the nanofur from the shape memory polymer Tecoflex®.

Next, a new nanofur fabrication process was introduced. In contrast to hot pulling, cold pulling is executed below the softening temperature of the polymer, which leads to a wider process window and, therefore, allows variations in the mold temperature. Similar to hot pulling, a steel plate roughened by sandblasting is heated up to a temperature above the softening temperature of the polymer and pressed into the polymer foil. The polymer surface melts and flows into the cavities of the rough mold. In contrast to hot pulling, where the hot mold is retracted, here the mold is cooled and the polymer foil is manually pulled from the rough steel at a temperature well below the softening temperature. This results in the elongation of the polymer and in the formation of a polymer surface covered with nanohairs. With this cold pulling technique, nanofur was successfully fabricated from PE and PP, with a WCA of approximately 150°. A further benefit of the cold pulling process compared to hot pulling is that the sandblasted molds can be reused and sandblasting is not required after every pulling process. Also, cold pulling, in contrast to hot pulling, does not require to fix the backside of the polymer foil to the counter plate. This reduces the number of process steps and allows the fabrication of a double sided nanofur, where both upper and lower side of the polymer foil are covered with a nanofur structure.

Finally, the cold pulling nanofur fabrication process is transferred to a roll-to-roll embossing machine. A preheater heats up the surface of the polymer foil to a temperature close to its softening temperature. The mold temperature of the roller mold which is roughened by sandblasting is chosen below the softening temperature of the polymer. The

rough surface structure of the roll is pressed into the polymer foil and the softened polymer is pressed into the cavities of the rough mold. Subsequently, the polymer foil is pulled from the structured roll which leads to the formation of the nanofur structure. The fabrication of the nanofur in a continuous roll-to-roll process paves the way towards a large-scale fabrication of nanofur and therefore is the basis for a future use in industrial applications.

5. Microperforated Nanofur for Selective Oil/Water Filtration

Membranes with special wetting properties enable the selective removal of either oil or water from oil/water mixtures by filtration. In this chapter, nanofur membranes are fabricated by perforating nanofur with microneedles. These superhydrophobic/superoleophilic membranes separate oil from oil/water mixtures. The as-prepared oil-removing membranes are converted into underwater superoleophobic water-removing membranes by argon plasma treatment. The plasma treated nanofur (p-nanofur) separates water from oil/water mixtures. The membrane permeability and breakthrough pressures are analyzed and compared to theoretical values. The efficiency of both types of membranes for oil/water separation is demonstrated.

5.1 Introduction to Oil/Water Filtration

Absorption of oil by selective oil sorbents (see Ch. 4) is the dominant method for separating oil/water mixtures and is used in many applications. However, the absorption of oil posseses issues such as a limited absorption capacity as well as challenging handling and difficult oil recovery. [34, 133, 134] A promising alternative oil/water separation technique to absorption is membrane-based filtration. The continuous mixture separation by filtration with a high separation capacity and a reduced material consumption is in general widely used in various industries. [135, 136] The effective oil/water filtration requires special wetting membrane materials with opposite affinities towards water and oil, which allow only one of the liquids to permeate while retaining the other. [133]

In general, two types of special wetting materials are suitable for oil/water filtration. [133] "Oil-removing" membranes with a superhydrophobic/superoleophilic surface have a high water contact angle (WCA) above 150° and low oil contact angles (OCA) close to 0°, and separate oil from oil/water mixtures by selective oil permeation. As explained in Ch. 2.1, such a wetting behavior occurs from a combination of surface chemistry and surface micro- and nanoscale roughness. [62, 137, 138] Underwater superoleophobic

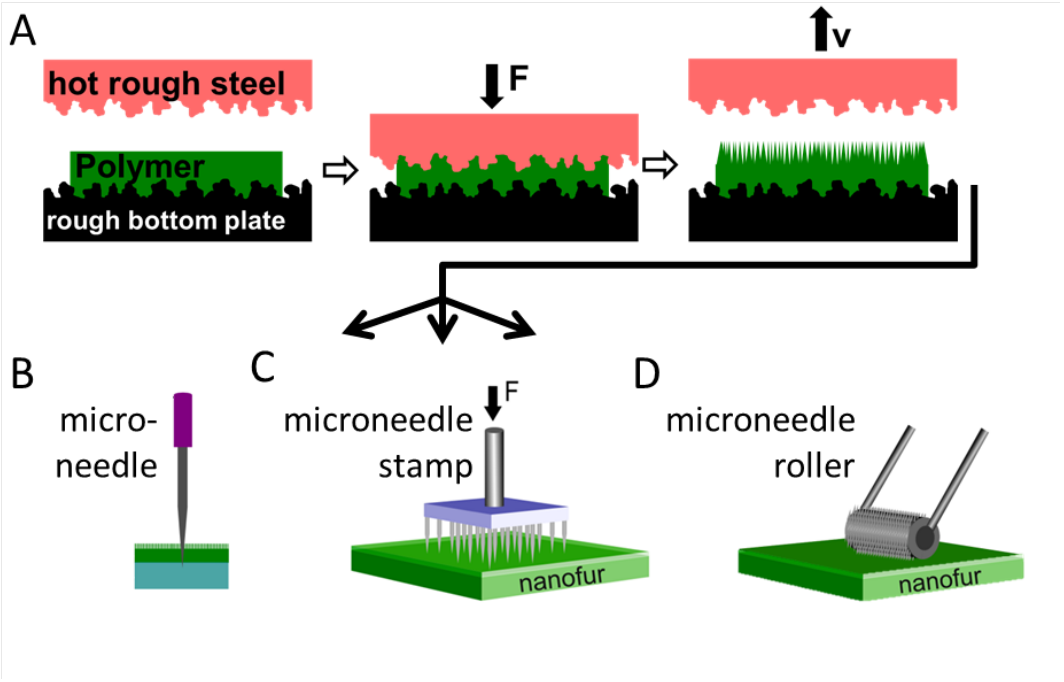

Figure 5.1: Schematic of the nanofur membrane fabrication process. **A)** A polymer film is fixed to the bottom plate and a sandblasted steel plate is heated and pressed into the polymer film. The softened polymer penetrates into the roughness of the heated plate and, after plate retraction, micro- and nanohairs are pulled from the film surface. Nanofur can be perforated with **B)** micro needles, **C)** a microneedle stamp, or **D)** a micro roller to create a porous membrane.

"water-removing" membranes, on the contrary, separate water by retaining the oil while water penetrates through the membrane. Underwater superoleophobicity requires the combination of a hydrophilic surface chemistry and a microstructured surface. It is a result of the water infiltration into the surface structure of the hydrophilic material and, thus, causes a decrease in the oil/solid contact area. [133, 139] The selection of the membrane type depends on the application. Oil-removing filters are typically used for oil purification and separation of heavy oil/water mixtures, in which water has a lower density compared to oil. [133–135, 139] Water-removing membranes are advantageous for light oil/water filtration processes, wastewater treatment, and other water purification processes. Such membranes are characterized by a reduced oil/solid contact area, which minimizes the risk of fouling and results in an increased membrane lifetime. [133, 134, 139]

A wide range of oil-removing and water-removing filtration materials has been developed in recent years, based on metallic meshes, textiles, fabrics, polymeric membranes, and filter papers. [133] Methods commonly used to achieve special wetting properties of oil- or water-removing membranes are a chemical modification such as the oxidization of the membrane material, and the deposition of coatings on the membrane surface. [29] Coating materials include polymers (polytetrafluorethylene, hydrogels), metal compounds ($Cu(OH)_2$, ZnO, nickel stearate), and various nanoparticles. [29, 37, 140–161] In contrast to superhydrophobic oil-removing membranes and underwater superoleophobic water-removing membranes, membrane materials with switchable wetting properties allow the selective separation of

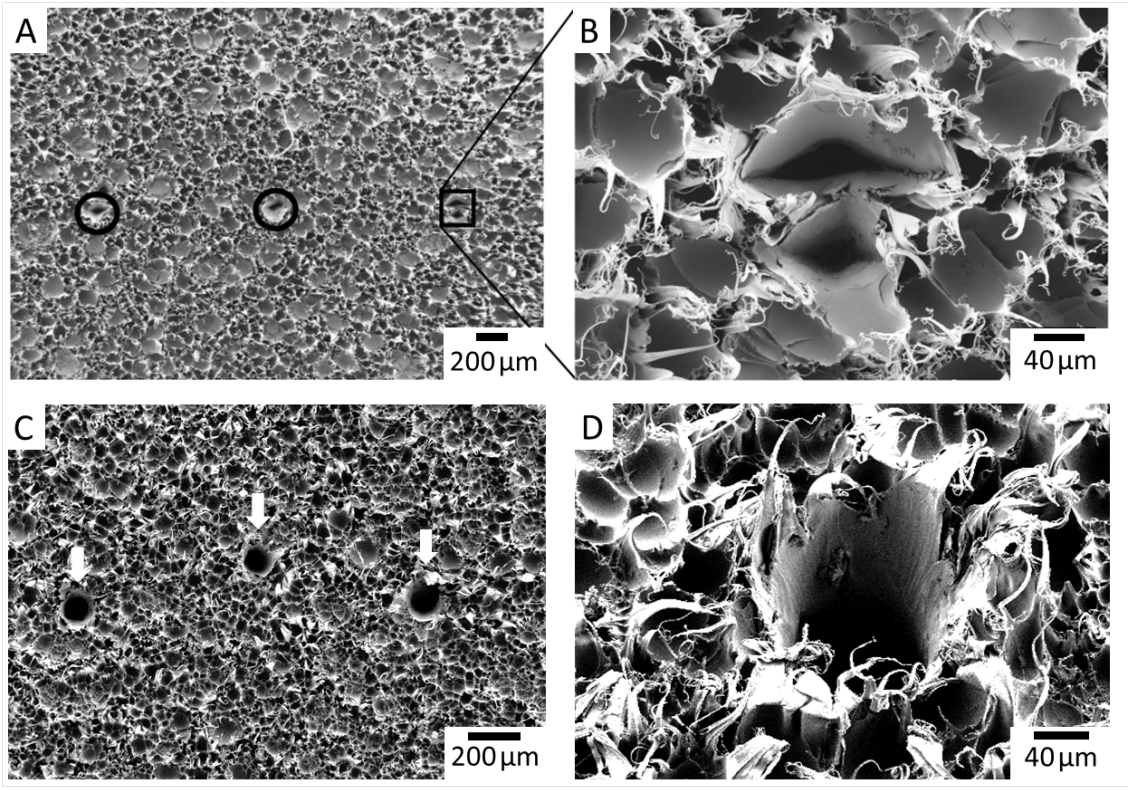

Figure 5.2: SEM images of the porous nanofur membrane fabricated with a microneedle roller and with a microneedle stamp. **A)** Overview showing four pores fabricated with a microneedle roller, indicated by black circles. **B)** Detailed view of two pores fabricated with a microneedle roller. Pores fabricated with the microneedle roller have a rhombic shape. **C)** Overview showing three pores fabricated with a microneedle stamp marked with an arrow and **D)** detailed view of a single pore. Pores fabricated with the microneedle stamp have a round shape with an average pore diameter of 80 ± 25 µm.

either oil or water from oil/water mixtures. Stimuli-responsive materials switch their wetting behavior in response to a change in an external stimulus such as temperature, electric or magnetic field. [138, 162–165] Other membrane materials with switchable properties require prewetting with either oil or water, and change their wetting properties in response to the prewetting liquid. [139, 166–168] However, most existing materials can separate only one of the two liquids (oil or water), and the development of environmentally friendly porous membranes, which enable selective separation of both liquids and can be fabricated on large scale, still remains a challenge. [133]

The nanofur membranes presented in this chapter can separate both oil and water from oil/water mixtures in a continuous filtration process. Pores were perforated in nanofur films with single microneedles, microneedle stamps, or microneedle rollers. The as-prepared porous membrane is superhydrophobic/superoleophilic and allows oil to penetrate through its pores while retaining water. It efficiently removes oil from oil/water mixtures in filtration processes. Additionally, the oil-removing porous nanofur can be converted into an underwater superoleophobic water-removing filter by plasma treatment, resulting in the removal of water from oil/water mixtures.

5.2 Methods and Materials for Oil/Water Filtration with Microperforated Nanofur

Porous nanofur membranes were fabricated from PE, PP, and PC. PE and PP nanofur is fabricated as described in Ch. 4.1, using the nanofur fabrication process introduced by Röhrig *et al.* [16] with adapted process parameters. For the fabrication of PC nanofur membranes, the thin nanofur fabrication process as described by Vüllers *et al.* [15] (see Ch. 2.2.5) is used. The nanofur fabrication is followed by a perforation step to fabricate pores (Fig. 5.1). The nanofur is perforated by manually punching pores with a microneedle stamp (Edvers, Germany, 32 microneedles) or microneedles with different diameters (100 µm, 120 µm (SEIRIN Co. Ltd., Japan), 160 µm (Phoenix Medical Ltd., United Kingdom), 450 µm (B. Braun Melsungen AG, Germany)). Alternatively, a microneedle roller (Sodacoda GmbH, Germany) is used for the efficient fabrication of high amounts of pores. SEM images of the porous nanofur membrane are presented in Fig. 5.2. They reveal that there is no significant change in the nanofur surface structure surrounding the pores compared to the original nanofur. Pores fabricated using single microneedles or microneedle stamps are round and their average diameter is smaller than the diameter of the microneedles. This is due to the creeping and stress relaxation effects occurring in polymers after punching holes with cold needles. In contrast, holes punched by the microneedle roller are not round but rhombic because of the small diameter of the microneedle roller and the non-round shape of the needles. The microneedle stamp is the method of choice for most experiments presented in this chapter. Single needles are less efficient and were used when variations in pore diameter were required, as microneedle stamps are available only with one specific needle diameter. The microneedle roller is most efficient for a high quantity pore fabrication, but neither pore size nor pore number can be controlled.

The nanofur surface is superhydrophobic with a typical water contact angle WCA $> 150°$ (Fig. 5.7a), and is superoleophilic with an OCA close to $0°$. [90] Due to these wetting properties, membranes fabricated from the as-prepared nanofur are oil-removing. In order to fabricate water-removing membranes, the wetting properties of as-prepared membranes are inverted to underwater superoleophobic by an argon plasma treatment step, which is performed using a reactive ion etch system (Sentech GmbH, Germany) at 0.2 mbar and 30 W for 120 seconds. The plasma treated nanofur (p-nanofur) is stored in water to ensure the long-term stability of its wetting properties by preventing hydrophobic recovery. [90] Experiments presented in this chapter were carried out by and in collaboration with Jana Kumberg as part of her master's thesis [169], plasma treatment was carried out by Uwe Köhler (IMT, Karlsruhe Institute of Technology).

5.3 Results and Discussion

5.3.1 Oil-Removing Membrane

The oil-removing nanofur membrane is superoleophilic and superhydrophobic in air with a typical WCA of $165°$. Besides superhydrophobicity in air, under oil superhydrophobicity is crucial for oil-removing membranes to prevent water from penetrating through the pores once the oil reaches the surface. In contrast to many superhydrophobic materials, which lose their superhydrophobic properties when in contact with oil [170], nanofur is

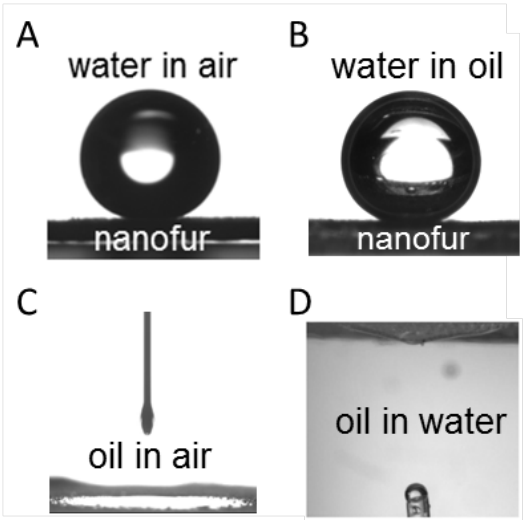

Figure 5.3: Water wetting behaviour of porous nanofur in air and in oil (hexane). Nanofur is superhydrophobic both in air **(A)** and in oil **(B)** with a typical WCA above 150°. Also, nanofur is superoleophilic both in air **(C)** and in water **(D)**.

superhydrophobic in oil, as can be seen in Fig. 5.3 and Fig. 5.4. In particular the low water roll-off angles both in air and in oil ensure that water droplets do not infiltrate the nanofur structure and therefore do not penetrate through the pores of the nanofur membrane.

The ability of the nanofur membrane to separate oil from an oil/water mixture is demonstrated in Fig. 5.5. The bottle opening of a vial is sealed with a PP nanofur membrane, into which pores were punched with a microneedle stamp. The vial is tilted a few degrees and droplets of oil (colored red) and water (colored blue) are simultaniously dispensed on the nanofur membrane. [171] While oil is soaked up by the nanofur surface and penetrates through the pores to be collected in the inside of the vial, water droplets roll off the nanofur membrane and are collected in a petri dish. This experimental setup proves that nanofur membranes are capable of separating oil from oil/water mixtures. Due to the low throughput and the inefficiency of this setup it however does not qualify for large scale oil/water separation.

As oil and water are immiscible liquids and as most oils have a lower density than water, oil and water barely mix, and oil normally floats on top of the water phase. In a simple experimental setup where an oil/water mixture is poured on top of the membrane, the membrane is blocked by a water layer and the oil can not touch the membrane surface and therefore not penetrate through the pores. Alternative experimental setups such a as coffee filter bag like membrane [172], a boat swimming on the surface of the liquid mixture [144], or a tilted setup [148, 173, 174] are more suitable for an experimental verification. In Fig. 5.6, a PP nanofur membrane with pores punched using a microneedle stamp is fixed in a tilted tube. The structured surface of the nanofur membrane faces upwards. The upside part of the tube is filled with a hexane/water mixture. The tilting angle and the maximum amount of water need to be chosen according to the diameter of the tube in a way that both water and oil touch the membrane surface. While oil penetrates through the membrane, the water is retained, which confirms that nanofur can separate oil/water mixtures.

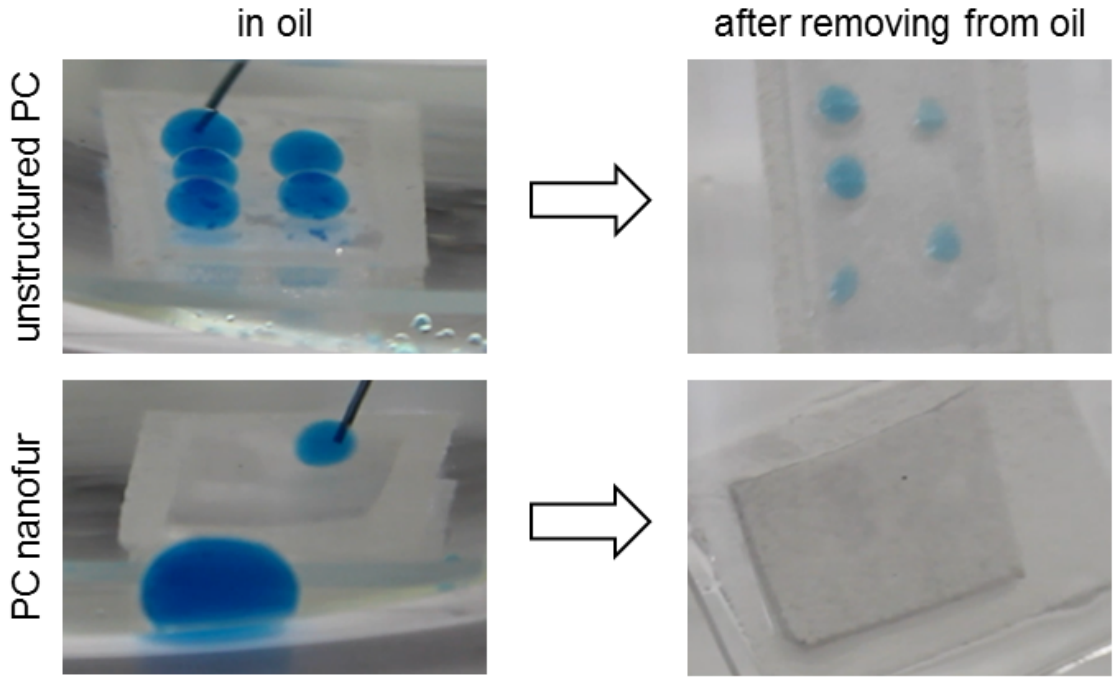

Figure 5.4: Water wetting behavior of porous nanofur in oil. Flat PC (top) and PC nanofur (bottom) in oil (hexane). Water droplets (colored blue) are dispensed on the surfaces. The water droplets stick to flat PC. In contrast, they roll off the nanofur surface. After both surfaces were removed from the oil, water droplets are visible on the flat PC, whereas no water can be observed on the nanofur, which indicates the under oil superhydrophobicity of the nanofur surface.

For an efficient large volume separation of oil from oil/water mixtures using oil-removing membranes, however, a different setup with a pressure driven separation is required, and the high water breakthrough pressure ΔP_{B} is a crucial parameter. ΔP_{B} indicates the maximum water column height which can be retained by the membrane. [135] To evaluate the ability of the porous superhydrophobic nanofur to retain water, and to study the influence of the pore diameter on ΔP_{B}, the breakthrough pressure of the nanofur membranes with different pore sizes was measured and compared. The porous membrane was sealed between two vertical tubes and pressure was applied to its surface by continuously increasing the height of a water column (Fig. 5.7a). The breakthrough pressure was calculated from $\Delta P_{\mathrm{B}} = \rho g h_{\mathrm{max}}$, where ρ is the density of water, g is the gravitational acceleration and h_{max} is the maximum height of the water column the membrane can support. [136] The water column height h_{max} was measured for membranes perforated with microneedles with different diameters (100 µm, 120 µm, 160 µm, 450 µm) and the microneedle stamp. The resulting pore diameters were determined from SEM images using ImageJ software [119]. Experimental results shown in Fig. 5.7b demonstrate the influence of pore diameters on ΔP_{B}. As predicted by theory, smaller pore diameters result in a higher breakthrough pressures. For example, nanofur with 90 ± 19 µm pores retains a water pressure of 2000 ± 186 Pa ($n = 4$), whereas pores with a diameter of 426 ± 16 µm retain only 477 ± 158 Pa ($n = 4$). The average diameter of pores fabricated with the microneedle stamp is 80 ± 25 µm and ΔP_{B} of these membranes is 1750 ± 197 Pa.

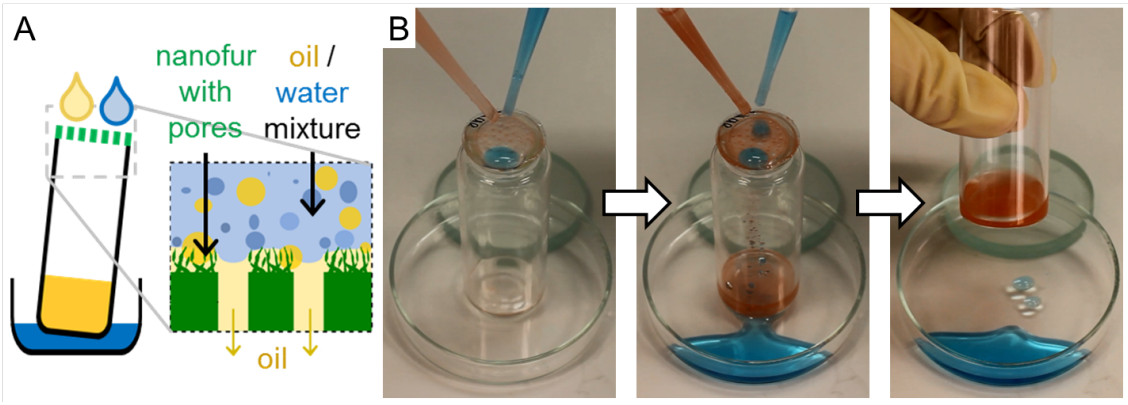

Figure 5.5: Oil/water filtration with a PC nanofur membrane with no pressure. **A)** Schematic of the experimental setup. A glass bottle (vial) is sealed with a porous nanofur membrane which selectively lets oil pass through the pores. **B)** Droplets of oil (n-hexane, colored red) and water (colored blue) are simultaneously dispensed on the nanofur membrane. Oil is soaked up by the nanofur surface and penetrates through the pores to be collected inside the vial. Water, in contrast, rolls of the tilted nanofur surface and is collected in a petri dish outside of the bottle.

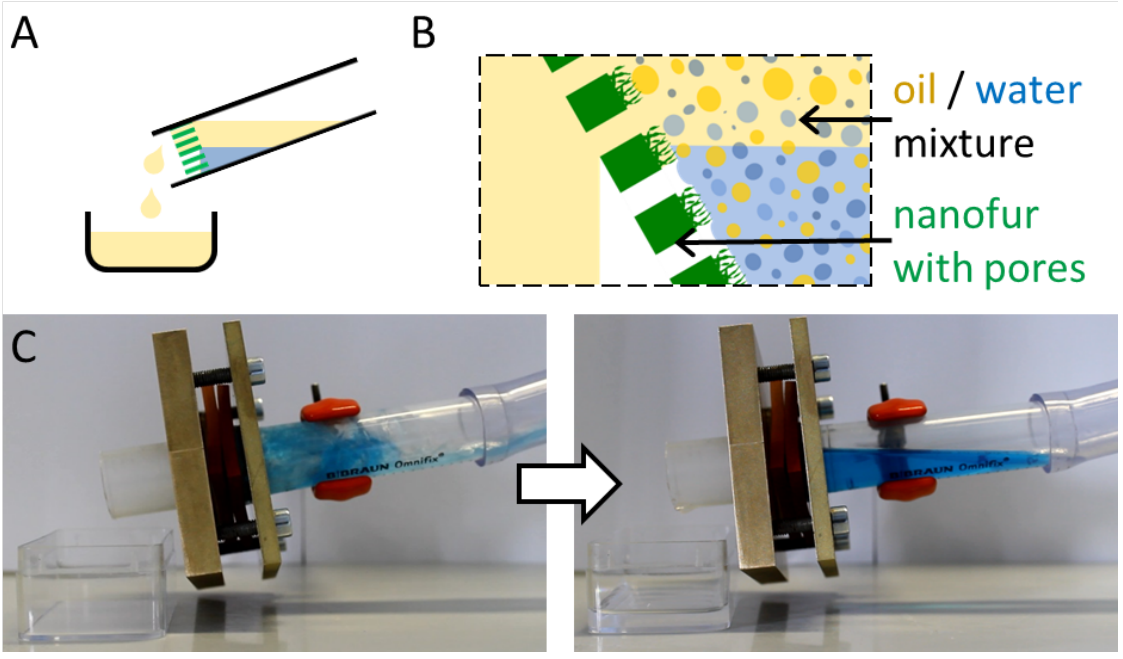

Figure 5.6: Oil/water filtration with PP nanofur membrane in a tilted tube. **A)** Sketch of the experimental setup and **B)** schematic view of nanofur inside the tube. **C)** The nanofur membrane is fixed in a tube with the structured surface facing upwards, and the tube is fixed in a tilted position. The upper part of the tube is filled with a hexane/water mixture. Tilting angle and maximum amount of water need to be chosen according to the diameter of the tube in a way that both water and oil touch the membrane surface. While oil (n-hexane, clear liquid) penetrates through the membrane, water (colored blue) is retained, which confirms that nanofur can separate oil/water mixtures.

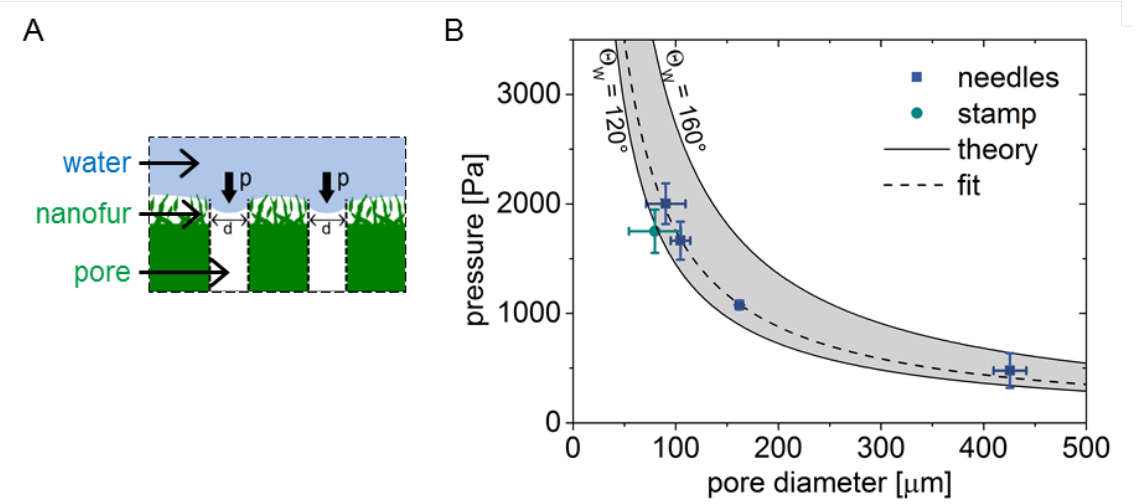

Figure 5.7: Water breakthrough pressure (ΔP_B) of superhydrophobic oil-removing nanofur membranes in air. **A)** Schematic of ΔP_B measurements on porous nanofur. **B)** Experimental ΔP_B as a function of the pore diameter. Pores with different diameters were fabricated using microneedles and a microneedle stamp. The theoretical ΔP_B for WCA ranging from 120° to 160° is indicated by the shaded area. The fitted curve (dashed line) corresponds to the WCA θ_W =127°. As predicted by theory, smaller pore sizes result in higher ΔP_B.

Next, experimentally measured breakthrough pressures of porous nanofur membranes are compared to the theoretical ΔP_B of hydrophobic membranes with cylindrical pores. ΔP_B is calculated using the Laplace-Young equation [136, 137, 175–177]

$$\Delta P_B = \frac{2\gamma \cdot |cos(\theta_W)|}{r}, \tag{5.1}$$

where θ_W is the WCA of the membrane surface, $\gamma_{water/air} = 72.8$ mN/m is the surface tension of the water-air interface and r is the pore radius. [178] As can be seen in Fig. 5.7b, the experimental measurements are in good agreement with the theory. Fitting the experimental ΔP_B values into Eq. (5.1) results in WCA $\theta_W = 127°$. The difference between this value and the measured WCA can be attributed to the variation in pore diameters and damage of nano- and microhairs at the pore edges. These results confirm that the breakthrough pressures of nanofur membranes depend on and are limited by the pore diameters. In practical applications, these limitation can be overcome by accordingly adapting the pore diameter. [135]

For effective oil/water filtration by an oil-removing porous membrane, water must be retained by the membrane in air as well as in oil. [179] ΔP_B measured on the nanofur membrane fabricated with the microstamp and pre-wetted with n-hexane is $\Delta P_{B,water/hexane} = 754 \pm 66$ Pa. According to Eq. (5.1), the lower value of ΔP_B of the membrane pre-wetted with hexane compared to the non-prewetted membrane is due to the lower surface tension of the water/hexane interface ($\gamma_{water/hexane} = 51$ mN/m) and the lower under oil WCA, compared to $\gamma_{water/air}$ of the water/air interface and the WCA in air.

The pressure-driven oil/water separation with oil-removing nanofur membranes is demonstrated in two ways utilizing two different experimental setups: One simple setup which

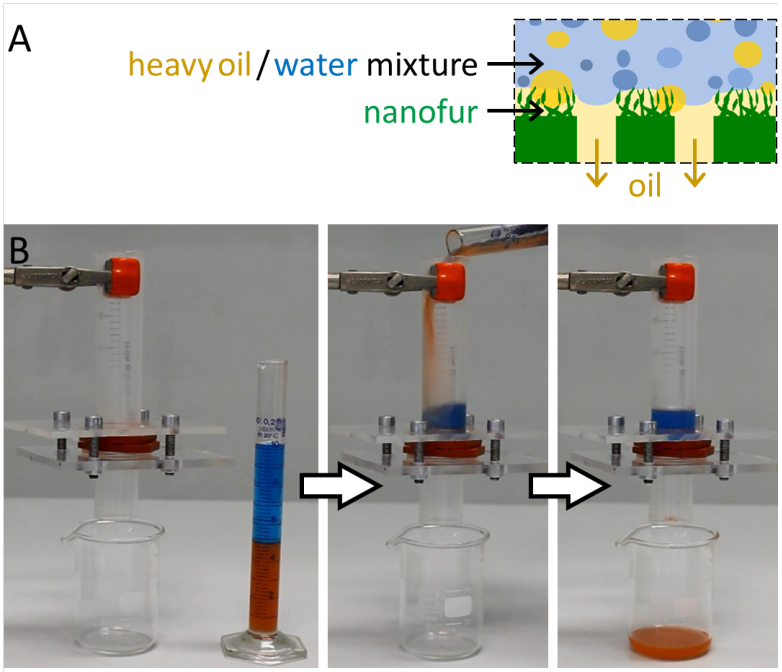

Figure 5.8: Heavy oil/water separation using an oil-removing nanofur membrane. **A)** Schematic of the heavy oil/water separation. As heavy oil has a higher density than water, water floats on top of the oil, and oil gets in contact with the nanofur membrane and penetrates through the pores. Water, in contrast, is retained. **B)** Nanofur is fixed in a pipe with the nanofur structure facing upwards. A mixture of water (colored blue) and oil (chloroforme, colored red) is poured on top of the nanofur membrane. Oil penetrates through the membrane and is collected in a beaker whereas water is retained and remains above the membrane.

is suitable only for heavy oil/water separation and a more complex U-pipe setup which allows the separation of an oil/water mixture with a lower oil density compared to the water density. A heavy oil/water separation is executed by fixing a PE nanofur membrane with pores punched using a microneedle stamp in a pipe and pouring a mixture of heavy oil (chloroforme) and water into the pipe. As heavy oil has a higher density compared to water, phase segregation causes the water to float on top of the oil. As a consequence, water does not form a layer on top of the membrane which blocks the filtration process. Rather, the oil touches the membrane, is soaked up by the nanofur structure, and penetrates through the pores. Once all oil penetrated through the membrane, the liquid flow stops, and the water is retained above the membrane, as presented in Fig. 5.8.

In addition, a porous PC nanofur membrane perforated with the microstamp was used to separate an n-hexane/water mixture in a filtration process. To overcome the limitation imposed by the lower density of hexane compared to water, an experimental setup in which the mixture is applied below the membrane (Fig. 5.9a) is used. It consists of a U-shaped tube in which the nanofur faces downwards. The pipe is filled with water and the water column height is used to pressurize the membrane with a pressure $\Delta P = \rho g \Delta h$ (with $\Delta P < \Delta P_{\mathrm{B,water/hexane}}$). Then the n-hexane/water mixture (1:1 (v/v)) is added under the membrane using a syringe (Fig. 5.9b). Due to its lower density, oil floats to the top and

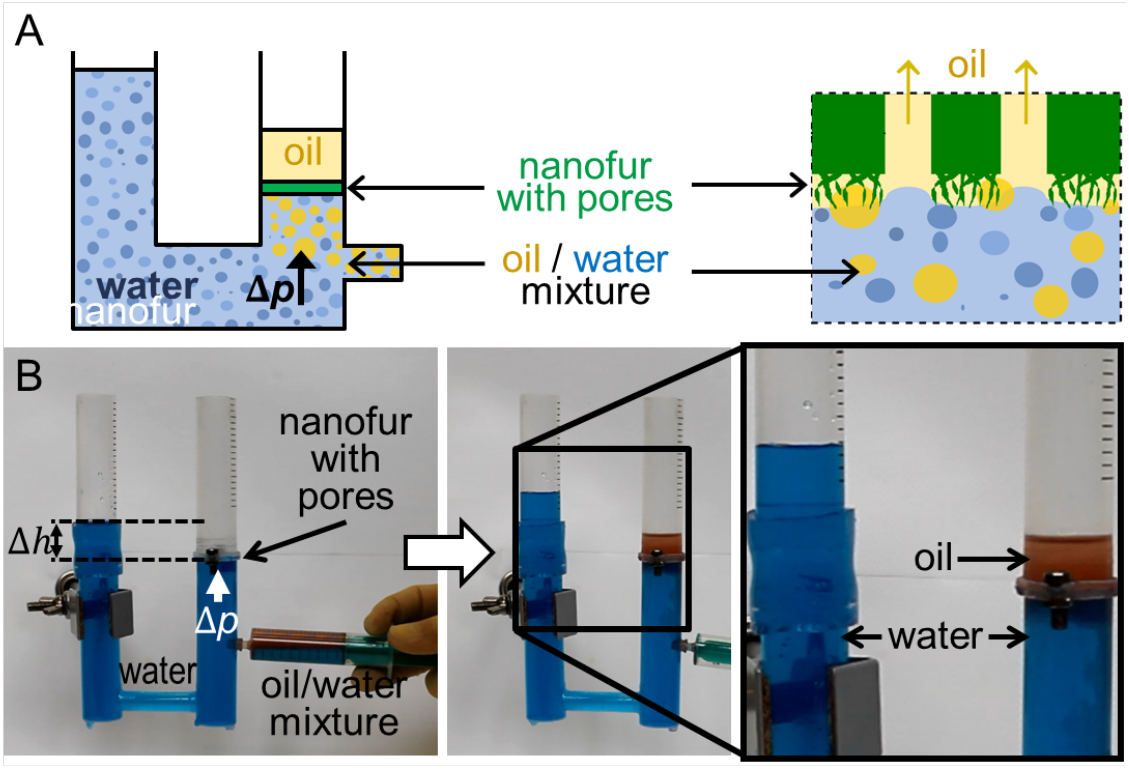

Figure 5.9: Oil/water separation using an oil-removing nanofur membrane. **A)** Schematic of the oil/water separation setup. **B)** The membrane is fixed in the right tube with the nanofur surface facing down. Pressure is applied through the water level. A hexane/water mixture is added under the membrane using a syringe. Oil penetrates through the pores while water is retained. No water is observed in the collected oil.

penetrates through the pores, while water is retained by the nanofur. The liquid flow stops when all oil is filtered through the nanofur, and no water is observed in the collected oil (Fig. 5.9b). The oil-removing membrane can be reused after washing it with isopropanol, which restores its wetting properties and oil absorption capacity (see Ch. 4.3.1). [90] The same quality of oil/water separation was achieved reusing it four times.

5.3.2 Water-Removing Membrane

To separate water from the oil/water mixture, a water-removing p-nanofur membrane was fabricated by argon plasma treatment of the as-prepared nanofur membrane. The comparison of SEM images of the nanofur before and after the argon plasma treatment did not reveal any changes of the surface topography (see Fig. 5.10a). The plasma treatment leads to the incorporation of hydrophilic carboxyl groups into the nanofur surface. The resulting increase in surface energy of the polycarbonate surface causes a reduced WCA and underwater superoleophobicity (see Fig 5.10b,c). [15, 90, 180, 181]

A high water permeability is an important parameter for efficient water-removing membranes. To characterize the water permeability of porous p-nanofur membranes, water flow rates through the membranes sealed between two tubes were measured. The porous p-nanofur membranes fabricated using the microstamp were used in this experiment ($n = 4$;

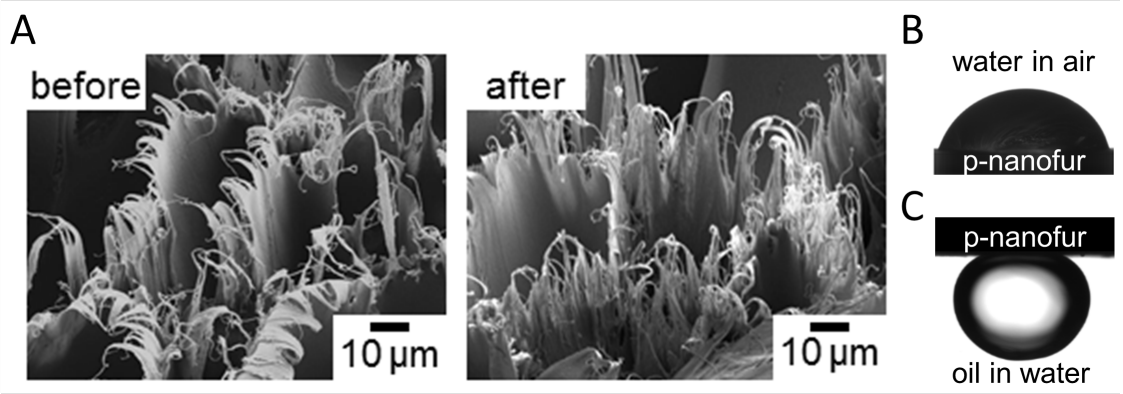

Figure 5.10: Surface topography of nanofur and of plasma treated nanofur (p-nanofur), and wetting behavior of plasma treated nanofur. **A)** SEM images of original nanofur before plasma treatment and of plasma treated nanofur (arbitrarily chosen areas of the same sample). The SEM images reveal no changes in the surface topography. **B)** The water droplet on p-nanofur with WCA $\approx 82°$ reveals hydrophilicity of the surface after plasma treatment. **C)** p-nanofur is underwater superoleophobic with OCA $\approx 152°$.

64 micropores with average pore diameter 83 ± 17 µm and pore length $t_{\mathrm{m}} \approx 168$ µm). The measured water flow rate depends linearly on the pressure, with a lower pressure resulting in a lower flow rate. In Fig. 5.11, experimental water flow rates are compared to theoretical flow rates calculated from

$$Q = \frac{\pi r^4 p \Delta P}{8 \eta t_m}, \tag{5.2}$$

where r is the pore radius, p is the number of pores, ΔP is the applied pressure, t_{m} is the pore length, and η is the water viscosity. [182] Experimental and theoretical results are in good agreement. According to the theory, membrane water flow rates can be further increased by increasing pore size, pressure, or number of pores.

When p-nanofur is submerged under water, oil droplets are repelled by the underwater superoleophobic surface with an underwater OCA of $\sim 152°$ and a roll-off angle below $5°$ (Fig. 5.10). [15, 90] The underwater superoleophobicity of p-nanofur is a result of the reduced contact between oil and solid due to water trapped in the surface micro- and nanostructures. [183] To separate water from the oil/water mixture, the water-removing porous p-nanofur membrane retains the oil while allowing the water to penetrate through, as schematically shown in Fig. 5.12a. To demonstrate this separation, a p-nanofur membrane was sealed between two tubes, and a mixture of crude oil (MiRO OK 679, Mineralölraffinerie Oberrhein, Germany) and water (1:1 (v/v)) is poured on the membrane. Water permeates through the porous p-nanofur membrane while oil is retained above (see Fig. 5.12b). No visible crude oil is observed in the collected water, demonstrating the high separation capability of the water-removing porous p-nanofur membrane. Due to the permeation of water and the reduced oil/membrane contact, the p-nanofur membrane is not contaminated by crude oil and can be reused several times for this process. The same separation results were observed after reusing the porous p-nanofur membrane up to four times.

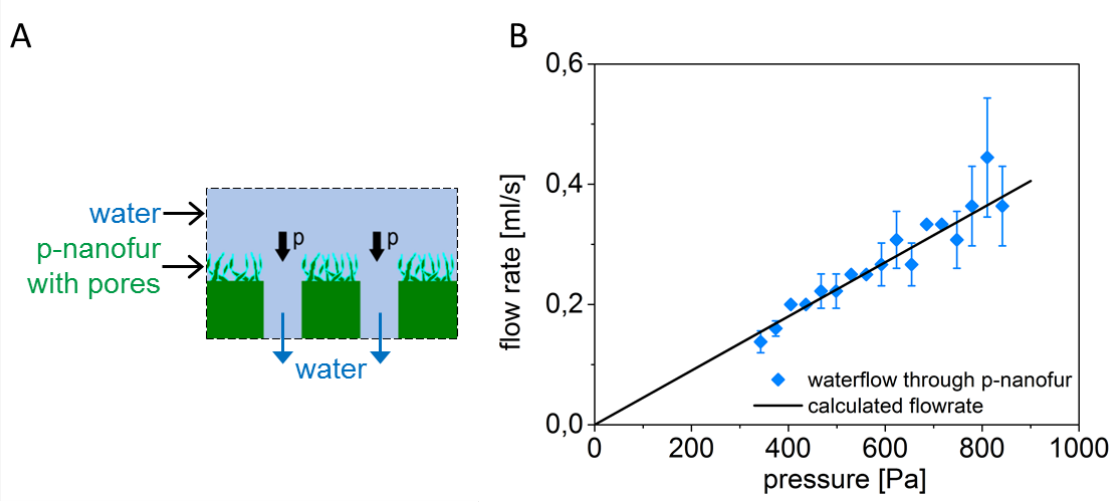

Figure 5.11: Demonstration of the water permeability of p-nanofur. **A)** p-nanofur is hydrophilic and water penetrates through the pores. **B)** The measured water flow rate through hydrophilic porous p-nanofur with 83 ± 17 µm pore diameter and 168 µm pore length is in agreement with the flow rate calculated with Eq. (5.2) ($p = 64$ micropores, $r = 41.5$ µm, $t_m = 168$ µm).

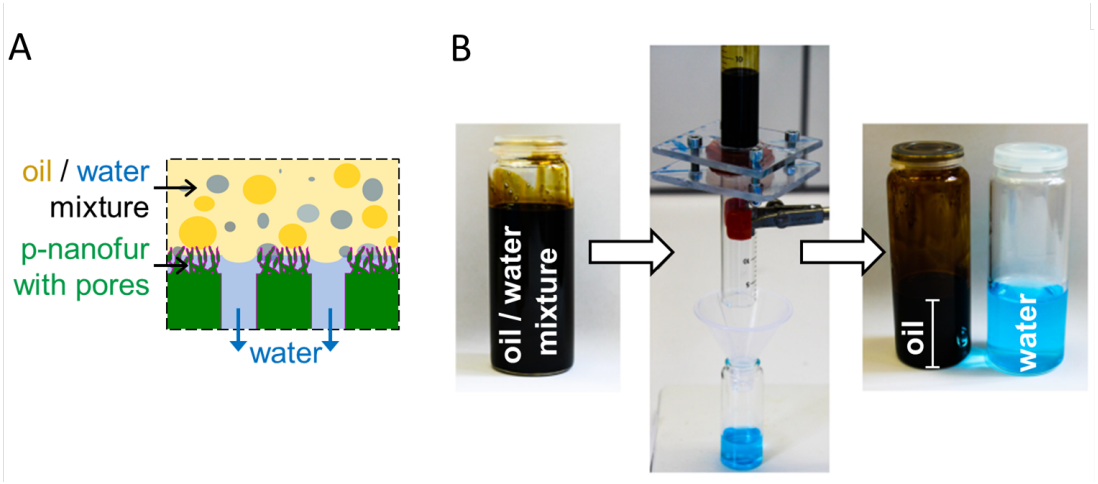

Figure 5.12: Oil/water separation using a water-removing p-nanofur membrane. **A)** Schematic of oil/water separation with p-nanofur. Hydrophilic and underwater superoleophobic p-nanofur allows water to penetrate through the pores and retains oil. **B)** Mixture of crude oil and water (colored blue) is separated using a p-nanofur membrane. The p-nanofur membrane is sealed between two tubes, and crude oil/water mixture is poured on top. Only water penetrates through the membrane and no crude oil is visible in the collected water.

5.4 Conclusions on Nanofur Membranes for Oil/Water Filtration

Selective separation of both oil and water from oil/water mixtures was demonstrated with porous nanofur membranes. Superhydrophobic oil-removing nanofur membranes are fabricated using the hot pulling technique followed by the perforation with microneedles. Underwater superoleophobic water-removing p-nanofur membranes were produced by an additional argon plasma treatment of the as-prepared nanofur membranes. Nanofur is one of the few membrane materials which allows selective separation of both oil and water from oil/water mixtures, whereas most membrane materials separate only one of the two liquids. Therefore, porous nanofur membranes can be used both for oil purification processes and in wastewater treatment technology. The control over the filtration fluid can also help to overcome separation efficiency limitations imposed by such oil properties as viscosity and density, and to reduce the membrane fouling by oil. Moreover, it was shown that smaller pore sizes lead to higher breakthrough pressures, but decrease the flow rate. The presented fabrication technique, in which pores are fabricated in the nanofur films by perforation with microneedles, allows the selection of the pore diameter and their number according to the specific requirements of the targeted separation process. Excellent performance, reusability, and adaptable separation properties make porous nanofur membranes a promising material for large scale industrial and environmental oil/water filtration applications.

A shortened version of this chapter was published as the article "Selective Filtration of Oil/Water Mixtures with Bioinspired Porous Membranes". Claudia Zeiger, Jana Kumberg, Felix Vüllers, Matthias Worgull, Hendrik Hölscher, Maryna Kavalenka: RSC Adv., 2017, ***7****, 32806.*

6. Summary and Outlook

The enormous worldwide consumption of oil and petroleum products leads to an increased risk of oil spillage and aquatic pollution. Although crude oil, which is commonly known as "black gold", is a naturally occurring product, it causes a massive negative impacts on the environment and on public health when spilled in unfavorable places. The search for environmental friendly and efficient oil absorption materials is challenging and most common oil sorption materials absorb considerable amounts of water in addition to oil. In contrast, materials with superhydrophobic properties repel water and ensure the selective absorption of oil from oil/water mixtures. The wetting behavior is quantified by contact angle measurement, with hydrophilic surfaces having a water contact angle below 90° and hydrophobic surfaces having a water contact angle above 90°. Surfaces are referred to as superhydrophobic when their water contact angle is at least 150°. While highest contact angles reached by smooth, unstructured surfaces are around 120°, superhydrophobicity always results from the combination of surface chemistry and surface structure.

In nature, superhydrophobicity prevents surfaces from getting wet or dirty, or leads to the retention of a stable air layer when dragged under water. Leaves of water fern *Salvinia* and water lettuce *Pistia stratiotes*, for example, achieve superhydrophobicity by their three-level hierarchical structure: Macroscopic trichomes with micro-size papillae are covered by nanoscale wax crystals. Water droplets roll off these plant leaves immediately, and even after having been submerged under water for hours or days, the leaves emerge completely dry. At the same time, these leaf surfaces are superoleophilic due to their wax surface. Similarly to the hairy oil absorbing legs of oil collecting bees, leaves of these water plants absorb huge amounts of oil. This absorption mechanism was studied in Ch. 3 by comparing the oil sorption capacity of leaves of different *Salvinia* species with different trichome types, as well as leaves of water lettuce and Lotus. The results reveal that leaves with trichomes absorb significantly more oil than leaves with no trichomes, and that not only the trichome height determines the oil absorption capacity, but also the trichome shape. Trichomes with connected tips lead to a higher oil sorption capacity compared to single standing trichomes. The increase in oil absorption capacity is due to connected trichomes offering better support of the oil/air interface whereas single trichomes break

through the interface. The latter leads to interstices between trichomes being partly not available for oil absorption and retention.

Leaves of the aquatic plants *Salvinia* and *Pistia stratiotes* serve as role model for biomimetic nanofur. Biomimetics is the idea of studying living nature and transferring its principles to human innovation. Famous examples are the hook-and-loop tape and the Lotus effect of self cleaning surfaces. The biomimetic polymeric nanofur surface is fabricated by hot pulling. Using a hot embossing machine, a heated sandblasted steel plate is pressed into the polymer surface. The surface melts and floats into the cavities of the rough mold. The retraction of the heated mold results in the elongation of the softened polymer and in the formation of nanofur. The polymeric surface is covered by a dense layer of a randomly distributed high aspect ratio hair-like structure with diameters in the micro- and nanometer range and a micro- to millimeter length. Similarly to its natural role models, nanofur is superhydrophobic and superoleophilic, and selectively absorbs oil from oil/water mixtures. A comparison of the oil absorption by a *Salvinia* leaf and nanofur is presented in Fig. 6.1. However, nanofur fabricated by the established hot pulling process has several issues. The serial fabrication of nanofur in a hot embossing machine leads to long cycle times, the sample size is limited by the maximum mold size. Also, nanofur as a single-use oil sorbent requires high material input and leads to increased disposal costs.

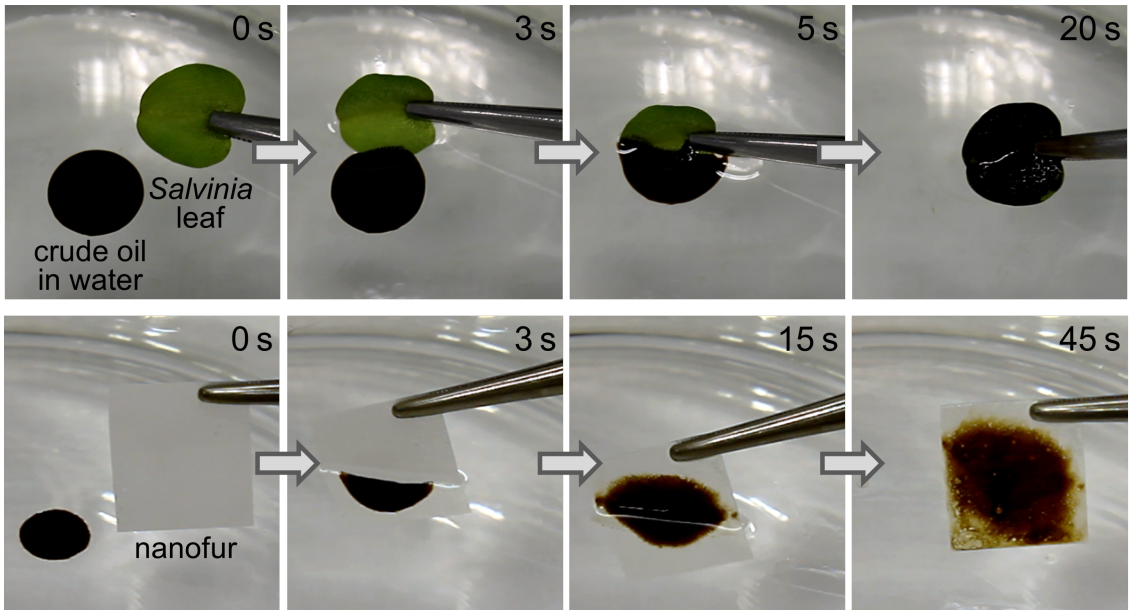

Figure 6.1: Oil absorption by a *Salvinia molesta* leaf (top) and by nanofur (bottom). Both polymeric nanofur and its natural role model *Salvinia molesta* selectively absorb oil from the water surface within seconds.

These challenges were addressed in this thesis and solutions were presented in Ch. 4. This includes the fabrication of nanofur from other polymers than polycarbonate such as polyethylene and polypropylene. Also, a cold pulling process was introduced, where the pulling of the nanofur surface is executed at a temperature significantly lower than the softening temperature of the polymer. Besides the possibility to fabricate a double-sided nanofur and various other advantages, this leads to the implementation of a roll-to-roll nanofur fabrication process. The continuous fabrication of nanofur leads to incomparably

shorter fabrication times and paves the way towards an industrial large-scale nanofur fabrication. Also, the resusability of nanofur was implemented by washing the nanofur with isopropanol. In addition, nanofur from the shape memory polymer Tecoflex® was developed to implement the reusability of the nanofur without the need of solvents. The shape memory effect allows to recover the nanofur structure after deformation. After oil absorption, the nanofur is temporarily flattened, which results in 95% of the absorbed oil being removed from the surface. After triggering the recovery of the nanofur structure by heat, the nanofur from Tecoflex® can be reused for oil absorption. Absorption, flattening, and recovering of the nanofur structure is repeated ten times with no significant change in the absorption capacity.

A promising alternative oil/water separation technique is the membrane-based filtration. The continuous mixture separation by filtration leads to a high separation capacity and a reduced material consumption compared to absorption. In Ch. 5, the nanofur was microperforated and implemented as a filter for continuous oil/water separation. Microperforation using microneedles, microneedle stamps, and microneedle rollers leads to porous nanofur with holes with diameters ranging from approximately 80 µm to 450 µm, depending on the diameter of the needles used for the perforation. Due to the superoleophilic and superhydrophobic properties of the nanofur surface, oil passes through the pores of the oil-removing nanofur membrane while the water is retained. The water breakthrough pressure as a characteristic property of membranes depends on the pore diameter, and experimental results are in good agreement with the theory. Oil-removing superhydrophobic nanofur membranes were converted into water-removing underwater superoleophobic membranes by a plasma treatment step. The plasma treated nanofur allows water to penetrate through the pores while the oil is retained. Water flow rates depend on the pore radius, the number of pores, the pore length, and the applied pressure. The experimental results are in good agreement with theoretical values. Finally, the performance of the plasma treated nanofur as a water-removing membrane was demonstrated by separating a crude oil/water mixture, with no visible leftover crude oil in the collected water.

All together the results presented in this thesis are a practical example for applied biomimetics. An overview over the addressed topics is presented in Fig. 6.2. Leaves of the *Salvinia* plant, which is a declared pest in many countries, qualify as natural oil sorbents. Collecting these plants could potentially be a cost efficient way to produce an environmentally friendly oil sorbent, as the leaves consist of bio-material and are biodegradable. However, an issue of the usage of fresh leaves for oil spill cleanup is that fresh leaves need to be regionally available at any time. Drying the leaves, in contrast, allows the storage of leaves as a natural oil sorbent. For drying, techniques such as air drying or vacuum drying can be implemented, as well as freeze-drying, which is a common process in food industry. As the ventral side of *Salvinia* leaves is hydrophilic when dried, coating the ventral side with a hydrophobic substance would reduce or avoid the absorption of water. *Pistia stratiotes* leaves, in contrast, remain superhydrophobic on both dorsal and ventral side even after drying. As leaves of both plants are highly biodegradable, a special storage solution would be required. Another challenge linked to the usage of a natural oil sorbent is that the production time is determined by nature. Also, *Salvinia* plants preferably grow in the tropical and subtropical parts of the world.

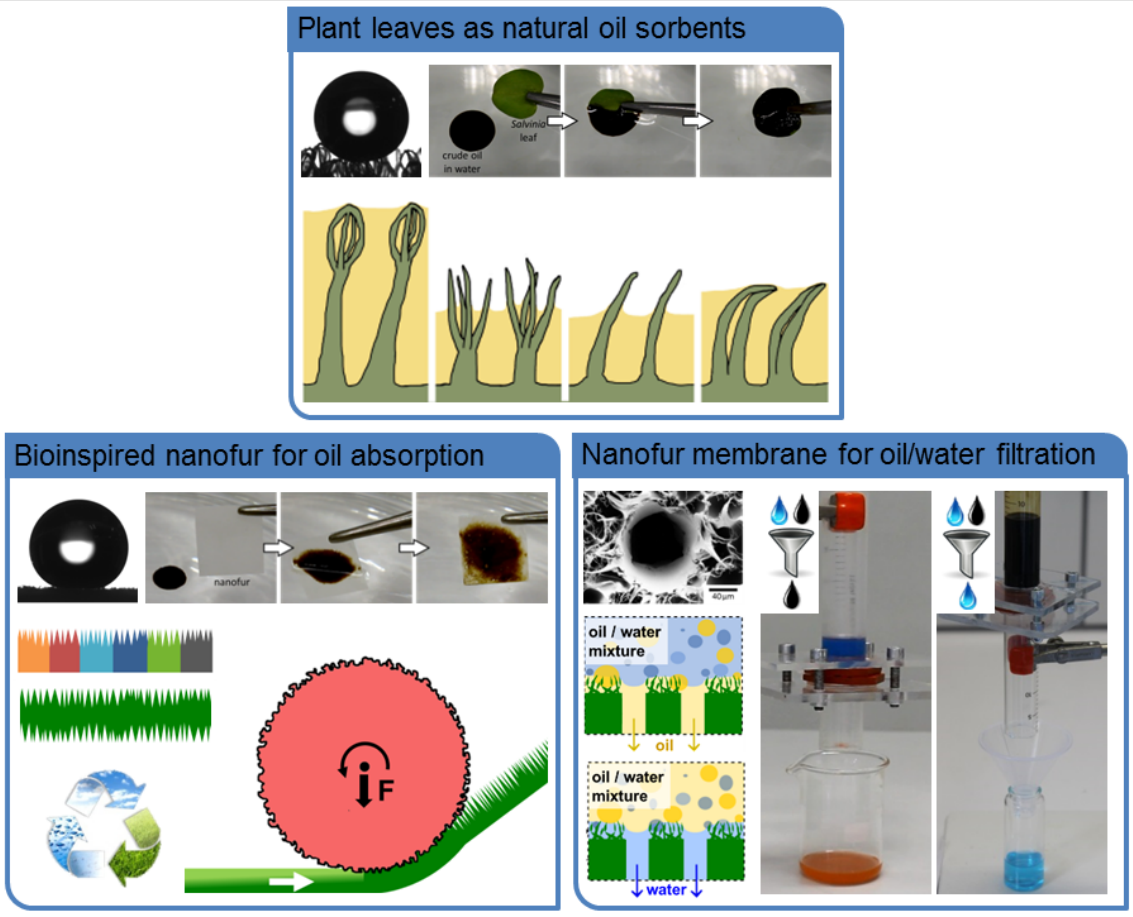

Figure 6.2: Summary of this thesis. Leaves of the water fern *Salvinia* achieve superhydrophobicity and superoleophilicity by the combination of their surface chemistry and their three-level hierarchical surface structure. They absorb large amounts of oil, and the absorption mechanism was studied in Ch. 3 by comparing oil sorption capacity of leaves of different *Salvinia* species with different trichome types. The results reveal that not only the trichome length determines oil absorption capacity, but also the trichome shape. *Salvinia* leaves are a role model for bioinspired polymeric nanofur, which also selectively absorbs huge amounts of water. Various enhancements of nanofur for oil absorption are presented in Ch. 4 of this thesis. This includes the fabrication of nanofur from PE, PP, and other polymers, and an increase of efficiency by reusing nanofur. Also, a cold pulling process was introduced, where pulling of the nanofur surface is executed at a temperature significantly lower than the softening temperature of the polymer. This enables the fabrication of double sided nanofur and leads to the implementation of a roll-to-roll nanofur fabrication process, which paves the way towards the industrial mass production of nanofur. A promising alternative oil/water separation technique is membrane-based filtration which is presented in Ch. 5. Continuous mixture separation by filtration leads to a high separation capacity and reduced material consumption compared to absorption. Both oil and water were selectively filtrated using nanofur membranes and plasma treated nanofur membranes.

These challenges are solved by the bioinspired nanofur. The polymeric micro- and nanostructured foil is resistant towards changes in temperature and humidity, and can therefore be stored under various conditions. Also, it can potentially be fabricated in large quantities within a short time period once the nanofur fabrication process on a roll-to-roll machine is industrially implemented. On the other hand, the polymeric nanofur consists of polymers which implies that petroleum is used for its fabrication. Also, most common polymers are not biodegradable and become waste after usage. Reusable nanofur and nanofur filters significantly reduce both the raw material input and the amount of waste.

For the absorption of one liter of oil, an average of 2 m^2 to 2.5 m^2 of polymeric nanofur is needed. In comparison, 1.3 m^2 *Salvinia molesta* leaves are sufficient, which corresponds to 270 g. Using *Pistia stratiotes* leaves as natural oil sorbents, 570 g of fresh leaves would be needed, or 100 g dried leaves. Öl-Ex, a widely and commercially used oil sorbent, is significantly less efficient, as approximately 4.5 kg are required to absorb one liter of oil. This depicts the high absorption capacity of nanofur. The required amounts of different sorption materials are illustrated in Fig. 6.3. To further reduce the nanofur material input, nanofur can be reused after oil absorption, or nanofur filters can be used. To separate one liter of oil from an oil/water mixture by filtration, a few square centimeters would suffice. In summary, the results presented in this thesis confirm that human innovations can take advantage of the biomimetic idea to transfer principles of the living nature, that have been optimized by evolution over millions of years, to technical applications.

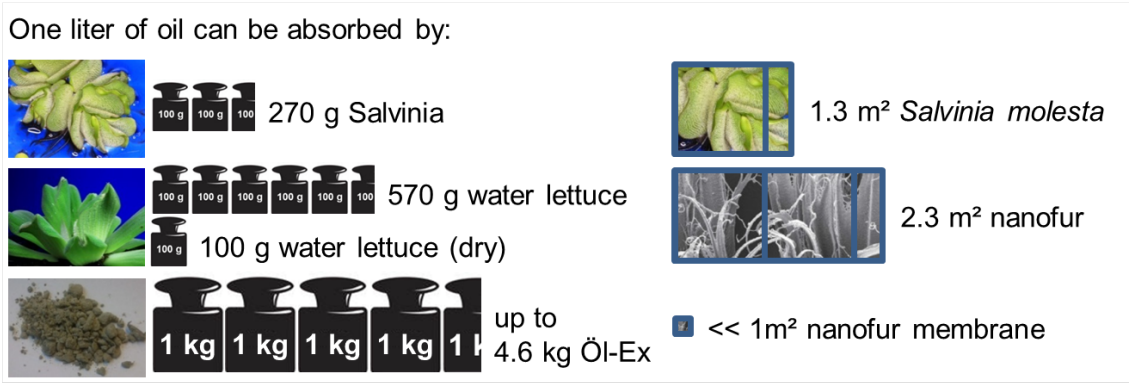

Figure 6.3: Comparison of approximately required amounts of sorbent materials for the absorption of one liter of oil. 270 g leaves of *Salvinia molesta* or 570 g leaves of *Pistia stratiotes* (water lettuce) have an oil absorption capacity of 1 L. When water lettuce is dried, the required amount of leaves weighs only 100 g. The commercial oil sorbent Öl-Ex is significantly less efficient and 4600 g are needed to absorb the same amount of oil. The surface area needed to absorb 1 L oil is 1.3 m^2 of *Salvinia molesta* leaf surface, or an average of 1.3 m^2 of nanofur foil. When an oil/water mixture is separated by filtration rather than absorption, the required amount of nanofur is drastically reduced and is well below 1 m^2.

List of Figures

Bibliography

[1] SCOPE Stanford Medicine. scopeblog.stanford.edu, 03/03/2018.

[2] Nature. nature.com, 03/03/2018.

[3] Charles Darwin. *On the Origin of Species by Means of Natural Selection, or the Preservation of Favoured Races in the Struggle for Life.* London: John Murray, 1859.

[4] W. Barthlott, M. Mail, and C. Neinhuis. Superhydrophobic hierarchically structured surfaces in biology: evolution, structural principles and biomimetic applications. *Phil. Trans. R. Soc. A*, 374:20160191, 2016.

[5] C. G. Bernhard. Structural and functional adaptation in a visual system. *Endeavour*, 26:79–84, 1967.

[6] D. G. Stavenga, S. Foletti, G. Palasantzas, and K. Arikawa. Light on the moth-eye corneal nipple array of butterflies. *Proc. R. Soc. B*, 273:661–667, 2006.

[7] H. Schmitz, A. Schmitz, and Horst Bleckmann. A new type of infrared organ in the australian "fire-beetle" *merimna atrata* (coleoptera: Buprestidae). *Naturwissenschaften*, 87(12):542–545, 2000.

[8] Tobias Mainz, Anke Schmitz, and Helmut Schmitz. Variation in number and differentiation of the abdominal infrared receptors in the Australian "fire-beetle" *merimna atrata* (coleoptera, buprestidae). *Arthropod Struct Dev.*, 33:419–430, 2004.

[9] Brian Dean and Bharat Bhushan. Shark-skin surfaces for fluid-drag reduction in turbulent flow: a review. *Philos. Trans. Royal Soc. A*, 368:4775–4806, 2010.

[10] John Davenport, Roger N. Hughes, Marc Shorten, and Poul S. Larsen. Drag reduction by air release promotes fast ascent in jumping emperor penguins - a novel hypothesis. *Marine Ecology Progress Series*, 430:171–182, 2011.

[11] Gregory D. Bixler and Bharat Bhushan. Fluid drag reduction and efficient self-cleaning with rice leaf and butterfly wing bioinspired surfaces. *Nanoscale*, 5:7685–7710, 2013.

[12] Wilhelm Barthlott, Matthias Mail, Bharat Bhushan, and Kerstin Koch. Plant surfaces: Structures and functions for biomimetic innovations. *Nano-Micro Letters*, 9(2):23, 2017.

[13] Jangsun Hwang, Yoon Jeong, Jeong Min Park, Kwan Hong Lee, Jong Wook Hong, and Jonghoon Choi. Biomimetics: forecasting the future of science, engineering, and medicine. *Int. J. Nanomedicine*, 10:5701–5713, 2015.

[14] M. N. Kavalenka, F. Vüllers, S. Lischker, C. Zeiger, A. Hopf, M. Röhrig, B. E. Rapp, M. Worgull, and H. Hölscher. Bioinspired air-retaining nanofur for drag reduction. *ACS Appl. Mater. Interfaces*, 7(7):10651–10655, 2015.

[15] F. Vüllers, G. Gomard, J. B. Preinfalk, E. Klampaftis, M. Worgull, B. Richards, H. Hölscher, and M. N. Kavalenka. Bioinspired superhydrophobic highly transmissive films for optical applications. *Small*, 12(44):6144–6152, 2016.

[16] M. Röhrig, M. Mail, M. Schneider, H. Louvin, A. Hopf, T. Schimmel, M. Worgull, and H. Hölscher. Nanofur for biomimetic applications. *Adv. Mater. Interfaces*, 1(4):1300083, 2014.

[17] Dorota Wolicka and Andrzej Borkowski. *Introduction to Enhanced Oil Recovery (EOR) Processes and Bioremediation of Oil-Contaminated Sites*. InTech, 2012.

[18] John Whitfield. How to clean a beach. *Nature*, 422:464–466, 2003.

[19] Ian R. MacDonald, Daniel M. Kammen, and Maohong Fan. Science in the aftermath: investigations of the DWH hydrocarbon discharge. *Environ. Res. Lett.*, 9:125006, 2014.

[20] Michel C. Boufadel and Xiaolong Geng. A new paradigm in oil spill modeling for decision making? *Environ. Res. Lett.*, 9:081001, 2014.

[21] Gianna Bern. *Investing in Energy: A Primer on the Economics of the Energy Industry*. John Wiley & Sons, 2011.

[22] Joseph H. Tarnecki and William F. Patterson. Changes in red snapper diet and trophic ecology following the Deepwater Horizon oil spill. *Marine and Coastal Fisheries*, 7:135–147, 2015.

[23] Marcia K. McNutt, Rich Camilli, Timothy J. Crone, George D. Guthrie, Paul A. Hsieh, Thomas B. Ryerson, Omer Savas, and Frank Shaffer. Review of flow rate estimates of the Deepwater Horizon oil spill. *Proceedings of the National Academy of Sciences*, 109(50):20260–20267, 2012.

[24] Timothy D. Bowman, Philip F. Schempf, and Jeffrey A. Bernatowicz. Bald eagle survival and population dynamics in Alaska after the "Exxon Valdez" oil spill. *The Journal of Wildlife Management*, 59(2):317–324, 1995.

[25] ITOPF. itopf.com, 03/03/2018.

[26] Dara O'Rourke and Sarah Connolly. Just oil? The distribution of environmental and social impacts of oil production and consumption. *Annu. Rev. Environ. Resour.*, 28:587–617, 2003.

[27] Samantha B. Joye. Deepwater Horizon, 5 years on. *Science*, 349(6248):592–593, 2015.

[28] Mark Schrope. Oil spill: Deep wounds. *Nature*, 472:152–154, 2011.

[29] Chee Huei Lee, Bishnu Tiwari, Dongyan Zhang, and Yoke Khin Yap. Water purification: oil-water separation by nanotechnology and environmental concerns. *Environ. Sci.: Nano*, 4:514–525, 2017.

[30] Despina Fragouli and Athanassia Athanassiou. Oil spill recovery: Graphene heaters absorb faster. *Nat. Nanotech.*, 12(5):406–407, 2017.

[31] WGCU. wgcu.org, 03 03/03/2018.

[32] tricycle. tricycle.org, 03/03/2018.

[33] The Hill. thehill.com, 03/03/2018.

[34] M.O. Adebajo, R.L. Frost, J.T. Kloprogge, O. Carmody, and S. Kokot. Porous materials for oil spill cleanup: A review of synthesis and absorbing properties. *J. Porous Mat.*, 10(3):159–170, 2003.

[35] B. Bhushan. *Biomimetics - Bioinspired Hierarchical-structured Surfaces for Green Science and Technology.* Springer International Publishing Switzerland, 2016.

[36] H. M. Chol and R. M. Cloud. Natural sorbents in oil spill cleanup. *Environ. Sci. Technol.*, 26:772–776, 1992.

[37] Lin Feng, Zhongyi Zhang, Zhenhong Mai, Yongmei Ma, Biquian Liu, Lei Jiang, and Daoben Zhu. A super-hydrophobic and super-oleophilic coating mesh film for the separation of oil and water. *Angew. Chem. Int. Ed.*, 116(15):2046–2048, 2004.

[38] Anish Tuteja, Wonjae Choi, Minglin Ma, Joseph M. Mabry, Sarah A. Mazzella, Gregory C. Rutledge, Gareth H. McKinley, and Robert E. Cohen. Designing superoleophobic surfaces. *Science*, 318:1618–1622, 2007.

[39] Philip S. Brown and Bharat Bhushan. Bioinspired, roughness-induced, water and oil super-philic and super-phobic coatings prepared by adaptable layer-by-layer technique. *Sci. Rep.*, 5:14030, 2007.

[40] Andreas Solga, Zdenek Cerman, Boris F. Striffler, Manuel Spaeth, and Wilhelm Barthlott. The dream of staying clean: Lotus and biomimetic surfaces. *Bioinsp. Biomim.*, 2:126–134, 2007.

[41] B. Wang, J. Li, G. Wang, W. Liang, Y. Zhang, L. Shi, Z. Guo, and W. Liu. Methodology for robust superhydrophobic fabrics and sponges from in situ growth of transition metal/metal oxide nanocrystals with thiol modification and their applications in oil/water separation. *ACS Appl. Mater. Interfaces*, 5:1827–1839, 2013.

[42] Q. Zhu, Q. Pan, and F. Liu. Facile removal and collection of oils from water surfaces through superhydrophobic and superoleophilic sponges. *J. Phys. Chem. C*, 115:17464–17470, 2011.

[43] J. Wu, J. Chen, K. Qasim, J. Xia, W. Lei, and B. P. Wang. A hierarchical mesh film with superhydrophobic and superoleophilic properties for oil and water separation. *J. Chem. Technol. Biotechnol.*, 87:427–430, 2012.

[44] C. Wang, T. Yao, J. Wu, C. Ma, Z. Fan, Z. Wang, Y. Cheng, Q. Lin, and B. Yang. Facile approach in fabricating superhydrophobic and superoleophilic surface for water and oil mixture separation. *ACS Appl. Mater. Interfaces*, 1:2613–2617, 2009.

[45] D. Deng, D. P. Prendergast, J. MacFarlane, R. Bagatin, F. Stellacci, and P. M. Gschwend. Hydrophobic meshes for oil spill recovery devices. *ACS Appl. Mater. Interfaces*, 5:774–781, 2013.

[46] J. Zhang and S. Seeger. Polyester materials with superwetting silicone nanofilaments for oil/water separation and selective oil absorption. *Adv. Funct. Mater.*, 21:4699–4704, 2011.

[47] S. Sabir. Approach of cost-effective adsorbents for oil removal from oily water. *Crit. Rev. Environ. Sci. Tech.*, 45:1916–1945, 2015.

[48] L. Wu, J. Zhang, B. Li, and A. Wang. Mechanical- and oil-durable superhydrophobic polyester materials for selective oil absorption and oil/water separation. *J. Colloid Interface Sci.*, 413:112–117, 2014.

[49] M. N. Kavalenka, A. Hopf, M. Schneider, M. Worgull, and H. Hölscher. Wood-based microhaired superhydrophobic and underwater superoleophobic surfaces for oil/water separation. *RSC Advances*, 59:31079–31083, 2014.

[50] J. T. Korhonen, M. Kettunen, R. H. A. Ras, and O. Ikkala. Hydrophobic nanocellulose aerogels as floating, sustainable, reusable, and recyclable oil absorbents. *ACS Appl. Mater. Interfaces*, 3:1813–1816, 2011.

[51] H.-C. Yang, K.-J. Liao, H. Huang, Q.-Y. Wu, L.-S. Wan, and Z.-K. Xu. Mussel-inspired modification of a polymer membrane for ultra-high water permeability and oil-in-water emulsion separation. *J. Mater. Chem. A*, 2:10225–10230, 2014.

[52] Jacob N. Israelachvili. *Intermolecular and Surface Forces.* Academic Press, 1992.

[53] K. Koch and W. Barthlott. Superhydrophobic and superhydrophilic plant surfaces: an inspiration for biomimetic materials. *Phil. Trans. R. Soc. A*, 367:1487–1509, 2009.

[54] N. Cohen, A. Dotan, H. Dodiuk, and S. Kenig. Superhydrophobic coatings and their durability. *Materials and Manufacturing Processes*, 31(9):1143–1155, 2016.

[55] Yu. I. Tarasevich. The surface energy of hydrophilic and hydrophobic adsorbents. *Colloid Journal*, 69(2):212–220, 2007.

[56] Jordi Fraxedas. *Water at Interfaces: A Molecular Approach.* CRC Press, 2014.

[57] Masashi Miwa, Akira Nakajima, Akira Fujishima, Kazuhito Hashimoto, and Toshiya Watanabe. Effects of the surface roughness on sliding angles of water droplets on superhydrophobic surfaces. *Langmuir*, 16(13):5754–5760, 2000.

[58] Robert N. Wenzel. Resistance of solid surfaces to wetting by water. *Ind. Eng. Chem.*, 28(8):988–994, 1936.

[59] A. B. D. Cassie and S. Baxter. Wettability of porous surfaces. *Trans. Faraday Soc.*, 40:546–551, 1944.

[60] Abraham Marmur. Wetting on hydrophobic rough surfaces: To be heterogeneous or not to be? *Langmuir*, 19(20):8343–8348, 2003.

[61] Erwin A. Vogler. Structure and reactivity of water at biomaterial surfaces. *Adv. Colloid Interface Sci.*, 74:69–117, 1998.

[62] C. Guo, S. Wang, H. Liu, L. Feng, Y. Song, and L. Jiang. Wettability alteration of polymer surfaces produced by scraping. *J. Adhes. Sci. Technol.*, 22(3-4):395–402, 2008.

[63] James W. Whalen. *Physical chemistry of surfaces, sixth edition.* Wiley-Interscience, 1997.

[64] DataPhysics Instruments GmbH. dataphysics.de, 03/03/2018.

[65] Julia Bur. Einstellbares Benetzungsverhalten von Formgedächtnispolymeren durch ortsaufgelöste Mikrostrukturierung. Diploma thesis, Karlsruhe Institute of Technology, 2013.

[66] L. B. Vernon and H. M. Vernon. US patent, 1941.

[67] J. Cui, K. Kratz, and A. Lendlein. Adjusting shape-memory properties of amorphous polyether urethanes and radio-opaque composites thereof by variation of physical parameters during programming. *Smart Materials and Structures*, 19(6):065019, 2010.

[68] J. Cui, K. Kratz, M. Heuchel, B. Hiebl, and A. Lendlein. Mechanically active scaffolds from radio-opaque shape-memory polymer-based composites. *Polymers for Advanced Technologies*, 22(1):180–189, 2011.

[69] A. Lendlein. *Shape-Memory Polymers (Advances in Polymer Science).* Springer, 2010.

[70] Andreas Lendlein and Steffen Kelch. Formgedächtnispolymere. *Angewandte Chemie*, 114(12):2138–2162, 2002.

[71] Tobias Meier. *Magnetoresistive and Thermoresistive Scanning Probe Microscopy with Applications in Micro- and Nanotechnology.* KIT Scientific Publishing, Karlsruhe, 2014.

[72] Andreas Lendlein, Marc Behl, Bernhard Hiebl, and Christian Wischke. Shape-memory polymers as technology platform for biomedical applications. *Expert Rev. Med. Devices*, 7:357–379, 2010.

[73] Matthias Worgull. *Hot Embossing. Theory and Technology of Microreplication, Micro and Nano Technologies.* William Andrew, 2009.

[74] Andreas Striegel, Marc Schneider, Norbert Schneider, Christian Benkel, and Matthias Worgull. Seamless tool fabrication for roll-to-roll microreplication. *Microelectron. Eng.*, 194:8–14, 2018.

[75] H. W. Bates. New species of butterflies from Guatemala and Panama, collected by Osbert Salvin and F. du Cane Godman, Esqs. *Entomologist's monthly Magazine*, 1(1), 1864.

[76] Kyungjae Chung and Jung H. Shin. Range and stability of structural colors generated by *morpho*-inspired color reflectors. *J. Opt. Soc. Am. A*, 30(5):962–968, 2013.

[77] Shichao Niu, Bo Li, Zhengzhi Mu, Meng Yang, Junqiu Zhang, Zhiwu Han, and Luquan Ren. Excellent structure-based multifunction of *morpho* butterfly wings: A review. *J. Bionic Eng.*, 12(2):170–189, 2015.

[78] Xuan Jiang, HaiBo Shi, TieLin Zuo, XueFeng Yang, WenJun Wu, and GuangLan Liao. Investigation on color variation of morpho butterfly wings hierarchical structure based on pca. *Sci. China Technol. Sci.*, 55:16–21, 2012.

[79] Gary Cook, Peter L Timms, and Christine Göltner-Spickermann. Exact replication of biological structures by chemical vapor deposition of silica. *Angewandte Chemie International Edition*, 42(5):557–559, 2003.

[80] Jingyun Huang, Xudong Wang, and Zhong Lin Wang. Controlled replication of butterfly wings for achieving tunable photonic properties. *Nano letters*, 6(10):2325–2331, 2006.

[81] Shenmin Zhu, Di Zhang, Zhixin Chen, Jiajun Gu, Wenfei Li, Haibo Jiang, and Gang Zhou. A simple and effective approach towards biomimetic replication of photonic structures from butterfly wings. *Nanotechnology*, 20(31):315303, 2009.

[82] Wang Zhang et al. Fabrication of ZnO microtubes with adjustable nanopores on the walls by the templating of butterfly wing scales. *Nanotechnology*, 17(3):840, 2006.

[83] Yu Chen, Xining Zang, Jiajun Gu, Shenmin Zhu, Huilan Su, Di Zhang, Xiaobin Hu, Qinglei Liu, Wang Zhang, and Dingxin Liu. ZnO single butterfly wing scales: synthesis and spatial optical anisotropy. *Journal of Materials Chemistry*, 21(17):6140–6143, 2011.

[84] Fang Song, Huilan Su, Jie Han, Di Zhang, and Zhixin Chen. Fabrication and good ethanol sensing of biomorphic SnO_2 with architecture hierarchy of butterfly wings. *Nanotechnology*, 20(49):495–502, 2009.

[85] Shao-Hui Kang, Tzu-Yao Tai, and Te-Hua Fang. Replication of butterfly wing microstructures using molding lithography. *Current Applied Physics*, 10(2):625–630, 2010.

[86] Keiichiro Watanabe, Takayuki Hoshino, Kazuhiro Kanda, Yuichi Haruyama, and Shinji Matsui. Brilliant blue observation from a *morpho*-butterfly-scale quasi-structure. *Japanese journal of applied physics*, 44:L48–L50, 2005.

[87] Radwanul Hasan Siddique, Silvia Diewald, Juerg Leuthold, and Hendrik Hölscher. Theoretical and experimental analysis of the structural pattern responsible for the iridescence of morpho butterflies. *Opt. Express*, 21:14351–14361, 2013.

[88] Norbert Schneider, Claudia Zeiger, Alexander Kolew, Marc Schneider, Juerg Leuthold, Hendrik Hölscher, and Matthias Worgull. Nanothermoforming of hierarchical optical components utilizing shape memory polymers as active molds. *Opt. Mat. Express*, 4:1895–1902, 2014.

[89] Alexander Kolew. *Heißprägen von Verbundfolien für mikrofluidische Anwendungen.* KIT Scientific Publishing, 2012.

[90] Maryna N. Kavalenka, Felix Vüllers, Jana Kumberg, Claudia Zeiger, Vanessa Trouillet, Sebastian Stein, Tanzila T. Ava, Chunyan Li, Matthias Worgull, and Hendrik Hölscher. Adaptable bioinspired special wetting material for multifunctional oil/water separation. *Sci. Rep.*, 7:39970, 2017.

[91] Claudia Zeiger, Jana Kumberg, Felix Vüllers, Matthias Worgull, Hendrik Hölscher, and Maryna N. Kavalenka. Selective filtration of oil/water mixtures with bioinspired porous membranes. *RSC Adv.*, 7:32806–32811, 2017.

[92] R. Wahi, L.A. Chuah, T.S.Y. Choong, Z. Ngaini, and M.M. Nourouzi. Oil removal from aqueous state by natural fibrous sorbent: an overview. *Sep. Purif. Technol.*, 113:51–63, 2013.

[93] T. R. Annunciado, T. H. D. Sydenstricker, and S. C. Amico. Experimental investigation of various vegetable fibers as sorbent materials for oil spills. *Mar. Pollut. Bull.*, 50:1340–1346, 2005.

[94] D. Li, F. Z. Zhu, J. Y. Li, P. Na, and N. Wang. Preparation and characterization of cellulose fibers from corn straw as natural oil sorbents. *Ind. Eng. Chem. Res.*, 52:516–524, 2012.

[95] X. Yang, S. Chen, and R. Zhang. Utilization of two invasive free-floating aquatic plants (*Pistia stratiotes* and *Eichhornia crassipes*) as sorbents for oil removal. *Environ. Sci. Pollut. Res.*, 21:781–786, 2014.

[96] A. M. Abd-Elnaby and M. A. Egorov. Efficiency of different particle sizes of dried *Salvinia natans* in the removing of Cu(II) and oil pollutions from water. *J. Water. Chem. Technol.*, 34:143–146, 2012.

[97] G. Sánchez-Galván, F. J. Mercado, and E. J. Olguín. Leaves and roots of *Pistia stratiotes* as sorbent materials for the removal of crude oil from saline solutions. *Water Air Soil Pollut*, 224:224, 2013.

[98] T. H. Ribeiro, J. Rubio, and R. W. Smith. A dried hydrophobic aquaphyte as an oil filter for oil/water emulsions. *Spill Sci. Technol. B*, 8:483–489, 2003.

[99] T. H. Ribeiro, R. W. Smith, and J. Rubio. Sorption of oils by the nonliving biomass of a *Salvinia* sp. *Environ. Sci. Technol.*, 34:5201–5205, 2000.

[100] Edyta Witka-Jeżewska and Jan Hupka. Investigation of oleophilic nature of straw sorbent conditioned in water. *Spill Sci. Technol. Bull.*, 8:561–564, 2003.

[101] M. J. Mayser, H. F. Bohn, M. Reker, and W. Barthlott. Measuring air layer volumes retained by submerged floating-ferns *Salvinia* and biomimetic superhydrophobic surfaces. *Beilstein J. Nanotechnol.*, 5:812–821, 2014.

[102] David Pimentel, editor. *Encyclopedia of Pest Management.* CRC Press, New York, USA, 2002.

[103] P. M. Room, K. L. S. Harley, I. W. Forno, and D. P. A. Sands. Successful biological control of the floating weed *Salvinia*. *Nature*, 294:78–80, 1981.

[104] C. Jacono and B. Pitman. *Salvinia molesta*: around the world in 70 years. *Aquatic Nuisance Species Digest*, 4:13–16, 2001.

[105] G. P. Chikwenhere. Biological control of water lettuce in various impoundments of Zimbabwe. *J. Aquat. Plant Manage.*, 32:27–29, 1994.

[106] S. A. Abbasi and P. C. Nipaney. Biogas production from the aquatic weed Pistia (*Pistia stratiotes*). *Bioresource Technology*, 37:211–214, 1991.

[107] G. Mbati and P. Neuenschwander. Biological control of three floating water weeds, *Eichhornia crassipes*, *Pistia stratiotes*, and *Salvinia molesta* in the Republic of Congo. *BioControl*, 50:635–645, 2005.

[108] R. de Moraes Ferreira, M. D. P. de Souza, I. Takase, and D. M. de Araujo Stapelfeldt. Pb(II) adsorption by biomass from chemically modified aquatic macrophytes, *Salvinia* sp. and *Pistia stratiotes*. *Water Sci. Tech.*, 73:2670–2679, 2016.

[109] Bhupinder Dhir. *Phytoremediation: Role of Aquatic Plants in Environmental Clean-Up*. Springer, 2013.

[110] W. Barthlott, Th. Schimmel, S. Wiersch, K. Koch, M. Brede, M. Barczewski, S. Walheim, A. Weis, A. Kaltenmaier, A. Leder, and H. F. Bohn. The *Salvinia* paradox: Superhydrophobic surfaces with hydrophilic pins for air retention under water. *Adv. Mater.*, 22:2325–2328, 2010.

[111] Harpreet S. Grewal, Il-Joo Cho, and Eui-Sung Yoon. The role of bio-inspired hierarchical structures in wetting. *Bioinspir. Biomim.*, 10:026009, 2015.

[112] John L. Neff and Beryl B. Simpson. Vogel,s great legacy: The oil flower and oil-collecting bee syndrome. *Flora*, 232:104–116, 2017.

[113] Stefan Vogel. Ölproduzierende Blumen, die durch ölsammelnde Bienen bestäubt werden. *Naturwissenschaften*, 58(1):58, Jan 1971.

[114] Stefan Vogel. A floral biologist's past fifty years: some thoughts and experiences. *Tyxpn*, 56:660–662, 2007.

[115] Stefan Vogel. Abdominal oil-mopping - a new type of foraging in bees. *Naturwissenschaften*, 68:627–628, 1981.

[116] S. L. Buchmann. The ecology of oil flowers and their bees. *Ann. Rev. Ecol. Syst.*, 18:343–369, 1987.

[117] A. Rüttgers, M. Griebel, L. Pastrik, H. Schmied, D. Wittmann, A. Scherrieble, A. Dinkelmann, and T. Stegmaier. Simulation of the oil storage process in the scopa of specialized bees. *Computer & Fluids*, 119:115–130, 2015.

[118] W. Barthlott, S. Wiersch, Z. Čolić, and K. Koch. Classification of trichome types within species of the water fern *Salvinia*, and ontogeny of the egg-beater trichomes. *Botany*, 87:830–836, 2009.

[119] ImageJ Software. imagej.net. online, 03/03/2018.

[120] puren® GmbH. puren.com, 03/03/2018.

[121] Deurex®. deurex.com, 03/03/2018.

[122] Z. Cerman, B. F. Striffler, and W. Barthlott. *Dry in the Water: The Superhydrophobic Water Fern Salvinia - a Model for Biomimetic Surfaces*, pages 97–111. Springer, Heidelberg, 2009.

[123] C.-Y. Yang, C.-Y. Yang, and C.-K. Sung. Enhancing air retention by biomimicking *Salvinia molesta* structures. *Jpn. J. Appl. Phys.*, 52:06GF08, 2013.

[124] Petra Ditsche, Elena Gorb, Matthias Mayser, Stanislav Gorb, Thomas Schimmel, and Wilhelm Barthlott. Elasticity of the hair cover in air-retaining *Salvinia* surfaces. *Appl. Phys. A*, 121:505–511, 2015.

[125] Alexander Storz. Fabrication, characterization and application of biomimetic nanofur made of polymers. Master's thesis, Karlsruhe Institute of Technology, 2016.

[126] Dong Wu, Jian-Nan Wang, Si-Zhu Wu, Qi-Dai Chen, Shuai Zhao, Hao Zhang, Hong-Bo Sun, and Lei Jiang. Three-level biomimetic rice-leaf surfaces with controllable anisotropic sliding. *Adv. Funct. Mater.*, 21:2927–2932, 2011.

[127] Gregory D. Bixler and Bharat Bhushan. Rice- and butterfly-wing effect inspired self-cleaning and low drag micro/nanopatterned surfaces in water, oil, and air flow. *Nanoscale*, 6:76–96, 2014.

[128] D.W. Bechert, M Bruse, Wolfram Hage, J.G.T. van der Hoeven, and G Hoppe. Experiments on drag-reducing surfaces and their optimization with an adjustable geometry. *J. Fluid Mech.*, 338:59–87, 1997.

[129] Gregory D. Bixler and Bharat Bhushan. Bioinspired micro/nanostructured surfaces for oil drag reduction in closed channel flow. *Soft Matter*, 9:1620–1635, 2013.

[130] Gregory D. Bixler and Bharat Bhushan. Bioinspired rice leaf and butterfly wing surface structures combining shark skin and lotus effects. *Soft Matter*, 8:11271–11284, 2012.

[131] Hanna Wund. Herstellung und Charakterisierung von wiederverwendbarem, biomimetischem Nanopelz aus Formgedächtnispolymer zur selektiven Absorption von Öl. Bachelor's thesis, Karlsruhe Institute of Technology, 2016.

[132] Christina Schmidt, A. M. Sarwaruddin Chowdhury, Klaus Neuking, and Gunther Eggeler. Studies on the cycling, processing and programming of an industrially applicable shape memory polymer Tecoflex® (or TFX EG 72D). *High Perform. Polym.*, 23(4):300–307, 2011.

[133] Qinglang Ma, Cheng Honfei, Anthony G. Fane, Wang Rong, and Zhang Hua. Recent development of advanced materials with special wettability for selective oil/water separation. *Small*, 12(16):2189–2202, 2016.

[134] Zonglin Chu, Yujun Feng, and Stefan Seeger. Oil/water separation with selective superantiwetting/superwetting surface materials. *Angew. Chem. Int. Ed.*, 54:2328–2338, 2015.

[135] Peng-Cheng Chen and Zhi-Kang Xu. Mineral-coated polymer membranes with superhydrophilicity and underwater superoleophobicity for effective oil/water separation. *Sci. Rep.*, 3:2776, 2013.

[136] Z. Xue, S. Wang, L. Lin, L. Chen, M. Liu, L. Feng, and L. Jiang. A novel superhydrophilic and underwater superoleophobic hydrogel-coated mesh for oil/water separation. *Adv. Mater.*, 23(37):4270–4273, 2011.

[137] A. Lafuma and D. Quéré. Superhydrophobic states. *Nat. Mater.*, 2:457–460, 2003.

[138] Zhongxin Xue, Yingze Cao, Na Liu, Lin Feng, and Lei Jiang. Special wettable materials for oil/water separation. *J. Mater. Chem. A*, 2:2445–2460, 2014.

[139] Jian Li, Dianming Li, Yaoxia Yang, Jianping Li, Fei Zha, and Ziqiang Lei. A prewetting induced underwater superoleophobic or underoil (super) hydrophobic waste

potato residue-coated mesh for selective efficient oil/water separation. *Green Chem.*, 18(2):541–549, 2016.

[140] J. Gu, P. Xiao, Y. Huang, J. Zhang, and T. Chen. Controlled functionalization of carbon nanotubes as superhydrophobic material for adjustable oil/water separation. *J. Mater. Chem. A*, 3:4124–4128, 2015.

[141] J. Y. Huang, S. H. Li, M. Z. Ge, L. N. Wang, T. L. Xing, G. Q. Chen, X. F. Liu, S. S. Al-Deyab, K. Q. Zhang, T. Chen, and Y. K. Lai. Robust superhydrophobic TiO_2@fabrics for uv shielding, self-cleaning and oil-water separation. *J. Mater. Chem. A*, 3:2825–2832, 2015.

[142] Lianbin Zhang, Yujiang Zhong, Dongkyu Cha, and Peng Wang. A self-cleaning underwater superoleophobic mesh for oil-water separation. *Sci. Rep.*, 3:2326, July 2013.

[143] Chao-Hua Xue, Ya-Ru Li, Jin-Lin Hou, Lei Zhang, Jian-Zhong Ma, and Shun-Tian Jia. Self-roughened superhydrophobic coatings for continuous oil-water separation. *J. Mater. Chem. A*, 3:10248–10253, 2015.

[144] Ling-Hao Kong, Xin-Hua Chen, Lai-Gui Yu, Zhi-Shen Wu, and Ping-Yu Zhang. Superhydrophobic cuprous oxide nanostructures on phosphor-copper meshes and their oil-water separation and oil spill cleanup. *ACS Appl. Mater. Interfaces*, 7(4):2616–2625, 2015.

[145] Zhenxing Wang, Yanchao Xu, Yuyan Liu, and Lu Shao. A novel mussel-inspired strategy toward superhydrophobic surfaces for self-driven crude oil spill cleanup. *J. Mater. Chem. A*, 3:12171–12178, 2015.

[146] Xi Chen, Yi He, Yi Fan, Qiangbin Yang, Guangyong Zeng, and Heng Shi. Facile fabrication of a robust superwetting three-dimensional (3D) nickel foam for oil/water separation. *J. Mater. Sci.*, 52(4):2169–2179, 2017.

[147] Chee Huei Lee, Nick Johnson, Jaroslaw Drelich, and Yoke Khin Yap. The performance of superhydrophobic and superoleophilic carbon nanotube meshes in water-oil filtration. *Carbon*, 49(2):669–676, 2011.

[148] Caiming Xiao, Lianxi Si, Yiming Liu, Guoqing Guan, Dihua Wu, Zhongde Wang, and Xiaogang Hao. Ultrastable coaxial cable-like superhydrophobic mesh with self-adaption effect: facile synthesis and oil/water separation application. *J. Mater. Chem. A*, 4:8080–8090, 2016.

[149] Weifeng Zhang, Na Liu, Yingze Cao, Yuning Chen, Liangxin Xu, Xin Lin, and Lin Feng. A solvothermal route decorated on different substrates: Controllable separation of an oil/water mixture to a stabilized nanoscale emulsion. *Adv. Mater.*, 27(45):7349–7355, 2015.

[150] Lin Li, Zhaoyue Liu, Qianqian Zhang, Chenhui Meng, Tierui Zhang, and Jin Zhai. Underwater superoleophobic porous membrane based on hierarchical TiO_2 nanotubes: multifunctional integration of oil-water separation, flow-through photocatalysis and self-cleaning. *J. Mater. Chem. A*, 3:1279–1286, 2015.

[151] Jian Li, Long Yan, Haoyu Li, Weijun Li, Fei Zha, and Ziqiang Lei. Underwater superoleophobic palygorskite coated meshes for efficient oil/water separation. *J. Mater. Chem. A*, 3:14696–14702, 2015.

[152] Chih-Feng Wang, Fan-Shiuan Tzeng, Hou-Guang Chen, and Chi-Jung Chang. Ultraviolet-durable superhydrophobic zinc oxide-coated mesh films for surface and underwater-oil capture and transportation. *Langmuir*, 28(26):10015–10019, 2012.

[153] Qiang Wen, Jiancheng Di, Lei Jiang, Jihong Yu, and Ruren Xu. Zeolite-coated mesh film for efficient oil-water separation. *Chem. Sci.*, 4:591–595, 2013.

[154] Xi Zheng, Zhenyan Guo, Dongliang Tian, Xiaofang Zhang, Wenxian Li, and Lei Jiang. Underwater self-cleaning scaly fabric membrane for oily water separation. *ACS Appl. Mater. Interfaces*, 7(7):4336–4343, 2015.

[155] Chuan Du, Jiadao Wang, Zhifu Chen, and Darong Chen. Durable superhydrophobic and superoleophilic filter paper for oil-water separation prepared by a colloidal deposition method. *Appl. Surf. Sci.*, 313:304–310, 2014.

[156] S. J. Maguire-Boyle and A. R. Barron. A new functionalization strategy for oil/water separation membranes. *J. Membrane Sci.*, 382:107–115, 2011.

[157] Ke He, Haoran Duan, George Y. Chen, Xiaokong Liu, Wensheng Yang, and Dayang Wang. Cleaning of oil fouling with water enabled by zwitterionic polyelectrolyte coatings: Overcoming the imperative challenge of oil-water separation membranes. *ACS Nano*, 9(9):9188–9198, 2015.

[158] Zhiyong He, Xiwang Zhang, and Warren Batchelor. Cellulose nanofibre aerogel filter with tuneable pore structure for oil/water separation and recovery. *RSC Adv.*, 6:21435–21438, 2016.

[159] Feng Zhang, Wen Bin Zhang, Zhun Shi, Dong Wang, Jian Jin, and Lei Jiang. Nanowire-haired inorganic membranes with superhydrophilicity and underwater ultralow adhesive superoleophobicity for high-efficiency oil/water separation. *Adv. Mater.*, 25(30):4192–4198, 2013.

[160] Jin Yang, Zhaozhu Zhang, Xianghui Xu, Xiaotao Zhu, Xuehu Men, and Xiaoyan Zhou. Superhydrophilic-superoleophobic coatings. *J. Mater. Chem.*, 22:2834–2837, 2012.

[161] Jun-Bing Fan, Yongyang Song, Shutao Wang, Jingxin Meng, Gao Yang, Xinglin Guo, Lin Feng, and Lei Jiang. Directly coating hydrogel on filter paper for effective oil-water separation in highly acidic, alkaline, and salty environment. *Adv. Funct. Mater.*, 25(33):5368–5375, 2015.

[162] G. Kwon, A. K. Kota, Y. Li, A. Sohani, J. M. Mabry, and A. Tuteja. On-demand separation of oil-water mixtures. *Adv. Mater.*, 24(27):3666–3671, 2012.

[163] Jing Wu, Nu Wang, Yong Zhao, and Lei Jiang. Simple synthesis of smart magnetically driven fibrous films for remote controllable oil removal. *Nanoscale*, 7:2625–2632, 2015.

[164] Ranwen Ou, Jing Wei, Lei Jiang, George P. Simon, and Huanting Wang. Robust thermoresponsive polymer composite membrane with switchable superhydrophilicity and superhydrophobicity for efficient oil-water separation. *Environ. Sci. Technol.*, 50(2):906–914, 2016.

[165] Zhongjun Cheng, Jingwen Wang, Hua Lai, Ying Du, Rui Hou, Chong Li, Naiqing Zhang, and Kening Sun. pH-controllable on-demand oil/water separation on the switchable superhydrophobic/superhydrophilic and underwater low-adhesive superoleophobic copper mesh film. *Langmuir*, 31(4):1393–1399, 2015.

[166] Mimi Tao, Lixin Xue, Fu Liu, and Lei Jiang. An intelligent superwetting PVDF membrane showing switchable transport performance for oil/water separation. *Adv. Mater.*, 26(18):2943–2948, 2014.

[167] Xin Du, Shijie You, Xiuheng Wang, Qiuru Wang, and Jiandong Lu. Switchable and simultaneous oil/water separation induced by prewetting with a superamphiphilic self-cleaning mesh. *Chem. Eng. J.*, 313:398–403, 2017.

[168] Dengteng Ge, Lili Yang, Chenbo Wang, Elaine Lee, Yongquan Zhang, and Shu Yang. A multi-functional oil-water separator from a selectively pre-wetted superamphiphobic paper. *Chem. Commun.*, 51:6149–6152, 2015.

[169] Jana Kumberg. Trennung von Öl/Wasser-Gemischen mit porösem, biomimetischem Nanopelz. Master's thesis, Karlsruhe Institute of Technology, 2015.

[170] Junhui He, editor. *Self-cleaning Coatings*. Smart Materials Series. The Royal Society of Chemistry, 2017.

[171] Colin R. Crick, James A. Gibbins, and Ivan P. Parkin. Superhydrophobic polymer-coated copper-mesh; membranes for highly efficient oil-water separation. *J. Mater. Chem. A*, 1:5943–5948, 2013.

[172] Indranee Das and Goutam De. Zirconia based superhydrophobic coatings on cotton fabrics exhibiting excellent durability for versatile use. *Sci. Rep.*, 5:18503, 2015.

[173] Chunai Dai, Na Liu, Yingze Cao, Yuning Chen, Fei Lu, and Lin Feng. Fast formation of superhydrophobic octadecylphosphonic acid (ODPA) coating for self-cleaning and oil/water separation. *Soft Matter*, 10:8116–8121, 2014.

[174] Zhongxin Xue, Zhongxue Sun, Yingze Cao, Yuning Chen, Lei Tao, Kan Li, Lin Feng, Qiang Fu, and Yen Wei. Superoleophilic and superhydrophobic biodegradable material with porous structures for oil absorption and oil-water separation. *RSC Adv.*, 3:23432–23437, 2013.

[175] Mohammed A. Gondal, Muhammad S. Sadullah, Mohamed A. Dastageer, Gareth H. McKinley, Divya Panchanathan, and Kripa K. Varanasi. Study of factors governing oil-water separation process using TiO_2 films prepared by spray deposition of nanoparticle dispersions. *ACS Appl. Mater. Interfaces*, 6(16):13422–13429, 2014.

[176] A. M. Vadya, P. J. Halling, and G. Bell. Surfactant-induced breakthrough effects during the operation of two-phase biocatalytic membrane reactors. *Biotechnol. Bioeng.*, 44(6):765–571, 1994.

[177] Jay W. Grate, Karl J. Dehoff, Marvin G. Warner, Jonathan W. Pittman, Thomas W. Wietsma, Changyong Zhang, and Mart Oostrom. Correlation of oil-water and air-water contact angles of diverse silanized surfaces and relationship to fluid interfacial tensions. *Langmuir*, 28(18):7182–7188, 2012.

[178] Georgios M. Kontogeorgis and Georgios K. Folas. *Thermodynamics and Colloid and Surface Chemistry*, pages 577–611. John Wiley & Sons, Ltd, 2009.

[179] Yao Lu, Sanjayan Sathasivam, Jinlong Song, Colin R. Crick, Claire J. Carmalt, and Ivan P. Parkin. Robust self-cleaning surfaces that function when exposed to either air or oil. *Science*, 347(6226):1132–1135, 2015.

[180] Edward Bormashenko, Gilad Chaniel, and Roman Grynyov. Towards understanding hydrophobic recovery of plasma treated polymers: Storing in high polarity liquids suppresses hydrophobic recovery. *Applied Surface Science*, 273:549–553, 2013.

[181] L. Zajíčková, D. Subedi, V. Bursikova, and K. Veltruská. Study of argon plasma treatment of polycarbonate substrate and its effect on film deposition. *Acta Phys. Slovaca*, 53:489–504, 2003.

[182] G. K. Batchelor. *An Introduction in Fluid Dynamics*. Cambridge University Press, Cambridge, 1970.

[183] Jiale Yong, Feng Chen, Qing Yang, Hao Bian, Guangqing Du, Chao Shan, Jinglan Huo, Yao Fang, and Xun Hou. Oil-water separation: A gift from the desert. *Adv. Mater. Interfaces*, 3(7):1500650, 2016.

List of Publications

SCIENTIFIC PAPERS

Claudia Zeiger, Jana Kumberg, Felix Vüllers, Matthias Worgull, Hendrik Hölscher, Maryna Kavalenka. Selective Filtration of Oil/Water Mixtures with Bioinspired Porous Membranes. *RSC Adv.*, 7:32806-32811, 2017.

Claudia Zeiger. Mikrostrukturierte Pflanzenblätter - Effiziente natürliche Ölabsorber und Inspiration für künstliche ölabsorbierende Materialien. GIT Labor-Fachzeitschrift, 3:36-38, 2017.

Maryna N. Kavalenka, Felix Vüllers, Jana Kumberg, Claudia Zeiger, Vanessa Trouillet, Sebastian Stein, Tanzila T. Ava, Chunyan Li, Matthias Worgull, and Hendrik HÏscher. Adaptable bioinspired special wetting material for multifunctional oil/water separation. *Sci. Rep.*, 7:39970, 2017.

Claudia Zeiger, Isabelle C. Rodrigues da Silva, Matthias Mail, Maryna N. Kavalenka, Wilhelm Barthlott, Hendrik Hölscher. Microstructures of superhydrophobic plant leaves - inspiration for efficient oil spill cleanup materials. *Bioinspir. Biomim.*, 11:056003, 2016.

Maryna N. Kavalenka, Felix Vüllers, Simone Lischker, Claudia Zeiger, Andreas Hopf, Michael Röhrig, Bastian E. Rapp, Matthias Worgull, and Hendrik Hölscher. Bioinspired air-retaining nanofur for drag reduction. *ACS Appl. Mater. & Interfaces*, 7(7):1065110655, 2015.

Norbert Schneider, Claudia Zeiger, Alexander Kolew, Marc Schneider, Juerg Leuthold, Hendrik Hölscher, and Matthias Worgull. Nanothermoforming of hierarchical optical components utilizing shape memory polymers as active molds. *Opt. Mat. Express*, 4:1895-1902, 2014.

PATENT APPLICATIONS

Claudia Zeiger, Maryna Kavalenka, Matthais Worgull, Hendrik Hölscher: WO2016096142 A1 (DE102014119183 A1)

Claudia Zeiger, Alexander Storz, Andreas Striegel, Maryna Kavalenka, Matthais Worgull, Hendrik Hölscher: 102018004339.9

CONFERENCE CONTRIBUTIONS

29-31 May 2017 **WE-Heraeus-Seminar Bio-Inspired Nano- and Microstructured Surfaces**, Bad Honnef, Germany. Poster presentation. Bioinspired Polymeric Nanofur for Oil/Water Separation. Claudia Zeiger, Matthias Worgull, Hendrik Hölscher, Maryna Kavalenka.

24-29 May 2015 **15th Conference of the International Association of Colloid and Interface Scientists**, Mainz, Germany. Oil/Water Separation with Bioinspired Superhydrophobic and Superoleopilic Nanofur. Claudia Zeiger, Maryna N. Kavalenka, Felix Vüllers, Marc Schneider, Matthias Worgull, Hendrik Hölscher.

4-6 May 2015 **SPIE Microtechnologies**, Barcelona, Spain. Bio-Inspired Nanofur for Oil Spill Cleanup and Underwater Drag Reduction. Claudia Zeiger, Maryna Kavalenka, Matthias Worgull, Hendrik Hölscher.

8-12 Mar. 2015 **SPIE Smart Structures/NDE conference**, San Diego, California, USA. Poster presentation. Biomimetic nanofur for drag reduction and oil-water separation. Hendrik Hölscher, Maryna N. Kavalenka, Claudia Zeiger, Matthias Mail, Marc Schneider, Stefan Walheim, Thomas Schimel, Matthias Worgull.

30 Nov. - 5 Dec. 2014 **MRS Fall Meeting & Exhibit**, Boston, USA. Fabrication of Hierarchical, Bio-inspired Nano- and Microstructures by Advanced Hot Embossing Techniques. Hendrik Hölscher, Michael Röhrig, Maryna Kavalenka, Claudia Zeiger, Marc Schneider, Alexander Kolew, Matthias Worgull.

24-26 Sept. 2014 **Statusworkshop Kompetenznetz funktionelle Nanostrukturen**, Bad Herrenalb, Germany. Poster presentation. Oil Water Separation with Biomimetic Nanofur. Claudia Zeiger, Maryna Kavalenka, Matthias Worgull, Hendrik Hölscher.

10-12 Apr. 2014 **Living Light: Uniting biology and photonics**, Namur, Belgium. Poster presentation. Lagre-Scale Nanothermoforming of Optical Nanostructures Inspired by Morpho Butterflies using Shape Memory Polymers. C. Zeiger, N. Schneider, A. Kolew, M. Schneider, R. H. Siddique, H. Hölscher, M. Worgull.

30 Mar. - 4 Apr. 2014 **DPG Spring Meeting**, Dresden, Germany. Large-scale Replication of Optical Nanostructures Inspired by Blue Morpho Butterflies. Claudia Zeiger, Norbert Schneider, Alexander Kolew, Marc Schneider, Radwanul H. Siddique, Hendrik Hölscher, Matthias Worgull

AWARDS AND HONORS

2017 **3rd price Best Poster Competition**
of the 644th WE-Heraeus-Seminar on Bio-inspired, Nano- and Microstructured Surfaces: New Functionality by Material and Structure, Bad Honnef, Germany

2016 **2nd price International Bionic Award 2016**
of the VDI / Schauenburg-Stiftung
Bioinspired Multifunctional Nanofur for Environmental Applications, together with Maryna Kavalenka and Felix Vüllers

2014 **1st price Poster Competition**
Statusworkshop Kompetenznetz funktionelle Nanostrukturen, Bad Herrenalb, Germany

2014 **3rd price Photo Competition**
Statusworkshop Kompetenznetz funktionelle Nanostrukturen, Bad Herrenalb, Germany